# Fatigue Crack Growth Behavior of Friction Stir Welded Joints for Dissimilar Aluminum Alloys Joined by Using a Bobbin Type Tool

（ボビン型ツールを用いた異種アルミニウム合金摩擦撹拌接合体の疲労き裂伝ぱ挙動）

**Panya Buahombura**

A dissertation submitted in partial fulfillment
Of requirements for the degree of

Doctor of Engineering
in
Materials Science

Graduate School of Engineering
Nagaoka University of Technology
Nagaoka, Niigata, JAPAN

October, 2013

# Fatigue Crack Growth Behavior of Friction Stir Welded Joints for Dissimilar Aluminum Alloys Joined by Using a Bobbin Type Tool

（ボビン型ツールを用いた異種アルミニウム合金摩擦撹拌接合体の疲労き裂伝ぱ挙動）

Friction stir welding (FSW) has been widely used mainly for aluminum alloys. Friction stir welding can join dissimilar materials and materials that difficult to join by conventional fusion welding. Many tools were developed in FSW to improve quality of the joint and productivity. Friction stir welding with a bobbin type tool has advantages compared to that with a conventional tool such as no backing plate, eliminate the root flaw, low distortion of the welded plate, joining thick plate in one-process, etc. In this study, fatigue crack growth (FCG) behavior of FSWed aluminum alloys joint joined by using a bobbin type tool was studied. Effect of FSW processes as comparison between bobbin type tool and conventional tool, effect of alloy type in similar material joint and effect of materials combination in dissimilar materials joint on the FCG behavior has been investigated. The results obtained in this research work were presented in details classified as below chapters.

**Chapter 1: Introduction –** Background and fundamental topic related to this study, such as friction stir welding of aluminum alloys and fatigue crack growth behavior of metallic material were introduced. A brief of literature review on FCG behaviors of FSWed aluminum alloys joints, research requirements, objective of this study and scope of the present work were also presented.

**Chapter 2: Fatigue crack growth behavior of FSWed 5052 aluminum alloy joint joined with a bobbin type tool and its comparison with single-passed and double-passed conventional FSWed joint –** Effect of FSW processes on FCG behavior of FSWed joints was studied in this chapter in 5052 aluminum alloy. Fatigue crack growth behavior at weld nugget zone (WNZ) and heat affected zone (HAZ) in the joints joined by using a bobbin type tool was investigated by comparing to those in the joints joined by using a conventional tool with single-passed and double-passed FSW processes. Friction stir welding process with the bobbin type tool introduced higher heat input compared to FSW processes with the single-pass and double-pass. Different FCG behavior was found in the joints joined with different FSW processing. Fatigue crack growth resistance of WNZ and HAZ in FSWed joint with single-passed process by using a conventional tool was higher compared to those observed in the FSWed joint with double-passed process by using a conventional tool and a bobbin type tool. However, the differences in FCG curves due to different FSW processes and positions in FSWed joints were arranged into a single curve when crack closure effect was taken into account. Grain size in the WNZ was dominant on threshold stress intensity factor range. Intrinsic FCG resistance of the FSWed joints were the similar regardless of FSW process.

**Chapter 3: Fatigue crack growth behavior of FSWed 5052, 6N01 and 7N01 similar aluminum alloy joints joined with a bobbin type tool -** Fatigue crack growth behavior at WNZ and HAZ in FSWed similar material joints joined by using a bobbin type tool in

5052, 6N01 and 7N01 aluminum alloys were investigated and compared to that of the BM. Different FCG behavior was found in FSWed joints with different aluminum alloys. The results showed that difference in FCG resistance was significantly observed in near threshold region, FCG resistance in WNZ of FSWed 5052 and 6N01 joints was lower than that in the BM and the HAZ. In contrast, FCG resistance in WNZ of FSWed 7N01 joint was higher than that in the BM and the HAZ. Difference in FCG behavior at different weld region was mainly due to difference in crack closure behavior in the FSWed joints. Grain size in the WNZ was dominant on threshold stress intensity factor range.

**Chapter 4: Fatigue crack growth behavior of FSWed 6N01-5052 dissimilar aluminum alloys joints joined with a bobbin type tool –**In this chapter, 5052 and 6N01 aluminum alloys which showed the similar FCG behaviors as shown in Chapter 3 were joined to FSWed 6N01-5052 dissimilar materials joint for investigating the effect of materials combination on fatigue crack growth behavior in the WNZ of the joint. FCG resistance in the WNZ of FSWed 6N01-5052 dissimilar materials joint was lower than that of the BMs and almost the same as that in WNZ of the FSWed 5052 and 6N01 similar material joints. In case of materials combination between two alloys which showed the similar FCG behavior in the joints, FCG behavior of the FSWed dissimilar materials joint was the similar with that of the similar materials joints in those alloys.

**Chapter 5: Fatigue crack growth behavior of FSWed 6N01-7N01 dissimilar aluminum alloys joints joined with a bobbin type tool -** In this chapter, 6N01 and 7N01 aluminum alloys which showed different FCG behavior as observed in Chapter 3 were joined to FSWed 6N01-7N01 dissimilar materials joint for investigating the effect of materials combination on fatigue crack growth behavior in the WNZ of the joint. Fatigue crack growth behavior in WNZ of the FSWed dissimilar aluminum alloys joints were investigated comparing to that of the FSWed similar aluminum alloy joints and the BMs. The result showed that the FCG resistance in WNZ of FSWed 6N01-7N01 dissimilar materials joint was higher than that observed in WNZ of FSWed 6N01 similar material joint, however, lower than that observed in WNZ of FSWed 7N01 similar material joint. Fatigue crack growth behavior of FSWed 6N01-7N01 dissimilar materials joint was influenced by combined effect of FCG behaviors of the both alloys joint. Difference in fatigue crack growth curves observed in WNZ of the dissimilar materials joints was smaller than difference in fatigue crack growth curves observed in different BMs when the curves were arranged by effective stress intensity factor range. Fatigue crack growth resistance in WNZ was the similar or higher than that of BMs for the similar and the dissimilar materials FSWed joints when crack closure effect was taken into account.

**Chapter 6: Conclusion –** General conclusions and recommendations for further work have been discussed and summarized.

# Acknowledgement

First of all, I would like to thank for my advisor, Prof. Yukio Miyashita for kindly support, advices and all of contributions for me during my studying and doing the research work in doctoral program.

My pleasure to thank Prof. Yoshiharu Mutoh who gave me opportunity and a contribution for studying in doctoral program in Nagaoka University of Technology (NUT), and valuable comments and suggestions on my research work.

I would like to thank Prof. Yuichi Otsuka for kindly support, comments and discussions on my research work and presentations on seminar in every week. I would like to thank Hosokai Sensei, Mr. Yamagishi and all of machine shop staffs for everything that they kindly supported for my experimental works. For all of lab members, I would like to thank for giving me a worm welcome, kindness and good memories while I was spending my life in Japan. I will remember all of you.

Particularly, I am grateful for the Japanese Government Scholarship for financial support in all period of doctoral program.

Finally, I would like to specially thank for my lovely wife, son, family and friends for their love, support and encouragement.

# List of Publication and Conference

**Publication:**

1. Panya BUAHOMBURA, Yukio MIYASHITA, Yuichi OTSUKA, Yoshiharu MUTOH and Seo NOBUSHIRO, *"Fatigue Crack Growth Behavior of FSWed Joint Joined with a Bobbin Type Tool in Different Aluminum Alloys"*, Applied Mechanics and Materials, Vol. 446-447 (2014), pp. 32-39.
2. Panya BUAHOMBURA, Yukio MIYASHITA, Yuichi OTSUKA, Yoshiharu MUTOH and Seo NOBUSHIRO, *"Fatigue crack growth behavior in weld nugget zone of FSWed similar and dissimilar aluminum alloys joints"*, IJS-JW Friction Based Welding and Processing, ISBN: 978-1-78242-163-4, Woodhead Publishing (2013) pp. 225-230.

**International Conference:**

1. Panya BUAHOMBURA, Yukio MIYASHITA, Yuichi OTSUKA, Yoshiharu MUTOH and Seo NOBUSHIRO, *"Fatigue Crack Growth Behavior of FSWed Joint Joined with a Bobbin Type Tool in Different Aluminum Alloys"*, 2013 2nd International Conference on Engineering and Innovative Materials (ICEIM 2013), Shanghai, China (September 7-8, 2013).
2. Panya BUAHOMBURA, Yukio MIYASHITA, Yuichi OTSUKA, Yoshiharu MUTOH and Seo NOBUSHIRO, *"Fatigue crack growth behavior in weld nugget zone of FSWed similar and dissimilar aluminum alloys joints"*, IJS-JW 2013-International Joint Symposium on Joining and Welding, Osaka, Japan (November 6-8, 2013).

**National Conference:**

1. Panya BUAHOMBURA, Yukio MIYASHITA, Yoshiharu MUTOH and Seo NOBUSHIRO, *"Fatigue Crack Growth Behavior of FSWed Joint in Different Aluminum Alloys"*, Japan Society of Mechanical Engineers Materials and Processing Division 20th Machine Materials and Materials Processing Technology Lecture (M&P2012), Osaka, Japan (November 30-December 2, 2012).

# Contents

# List of Figures

**Chapter 1**

**Chapter 2**

**Chapter 3**

**Chapter 5**

# List of Tables

# Chapter 1

# Introduction

Background and fundamental topic related to this study, such as friction stir welding of aluminum alloys and fatigue crack growth behavior of metallic material were introduced. A brief of literature review on FCG behaviors of FSWed aluminum alloys joints, research requirements, objective of this study and scope of the present work were also presented.

## 1.1 Introduction to Friction Stir Welding

### 1.1.1 Basic concept of friction stir welding

The high strength aluminum alloys are generally classified as non-weldable due to difficult to join and obtain high-strength, fatigue and fracture resistance welded joints in these alloy. Joining of these materials by conventional fusion welding is resulted in poor solidification microstructure and porosity in the fusion zone [1]. Moreover, reduction in mechanical properties compared to the base material is very significant [2].

Friction stir welding (FSW) was invented at The Welding Institute (TWI) of UK in 1991 as a solid-state joining technique, and it was initially applied to aluminum alloys [3, 4] The basic concept of FSW is a non-consumable rotating tool with a specially designed pin and shoulder is inserted into the butt-edges of sheets or plates to be joined and travelled along the line of joint as shown in Fig. 1.1. The tool served two primary functions: (a) heating of workpiece, and (b) movement of material to produce the joint [2]. The heating is accomplished by friction between the tool and the workpiece and plastic deformation of workpiece. The localized heating softens the material around the pin and combination of tool rotation and translation leads to movement of material from the front of the pin to the back of the pin. As a result of this process, a joint is produced in solid state. During FSW process, the material undergoes intense plastic deformation at elevated temperature, resulting in generation of fine-equiaxed recrystallization grains [5-8]. The fine microstructure in friction stir welds produced good mechanical properties.

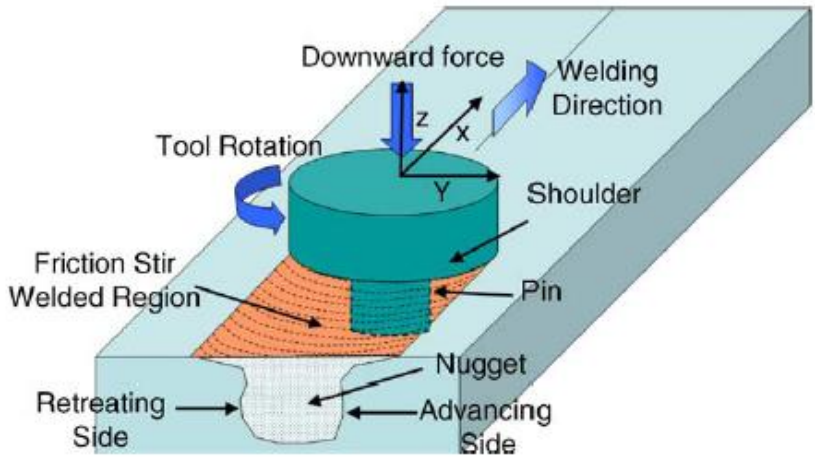


Fig. 1.1 Schematic diagram of friction stir welding [2].

As compared to the conventional welding method, the joining does not involve any use of filler metal and therefore any aluminum alloy can be joined without concerning the compatibility of compositions, which is an issue in fusion welding. Dissimilar aluminum alloys and composites can be joined by FSW process [9-12]. Mechanical properties and fatigue strength of the joint joined by the friction stir welding was better than that joined by the conventional fusion welding according to previous reports [13, 14].

### 1.1.2 Microstructure evolution in FSW

The contribution of intense plastic deformation and high-temperature exposure within the stirred zone during FSW results in recrystallization and development of texture within the stirred zone [8, 9, 11, 15-18, 19-35] and precipitate dissolution and coarsening within and around the stirred zone [9, 11, 16-18]. Based on microstructure characterization of grains and precipitates, three different zones, stirred (nugget) zone, thermo-mechanically affected zone (TMAZ), and heat-affected zone (HAZ), have been identified as shown in Fig. 1.2. The microstructural changes in various zones have significant effect on postweld mechanical properties. Therefore, the microstructural evolution during FSW has been studied by a number of investigators.

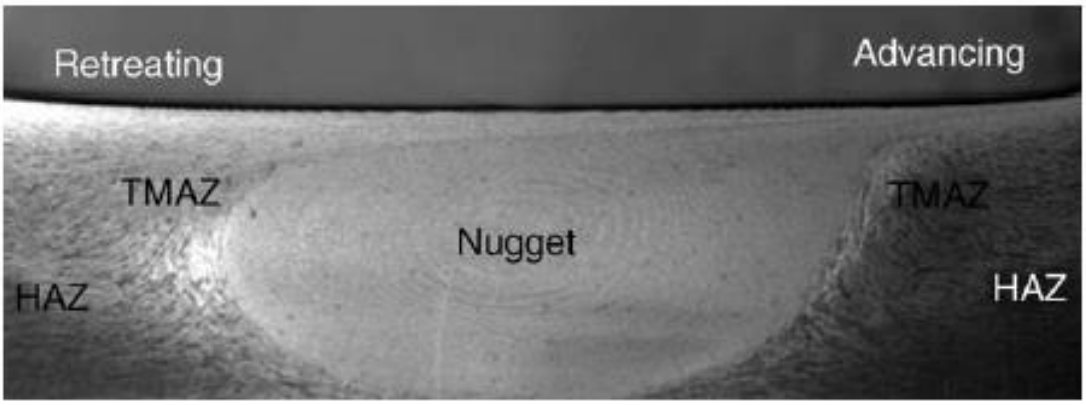


Fig. 1.2 A typical macrograph showing various microstructural zones in FSW joint (Ref. [2]).

**Nugget zone**

Intense plastic deformation and friction heating during FSW result in generation of a fine-equiaxed recrystallized grained microstructure within stirred zone as shown in Fig. 1.3. This region is usually referred to as nugget zone (or weld nugget) or dynamically

recrystallized zone (DXZ). In the interior of the recrystallized grains, there is usually low dislocation density [5, 6]. However, some investigators reported that the small recrystallized grains in the nugget zone contain high density of sub-boundaries [36], subgrains [19], and dislocation [37]. The interface between the recrystallized nugget zone and the parent metal is relatively diffuse on the retreating side of the tool, but quite sharp on the advancing side of the tool [38].

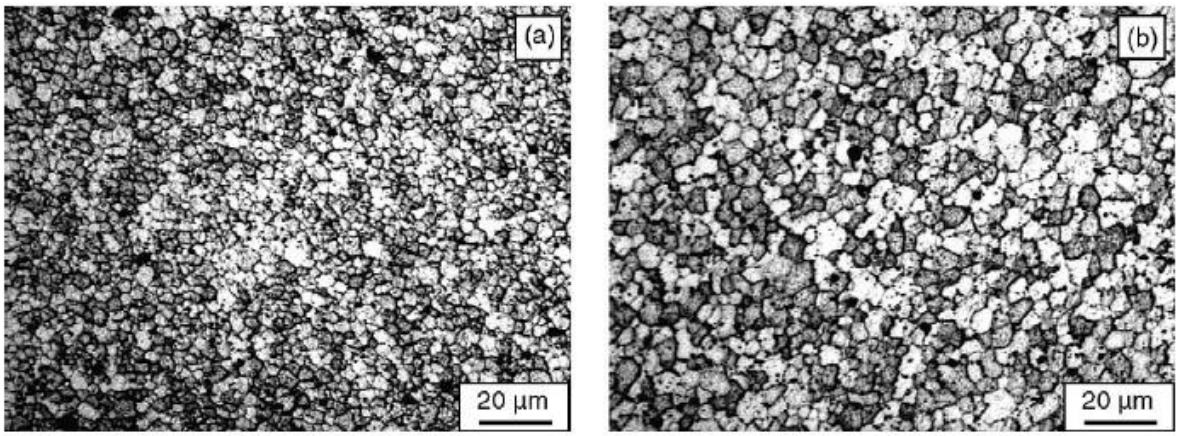


Fig. 1.3 Dynamic recrystallized grains in nugget zone of 7075-T7651 FSW aluminum alloys joint by different processing parameter (a) 350 rpm, 152 mm/min and (b) 400 rpm, 102 mm/min [15].

Depending on processing parameter, tool geometry, temperature of workpiece, and the thermal conductivity of the material, various shapes of nugget zone have been observed. It is well accepted that the dynamic recrystallization during FSW results in generation of fine equiaxed grains in the nugget zone [8, 9, 11, 15-35]. FSW parameters, tool geometry, composition of workpiece, temperature of the workpiece, vertical pressure, and active cooling exert significant influence on the size of the recrystallized grains in the FSW materials. The typical recrystallized grain size in the FSW aluminum alloys is in the micron range. Li et al. [11], Ma et al. [15], Sato et al. [39] and Kwon et al. [18, 34, 35] studied the influence of processing parameters on the microstructure of FSW aluminum alloys. It was noted that the recrystallized grain size can be reduced by decreasing the tool rotation rate at a constant tool travelling speed [11, 18, 34, 35, 39] or decreasing the ratio of tool rotation rate/travelling speed [15]. FSW at higher tool rotation rate or higher ratio of tool rotation rate/travelling speed results in an increase in both of degree of deformation and peak temperature of the thermal cycle. The increase in the degree of deformation during FSW results in a reduction in the recrystallized grain size according to the general

principles for recrystallization [40]. On the other hand, the increase in peak temperature of FSW thermal cycle leads to generation of coarse recrystallized grains, and also results in remarkable grain growth. Moreover, Chenelle and Lados (Ref. [12]) studied the effect of processing parameters on both the grain size and band spacing in FSW. They observed that as the rotating speed of the tool increased from 1000 to 1500 rpm, the grain size in the DXZ increased from 8 to 18 micron. The increasing in grain size was attributed to an increased stirring, which introduced additional frictional heat input, and therefore, additional energy for grain growth after recrystallization. The changes in material flow in nugget zone as band spacing were also observed with the changes in rotating and travelling speeds as shown in Fig. 1.4.

FSW results in the temperature increase up to 400-550 $^{o}$C within the nugget zone due to friction between tool and workpieces and plastic deformation around rotating pin [5, 6, 16-18, 36, 39, 41]. At a high temperature, precipitates in aluminum alloys can coarsen or dissolve into aluminum matrix depending on alloy type and maximum temperature. Liu et al. [6] reported that the homogenously distributed precipitates are generally smaller in the workpiece than in the nugget zone. However, there were far fewer large precipitates in the nugget zone than in the base material. This implies that the occurrence of both dissolution and coarsening of precipitates during FSW. Sato et al. [36], Heinz and Skrotzki [19] and Jata et al. [37] reported that they did not observe precipitates within the nugget zone. Their study indicated that all the precipitates were dissolved into aluminum matrix during FSW. The overall response includes a combination of dissolution, coarsening and re-precipitation of strengthening precipitates during FSW.

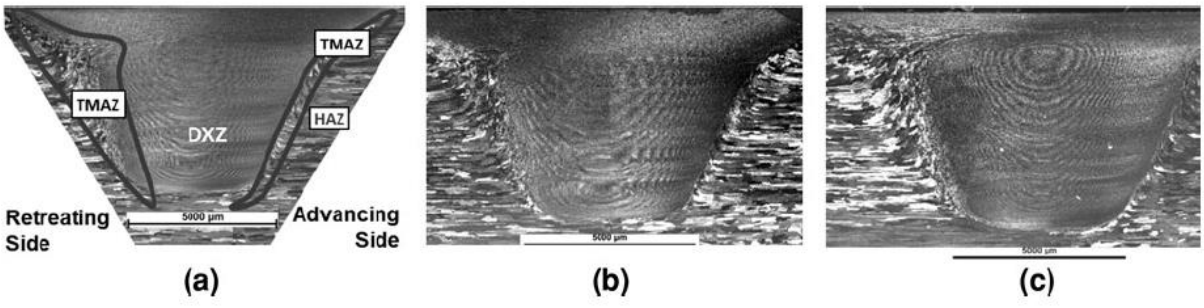


Fig. 1.4 Effect of process parameters on grain size and band spacing in 6061-T651 FSW for (a) 1000 rpm at 2.0 mm/s, (b) 1000 rpm at 3.0 mm/s and (c) 1500 rpm at 2.0 mm/s (Ref. [12]).

**Thermo-mechanically affected zone**

The FSW process is created of a transition zone of the thermo-mechanically affected zone (TMAZ) between the parent material and the nugget zone [5, 15, 16] as shown in Fig. 1.2. The TMAZ experiences both temperature and deformation during FSW. A typical micrograph of TMAZ is shown in Fig. 1.5. The TMAZ is characterized by a highly deformed structure. The parent metal elongated grains were deformed in an upward flowing pattern around the nugget zone. Although the TMAZ underwent plastic deformation but recrystallization did not occur in this zone due to insufficient deformation strain. However, dissolution of some precipitates was observed in the TMAZ, as shown in Fig. 1.6 c and d, due to high-temperature exposure during FSW [36, 42]. The extent of dissolution depends on the thermal cycle experienced by TMAZ. Furthermore, it was revealed that the grains in the TMAZ usually contain a high density of sub-boundaries [36].

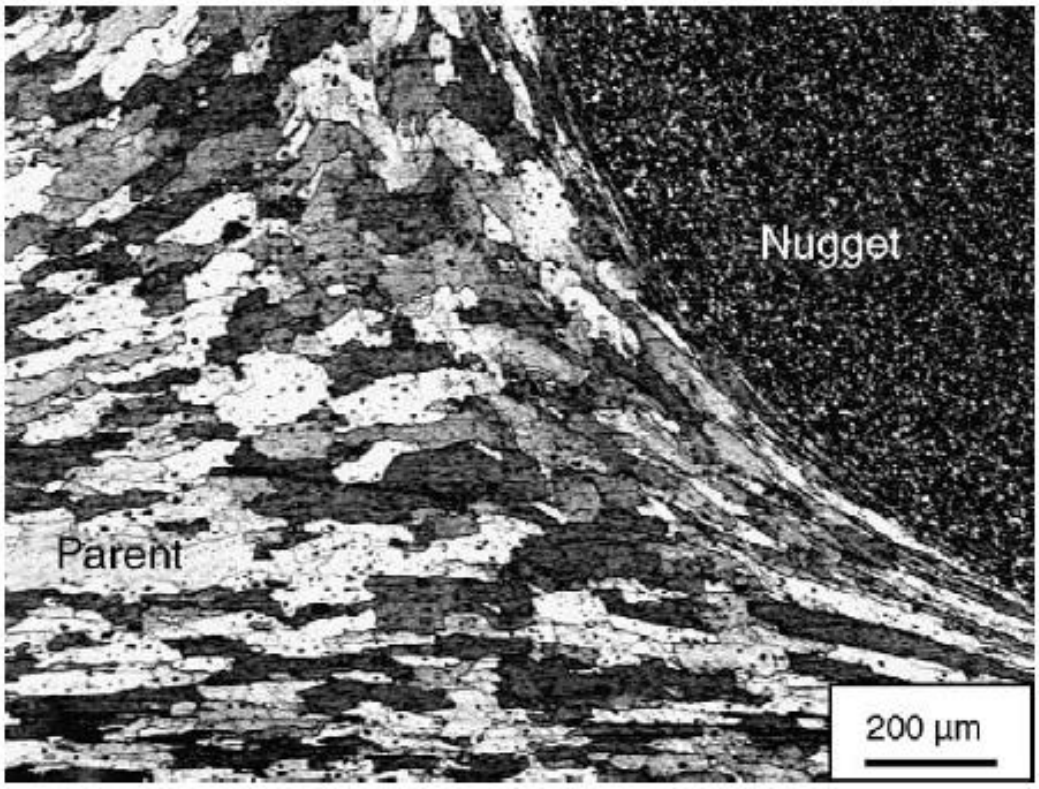


Fig. 1.5 Microstructure of thermo-mechanical affected zone (TMAZ) [15].

**Heat-affected zone**

Beyond the TMAZ there is a heat-affected zone (HAZ). This zone experiences a thermal cycle, but does not undergo any plastic deformation. Mahoney et al. [16] defined the HAZ as a zone experiencing a temperature rise above 250 $^{o}$C for a heat-treatable aluminum alloy. The HAZ retains the same grain structure as the parent material. However, the thermal exposure above 250 $^{o}$C exerts a significant effect on the precipitate structure. Jata et al. [37] reported that FSW process has relatively little effect on the size of the subgrains in the HAZ, it results in coarsening of the strengthening precipitates and the precipitate-free-zone (PFZ) increases by a factor of 5. Similar observation was also made by Su et al. [42] in a detailed TEM examination as shown in Fig. 1.6 b. The coarsening of precipitates and widening of PFZs is evident. Similarly, Heinz and Skrotzki [19] also observed significant coarsening of the precipitates in the HAZ.

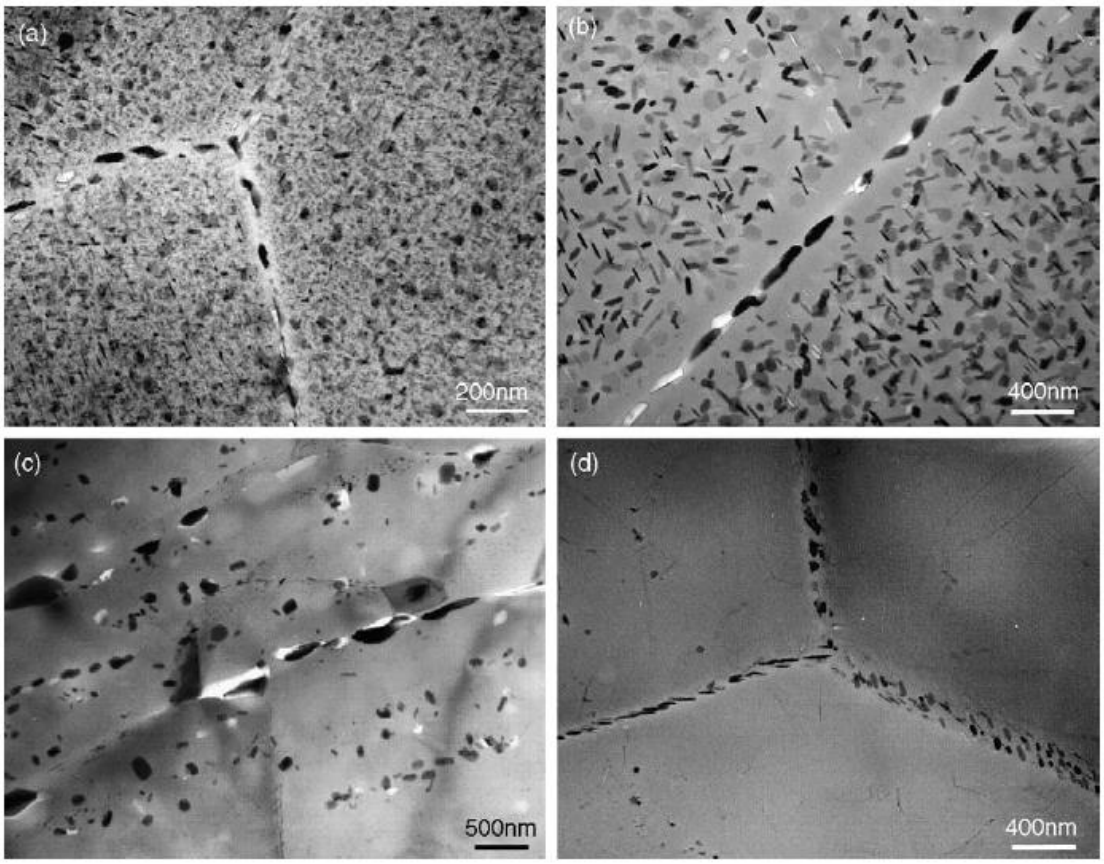


Fig. 1.6 Precipitate microstructures in the grain interior and along grain boundaries in: (a) base metal, (b) HAZ, (c) TMAZ near HAZ, and (d) TMAZ near nugget zone [42].

## 1.2 Introduction to Fatigue Crack Growth

### 1.2.1 Fracture mechanics approach

Many engineering materials and structures are contained crack-like defects or flaws which introduced during manufacturing process, especially in case of welding, or form early during service. Fatigue life of these structures can be occupied by fatigue crack growth from this cracks or flaws. Therefore, fatigue crack growth is dominated for determining fatigue life of these materials components or structures that was under cyclic loading during services. Understanding fatigue crack growth behavior of these components can be allow the flawed parts to remain in their services, also reducing maintenance and unnecessary parts replacement costs.

The main topic concerning fatigue crack growth is how long does it take for a crack or flaws to grow from initial size to the maximum permissible or critical size which cause to structures failure. The rate of growth of a fatigue crack subjected to constant amplitude stress reversals is expressed in terms of the crack length increment per cycle, da/dN. Value of crack growth rate for different loading conditions is determined from experimentally determined changes in crack length over a number of elapsed fatigue cycles.

The method for characterizing the crack growth rate in terms of an appropriate loading parameter which enables a quantification of the intrinsic resistance of the material to fatigue crack growth for different combinations of applied stresses, specimen geometry and crack geometry was established. When cyclic stresses applied to a component are so small that the zone of plastic deformation ahead of the advancing fatigue crack is a minor perturbation in an otherwise elastic field, linear elastic fracture mechanics (LEFM) solutions is provided appropriate continuum descriptions for fatigue fracture [43]. As note, Paris, Gomez & Anderson (1961) and Paris & Erdogan (1963) suggested that for a cyclic variation of the imposed stress field, the LEFM characterization of the rate of fatigue crack growth should be based on the stress intensity factor range,

$$\Delta K = K_{\max} - K_{\min} \qquad (1)$$

$K_{max}$ and $K_{min}$ are the maximum and minimum values, respectively, of the stress intensity factor during a fatigue stress cycle. The stress intensity factor is strongly depending on the flaw size, geometry of the flaw and the applied stress. For an edge-cracked fatigue test specimen,

$$K_{max} = Y\sigma_{max}\sqrt{\pi a}, \quad K_{min} = Y\sigma_{min}\sqrt{\pi a}, \tag{2}$$

$$\Delta K = Y\Delta\sigma\sqrt{\pi a}, \quad \Delta\sigma = \sigma_{max} - \sigma_{min}, \tag{3}$$

where Y is a geometrical factor which depends on the ratio of crack length $a$ to the width of the specimen W, and $\sigma_{max}$ and $\sigma_{min}$ are the maximum and minimum values, respectively, of the fatigue stress cycle.

Paris, Gomez & Anderson (1961) and Paris & Erdogan (1963) showed that the fatigue crack growth increment da/dN is related to the stress intensity factor range by the power law relationship

$$\frac{da}{dN} = C(\Delta K)^m, \tag{4}$$

Where C and m are empirical constants influenced by variables as material microstructure, environment and temperature (both of which could promote a strong effect of cyclic loading frequency and waveform), and stress ratio, R. The stress ratio is defined as

$$R = \frac{\sigma_{min}}{\sigma_{max}} = \frac{K_{min}}{K_{max}} \tag{5}$$

### 1.2.2 Fatigue crack growth curve and it regions

Schematic diagram of typical fatigue crack growth behavior in engineering materials is shown in Fig 1.7. Log-log plot between crack growth rate (m/cycle) and stress intensity factor range (MPa.m$^{1/2}$) in fatigue crack growth curve exhibits a sigmoidal shape is classified into three different regions depend on curve shape, mechanism of crack extension and factors influences on the curve. In region I, near-threshold region, fatigue crack was propagated in slow rate and extremely low crack growth rate or stop to propagate when reach a threshold stress intensity factor range, $\Delta K_{th}$. Above the threshold value, crack growth rate increases rapidly with increasing $\Delta K$. In region II or Paris region, crack growth rate (da/dN) is in power function of stress intensity factor range ($\Delta K$) in linear relationship between log (da/dN) and log ($\Delta K$). The fatigue crack growth behavior in this region was usually described by empirical formula as known Paris Equation:

$$\frac{da}{dN} = C(\Delta K)^m \tag{6}$$

where da/dN is crack growth rate, ΔK is stress intensity factor range, C and m are empirical parameters.

In region III, high fatigue crack growth rate in this region with high stress intensity factor range ΔK. The crack growth rate curve rise to an asymptote where the maximum stress intensity factor, $K_{max}$, in the fatigue stress cycle becomes equal to the critical stress intensity factor, $K_c$, where crack growth rate increase rapidly causing catastrophic failure. In generally, region I and region II was relied to predict and dominate fatigue crack propagation life [44].

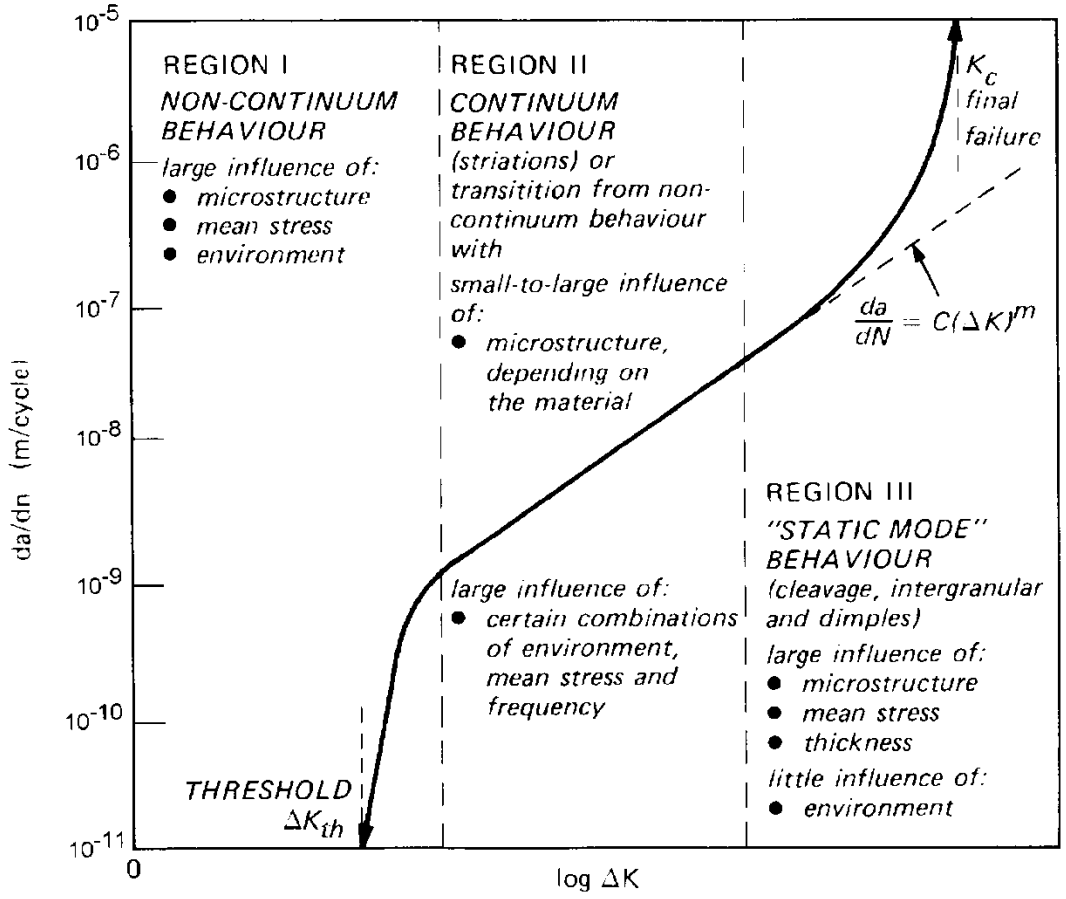


Fig. 1.7 Characteristic in the three different regions of fatigue crack growth curves (Ref. [44]).

### 1.2.3 Crack closure

The theory that fatigue crack can close even at a far-field tensile loading was first proposed by Elber (1970, 1971) on the basis of experimental observations. By monitoring changes in the compliance of thin sheets of cracked 2024-T3 aluminum alloy, Elber argued that a zone of residual tensile deformation was left in the wake of a fatigue crack tip. The attendant reduction in crack opening displacement gives rise to premature contact between the faces of the crack and causes a reduction in the apparent "driving force" for fatigue crack growth.

Moreover, additional mechanisms of crack closure have been identified which have broadened the application of crack closure to a significantly greater number of fatigue crack growth characteristics than what was originally anticipated from Elber's work. Experimental observations published in the later 1970s and early 1980s established that Elber's mechanism was not the sole cause of closure, but other types of closure phenomena also influence the fatigue crack growth rate. On the basis of their own results and the work of other researchers, Ritchie, Suresh & Moss (1980), Suresh, Zamiski & Ritchie (1981), and Suresh & Ritchie (1982a, 1984a) categorized the various forms of fatigue crack closure that are induced by a variety of mechanical, microstructural and environmental factors, and coined the expression plasticity-induced crack closure for Elber's closure due to residual plastic stretch at crack wake. The additional sources of closure arise as a result of: (i) corrosion layers formed within a fatigue crack (oxide-induced crack closure), (ii) microscopic crack closure, (iii) viscous fluids penetrated inside the crack (viscous fluid-induced crack closure), and (iv) stress- or strain-induced phase transformations at the crack tip (transformation-induced crack closure). These various mechanisms retarded the fatigue crack growth.

Elber argued that the crack can propagate only when the fraction of the fatigue loading cycle in the crack faces are separated. The effective stress range, $\Delta\sigma_{eff}$, and the corresponding effective stress intensity factor range, $\Delta K_{eff}$, which are responsible for crack growth as given by

$$\Delta\sigma_{eff} = \sigma_{\max} - \sigma_{op} = U\Delta\sigma, \tag{7}$$

$$\Delta K_{eff} = K_{\max} - K_{op} = U\Delta K, \tag{8}$$

where Δσ and ΔK are the applied stress range and the stress intensity factor range, respectively, and $K_{op}$ is the crack opening stress intensity factor as shown in Fig. 1.8. The corresponding characterization of fatigue crack growth rates based on LEFM becomes

$$\frac{da}{dN} = C(\Delta K_{eff})^m = C(U\Delta K)^m \quad (9)$$

For variation in stress ratio, R, of -0.1 to 0.7, Elber determined that

$$\frac{K_{op}}{K_{\max}} = 0.5 + 0.1R + 0.4R^2 \quad (10)$$

while a plot of da/dN versus nominal ΔK (in the Paris region) varied noticeably with the stress ratio R in Elber's experiments, a reformulation of the same set of data in terms of the effective stress intensity factor range $\Delta K_{eff}$ using Eq. 8 collapsed the results for different R values into a single curve.

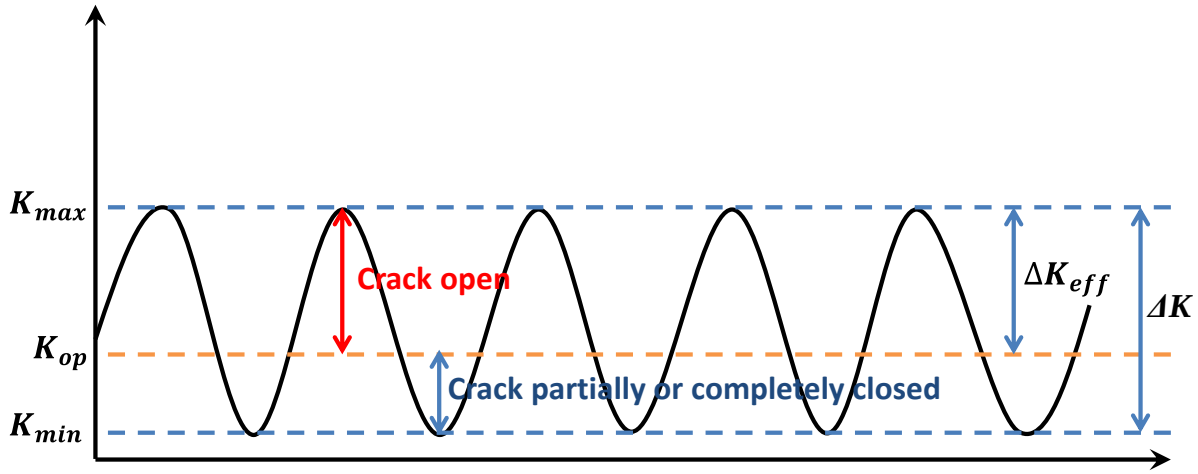


Fig. 1.8 Definition of effective stress intensity factor range.

## 1.3 Literature Reviews

Fatigue properties are critical for engineering materials in many applications such as aerospace structure, transport vehicles, platforms and bridge constructions. Therefore, it is important to understand the fatigue characteristics of FSW joints due to in currently FSW technique is used in wide range of engineering applications. This lead to increasing

research interest on evaluating the fatigue behavior of FSW joints, including fatigue properties [45-52] and fatigue crack growth behavior [46, 53-58].

### 1.3.1 Fatigue properties in FSW aluminum alloys

Recently, several investigations were conducted on fatigue strength of FSWed 6006Al-T5 [47, 48], 2024Al-T351 [49], 2024Al-T3 [45], 2219Al-T8751 [52] and 2519Al-T87 [46] joints. These studies resulted in the following important observations. First, the fatigue strength of the FSW joint was lower than that of the base material because of the FSW joints are susceptible to fatigue crack initiation [45, 50, 51, 52, 56]. Fatigue strength of the transverse FSW specimens had lower fatigue strength than the longitudinal FSW specimens were investigated by Bussu and Irving [57]. However, the fatigue strength of the FSW joint was higher than that of conventional fusion welding as MIG and laser welds [48, 49]. S-N curves for FSW joint, laser weld, MIG weld, and the base metal of 6005Al-T5 are shown in Fig. 1.9. The finer and uniform microstructure after FSW leads to better properties as compared to fusion (laser and MIG) welds. Secondly, surface quality of the FSW welds was significant effect on the fatigue strength of the welds. Hori et al. [45] reported that the fatigue strength of the FSW weld decreased with increasing tool traverse speed/rotation rate ($\nu/\omega$) due to the increase of non-welded groove on the root side of the weld. However, when the non-welded groove was skimmed, the fatigue strength of the FSW weld remained unchanged by changing the $\nu/\omega$ ratio. Furthermore, Bussu and Irving [49] reported that skimming 0.5 mm thick layer from both root and top sides that removed all the profile irregularities then resulted in fatigue strength of both transverse and longitudinal FSW specimens were comparable to the base metal. These observations suggested that the fatigue life is limited by surface crack nucleation and there are no inherent defects or internal flaws in successful FSW welds joints. Third, the effect of FSW parameters on the fatigue strength is complicated and no consistent trend is obtained. Hori et al. [47] reported that for a specific $\nu/\omega$ ratio, the fatigue strength of the FSW weld was not affected by the tool travelling speed. However, Biallas et al. [45] observed that for a constant $\nu/\omega$ ratio, the fatigue strength of FSW 2024Al-T3 welds with thickness of 1.6 and 4 mm was considerably enhanced with increasing tool rotation rate and travelling speed. The fatigue strength of 1.6 mm thick FSW weld made at a high tool rotation rate at 2400 rpm and a travelling speed of 240 mm/min were identical to the base metal. Forth, low plasticity burnishing (LPB) after FSW can enhance the fatigue life of the FSW joints. Jayaraman et al. [52] reported that LPB processing increased the high cycle fatigue

endurance of aluminum alloy FSW 2219Al-T8751 by 80% due to introduction of a deep surface layer of compressive residual stress. In addition, the surface becomes highly polished after LPB and as noted earlier the fatigue life of FSW welds is limited by surface crack nucleation. Compressive residual stresses at surface and high-quality surface finish are desirable for good fatigue properties. Fifth, the fatigue resistance of FSW specimens tested in air is lower than that of the base material. Pao et al. [46] reported that FSW 2519Al-T87 and base material specimens have similar fatigue lives and fatigue thresholds in 3.5% NaCl solution. The corrosion products at the surface are likely to influence the fatigue crack nucleation and influence of FSW on a complexity of corrosion-fatigue interaction.

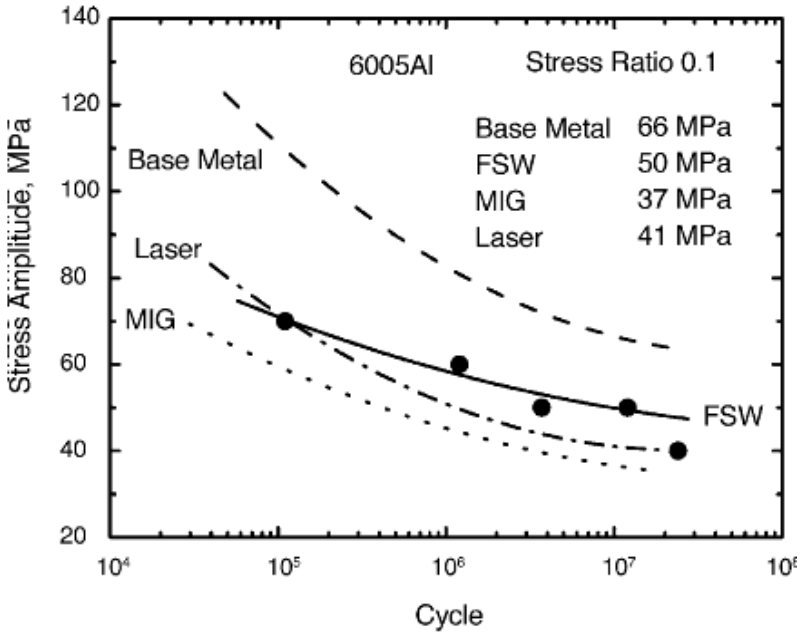


Fig. 1.9 S-N curves of base metal, FSW weld, laser weld and MIG weld for 6005Al- T5 [47].

### 1.3.2 Fatigue crack growth behavior in FSW aluminum alloys

Several investigations were undertaken to evaluate the effect of FSW on the fatigue crack growth behavior [46, 53-58]. Different conclusions from several investigators studied on FCG behavior of FSW joint was revealed as below.

Donne et al. [54] investigated the effect of weld imperfections and residual stresses on the fatigue crack growth in FSW 2024Al-T3 and 6013Al-T6 welds using compact tension specimens. Their study revealed following important observations. First, the quality of the FSW welds only limited effects on the fatigue crack growth curve. Second,

at low ΔK and lower R-ratio of 0.1, the FCG resistance of the FSW welds was superior to that of the base material for both FSW joints, whereas at high ΔK and higher R-ratios of 0.7-0.8, base materials and FSW welds exhibited similar FCG behavior. This was attributed to the presence of compressive residual stresses at the crack tip region in the FSW welds, which decreases the effective stress intensity factor range ($\Delta K_{eff}$) at the crack front. In this case, FCG rate at low ΔK and low R-ratio were apparently reduced due to reduced effective stress intensity factor range. However, at high ΔK and higher R-ratio, the effect of the compressive residual stress becomes less important, therefore, fatigue crack growth resistance of base material and FSW were the similar. Donne et al. [54] further showed that after subtracting the effect of the residual stress, the da/dN-ΔK curves of the base materials and the FSW welds overlapped. Third, specimen geometry exhibited a considerable effect on the FCG behavior of the FSW welds. Donne et al. [54] compared the FCG curves obtained by compact tension specimens and middle cracked tension specimens for both base material and FSW weld at low R-ratio of 0.1. While the base material curves overlapped, a large different was found in the case of FSW welds. This was attributed to different distribution of the residual stresses in two specimens with different geometries.

The improvement in FCG resistance after FSW was investigated in FSW 2519Al-T87, 2024Al-T351 5083-H32 and 6061-T651 by Pao et al. [46], Bussu and Irving [57] and S. Kim et al. [58] respectively. Pao et al. [46] reported that the nugget zone and HAZ of FSW 2519Al-T87 exhibited lower fatigue crack growth rate and higher fatigue crack growth threshold, $\Delta K_{th}$, at both R=0.1 and 0.5, in air and in 3.5% NaCl solution, compared to the base material. Furthermore, the FCG resistance of the nugget zone was higher than those of the HAZ. Compared to the FCG rate in air, the FCG rate in 3.5% NaCl solution for the base material, HAZ, and nugget zone, in the intermediate and high ΔK regions, were about two times higher than those observed in air. However, at crack growth rate below about $10^{-8}$ m/cycle, $\Delta K_{th}$ values in 3.5% NaCl solution were substantially higher than those in air because corrosion product wedging became increasingly dominant and corrosion product induced crack closure also lowered the effective stress intensity factor range and eventually stopped the crack growth. Bussu and Irving [57] reported that crack growth behavior in the FSW 2024Al-T351 joints was generally dominated by the weld residual stress and that microstructure and hardness changes in the FSW welds had minor influence. Furthermore, they reported that FCG rate in FSW 2024Al-T351 depended

strongly on their location and orientation with respect to the weld centerline. However, in FSW weld which were mechanically stress relieved by applying of 2% plastic strain, crack growth rate were almost identical to those of the base material, irrespective of location and orientation. S. Kim et al. also reported that FCG resistance in WNZ of FSWed 5083-H32 and 6061-T651 joints were higher than FCG resistance in the BM as shown in Fig. 1.10. It was suggested that compressive residual stress in WNZ decreased effective stress intensity factor range, $\Delta K_{eff}$ and resulted in reduction of FCG rate. [58].

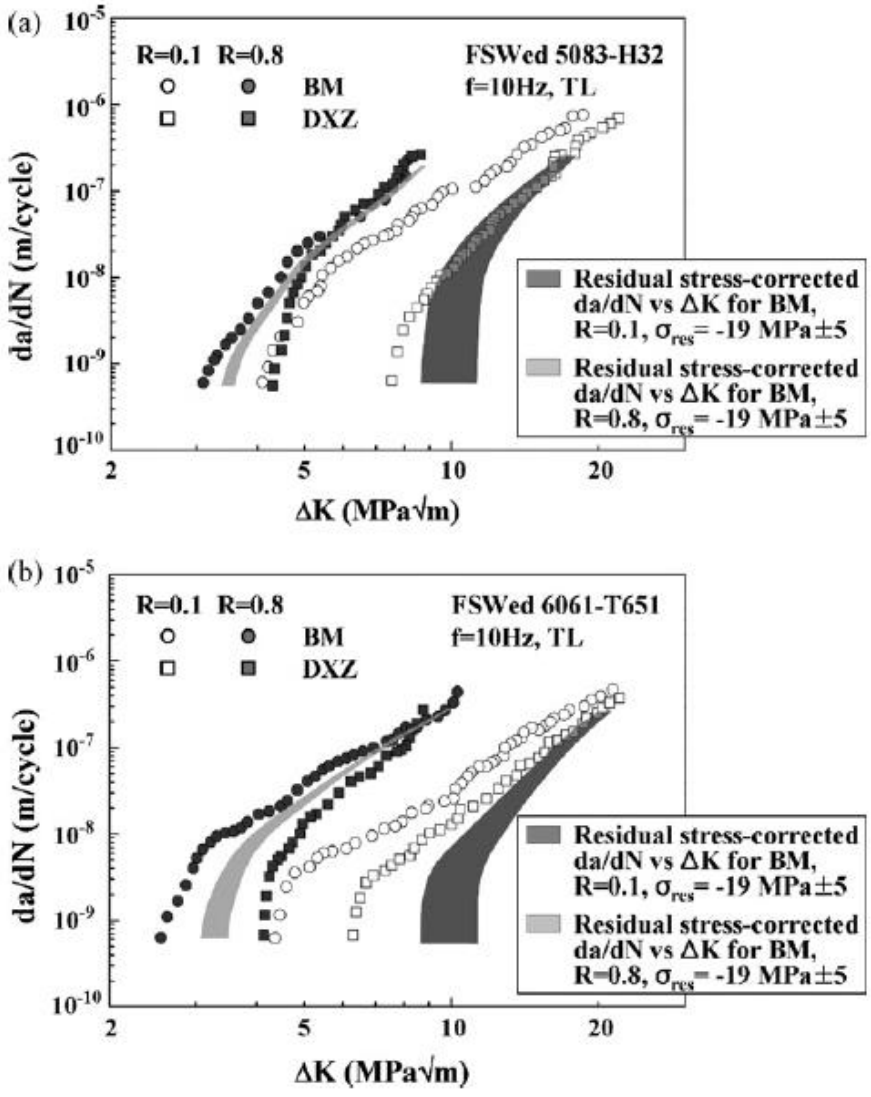


Fig. 1.10 Fatigue crack growth curves for FSWed (a) 5083-H32 and (b) 6061-T651 specimen along the BM and DXZ respectively, at R-ratio of 0.1 and 0.8 respectively [58].

In contradiction, in an investigation of fatigue crack growth behavior of FSW 7050Al-T7451 in the as-FSW + T6 condition at lower stress ratio of 0.33, Jata et al. [53] observed that the nugget zone had the lowest near-threshold FCG resistance and the HAZ the highest near-threshold FCG resistance as shown in Fig. 1.11. At the higher stress ratio of 0.7, the differences in the FCG rate of the base material, nugget zone and HAZ were almost negligible. They suggested that the decrease in the FCG resistance of the nugget zone was due to an intergranular failure mechanism. In the HAZ, residual stresses were more dominant than the microstructure improving the FCG resistance. Similarly, Pao et al. [55] found that the HAZ of FSW 7050Al-T7451 in the as-FSW + aged (121 $^{o}$C/12 h) condition exhibited significantly lower FCG and much higher $\Delta K_{th}$ at a stress ratio of 0.1 in both air and 3.5% NaCl solution. However, the FCG resistance of the weld nugget zone was identical to those of the base metal in both air and 3.5% NaCl solution. The low FCG rate in the HAZ was attributed to residual stress and roughness induced crack closure. Furthermore, they reported that a significant increase in the $\Delta K_{th}$ values in 3.5% NaCl solution for the nugget zone, HAZ, and base material. This observation is similar to that in FSW 2519Al-T87 and attributed to the corrosion product wedging phenomenon.

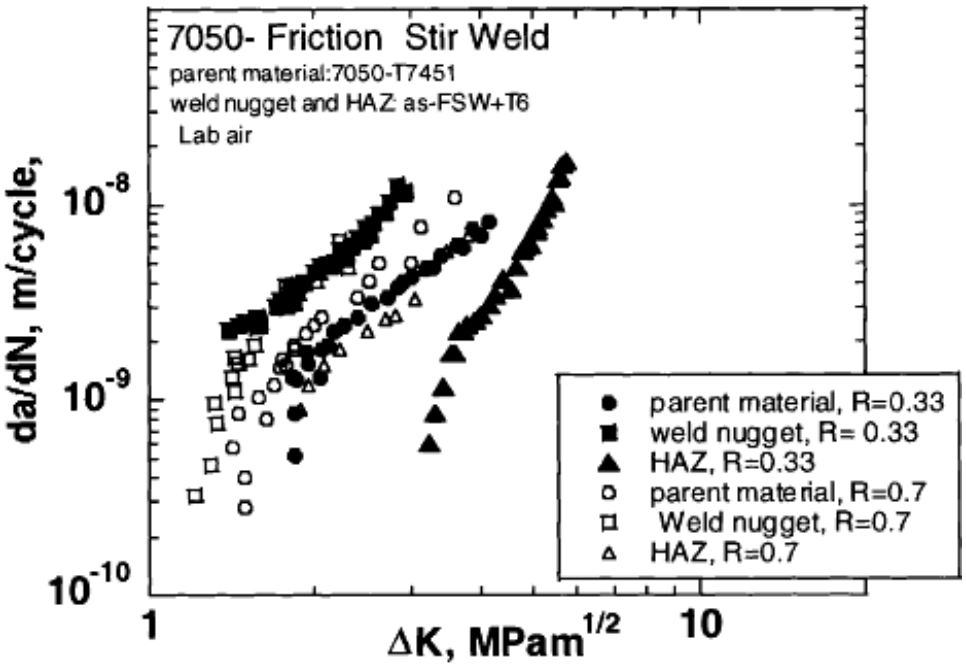


Fig. 1.11 Comparison of FCGRs between WNZ, HAZ and the parent material, at R-ratio 0.33 and 0.7. FCGRs were evaluated in the as-FSW+T6 condition. Tests were conducted in laboratory air [53].

## 1.4 Research Requirements and Objectives

In according to friction stir welding was increasing and widely used in currently to join the engineering materials in many applications including automotive body, railway components, ship, aerospace parts, nuclear and military applications [2, 12] as shown in Table 1.1 and 1.2 due to the joint properties overcome the conventional fusion welding [2, 12-14]. In order to understanding and preventing fatigue failure occurred in the structural and vehicle components which these parts are prone to fatigue failure. Fatigue crack growth behavior of these parts was required to study in case of materials that easy to deform and initiate crack in early stage during service or contain defects or flaws from manufacturing process.

Table 1.1 Applications and type of aluminum where FSW has been used in automotive industry [Ref. 12].

| Aluminum in the Auto Industry | |
|---|---|
| Inner and outer body panels | 2008, 2010, 2036, 3004, 5052, 5192, 5754, 6009, 6010, 6016, 6022, 6111 |
| General structural components | 6005, 6005A, 6009, 6061 |
| Extrusions | 6063, 6082, 7005 |
| Luggage racks, air deflectors | 6463 |
| Spare tire carrier parts | 6061 |
| Bumper components | |
| Ace bars | 5052, 6009 |
| Reinforcements | 6009, 6061, 7003, 7004, 7021, 7029 |
| Brackets | 6009, 7021 |
| Seats | |
| Shells | 7036, 6010 |
| Headrest bars | 7116, 7129 |
| Tracks | 6010, 5182, 5754, 6009 |
| Load floors | 2036, 5182, 5754, 6009 |
| Wheels | 5454, 6061, A356.0 |
| Suspension components | 6061 (forging) |
| Drive shaft | 6061 (tube), aluminum metal matrix composites |
| Engine mounts | 5454, 5754 |
| Sub-frames & engine cradles | 5454, 5754, 6061, 6063 |
| Radiator tubes & fins | 3003, 3005 |
| Condenser tubes | 3102 |
| Condenser fins | 7072 |

Table 1.2 Applications of FSW in aerospace industry [Ref. 12].

| Name | Y-Chord Demonstration | HIMARS Sponson Door | Fighter Wing Box | Circular Weld Demonstration | C-130 Cargo Floors |
|---|---|---|---|---|---|
| Alloy | Al2014 | Al5052 | Al7075 and Al2297 | Al2195 and Al2297 | Al7249 |
| Joint configuration | 0.250″ butt | 0.100 to 0.125″ T-joint | 0.125″ butt, L-T and lap-joints | 0.200 to 0.280″ butt | 0.090 to 0.150″ butt |
| Size | 2′ × 2′ | 2′ × 4′ | 4′ × 4′ | up to 12″ diameter | 16′ length |
| Status | development | development | development | development | development |

Currently, study on fatigue crack growth behavior of FSWed joints was limited and has contradiction in trend as discussed in literature review. Moreover, in previous study was almost investigated the fatigue crack growth behavior of conventional friction stir welding which FSW tool insert into joining material plates on one side. Even through, the conventional friction stir welded joint was better tensile and fatigue properties compared to conventional fusion welding as mentioned in earlier. However, there are reported that kissing bond or root flaws generating at the bottom part of conventional friction stir welded joint and affected to decrease fatigue properties of the joint as shown in Fig. 1.12 and 1.13 [59]. Moreover, conventional friction stir welding required highly constrained to fix the joining material plates during welding process as shown in Fig. 1.14 [60].

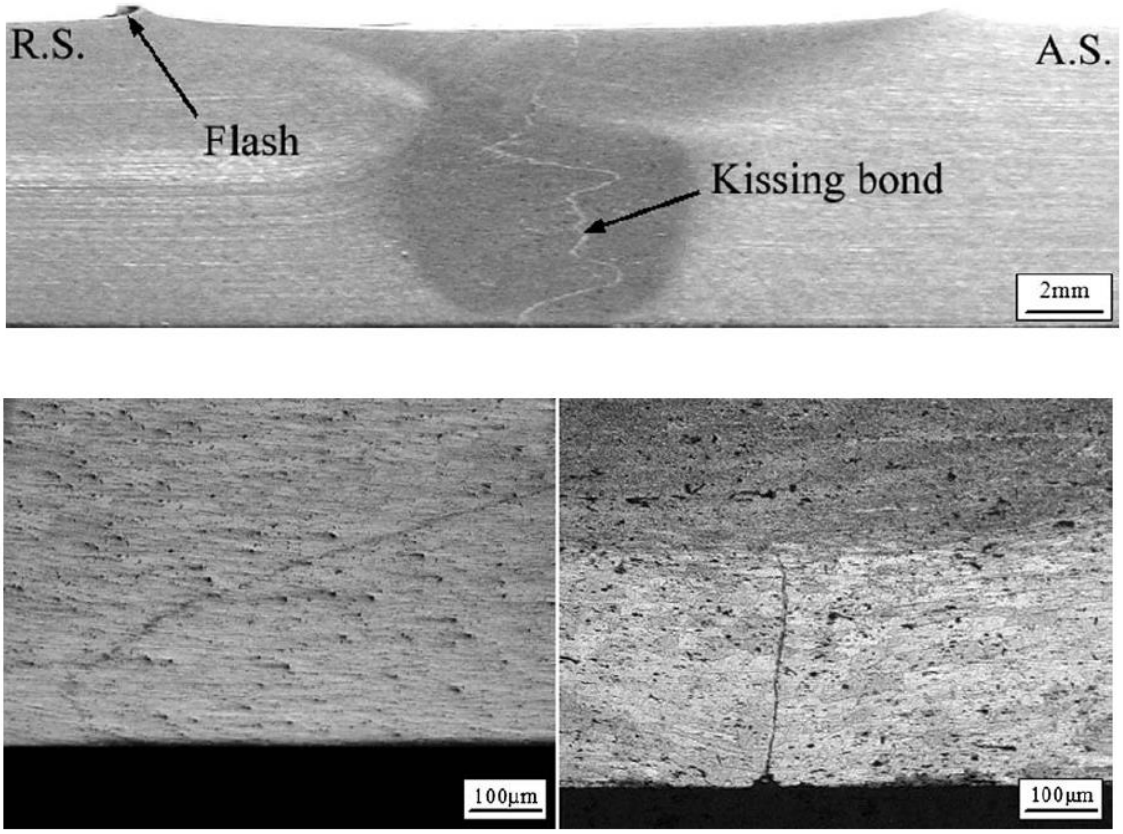


Fig. 1.12 Optical micrograph of kissing bond and root flaw in conventional FSW joint [59].

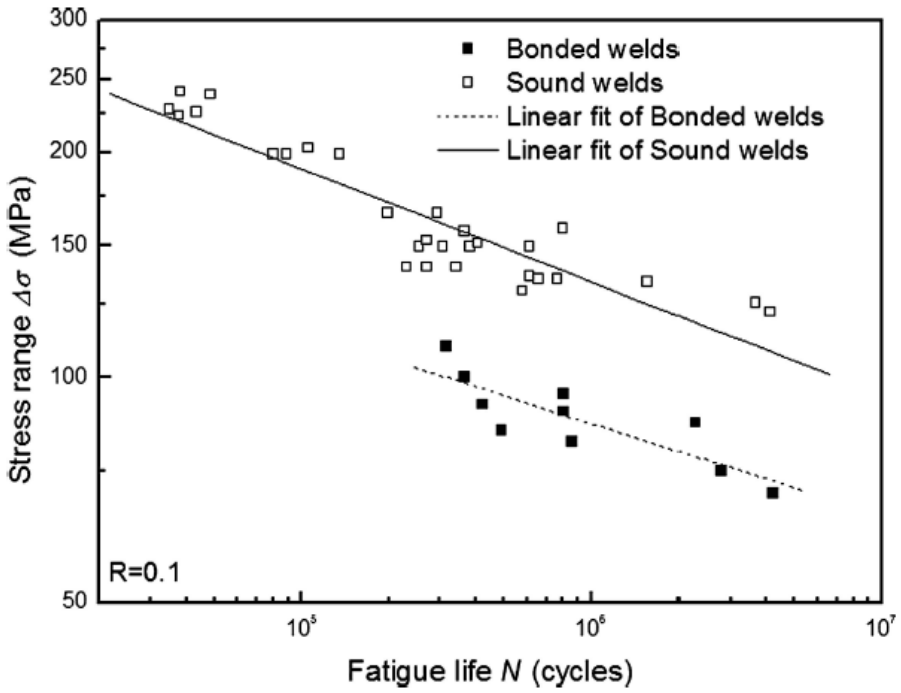


Fig. 1.13 S-N curves of flaws (bonded) and sound conventional FSW joint [59].

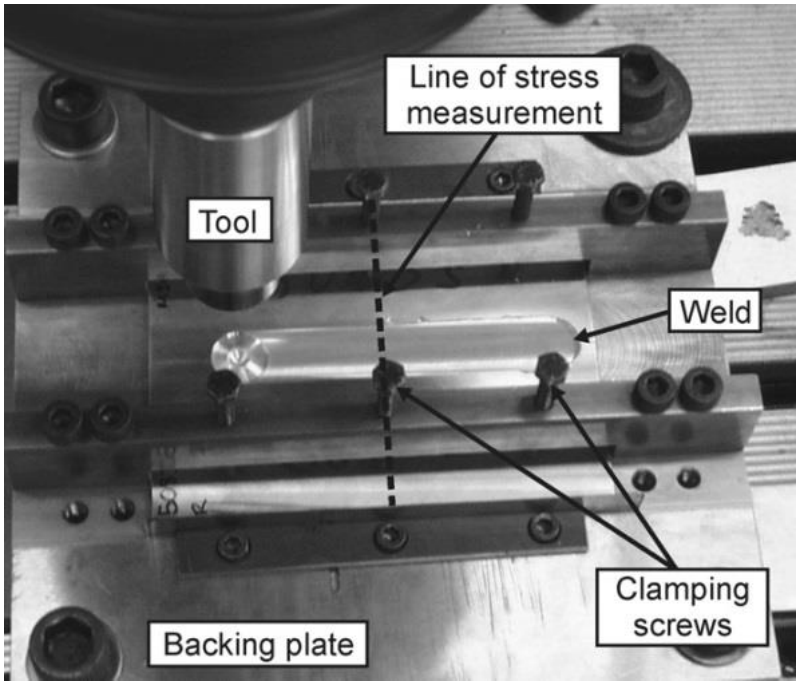


Fig. 1.14 Tool set-up for conventional friction stir welding process [60].

Friction stir welding process by using a bobbin type tool and their FSWed joint were shown in Fig. 1.15 [61]. It has been reported [61] that bobbin type FSW have many advantages over than that of conventional FSW such as obtain symmetry welded structure in thickness direction, low distortion of welded parts, eliminate root flaws or kissing bond, no backing plate require and low constrain for fixing the weld plate and able to join thick plate in single step. The study on fatigue crack growth behavior of FSWed joint joined by bobbin type tool is a new and limited data. In order to understanding the crack advancing in this kind of material joining process, 5052, 6N01 and 7N01 aluminum alloys were used to join in this study. Rolled 5052 aluminum alloy was widely used in commercial for structure parts, ship and automotive components. Extruded 6N01 and 7N01 aluminum alloys was used for specific purpose such as body of high-speed train. Several combinations of materials couples in both similar and dissimilar aluminum alloys joints were joined by using a bobbin type tool in the present work.

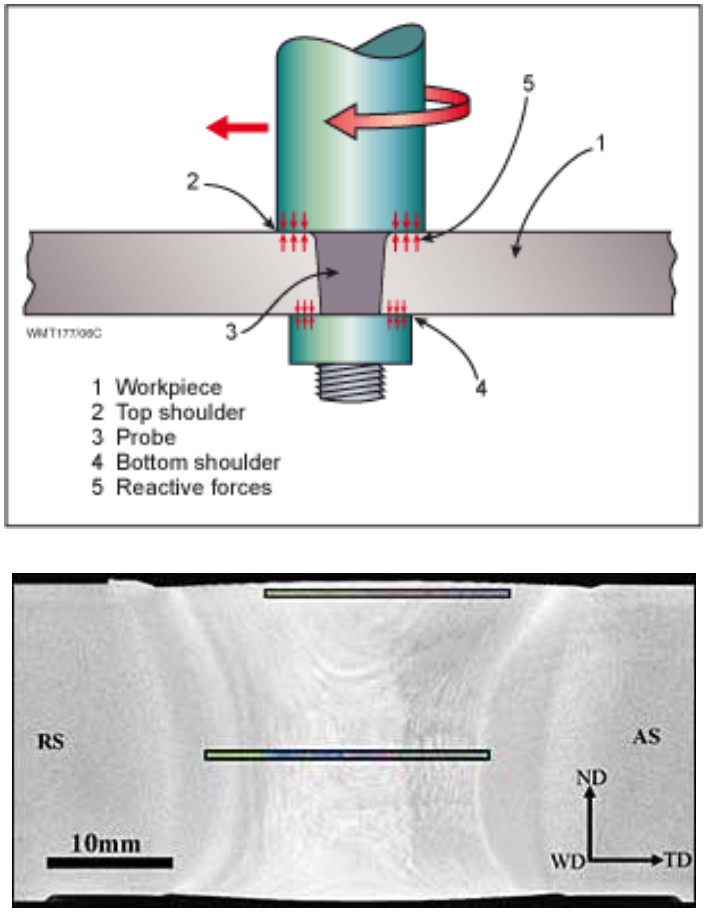


Fig. 1.15 Schematic illustration of bobbin type tool friction stir welding and welded joint [61].

The objective of the present work is to study the FCG behavior of friction stir welded (FSWed) similar and dissimilar aluminum alloys joints joined by using a bobbin type tool. Firstly, the FCG behavior of FSWed 5052 joint joined by using a bobbin type tool were compared with the FSWed joints joined by using conventional FSW tool which applying single and double-passed to investigate the effect of welding process. Secondly, the FCG behavior of FSWed 5052, 6N01 and 7N01 similar aluminum alloys joints were studied to investigate the effect of materials on FCG behavior of the joints joined by using a bobbin type tool. Finally, the FCG behavior of FSWed 6N01-5052 and 6N01-7N01 dissimilar aluminum alloys joints were studied and evaluated the effect of material combinations in the joints joined by using a bobbin type tool.

## 1.5 Dissertation outline

In **Chapter 1** Background and fundamental topic related to this study, such as friction stir welding of aluminum alloys and fatigue crack growth behavior of metallic material were introduced. A brief of literature review on FCG behaviors of FSWed aluminum alloys joints, research requirements, objective of this study and scope of the present work were also presented.

**Chapter 2** Fatigue crack growth behavior at weld nugget zone (WNZ) and heat affected zone (HAZ) in friction stir welded (FSWed) 5052 aluminum alloy joints joined by using a bobbin type tool was investigated comparing to single-passed and double-passed conventional FSWed and the base materials (BM). The effect of FSW processes on FCG behavior of FSWed joints was studied in this chapter in 5052 aluminum alloy.

**Chapter 3** Fatigue crack growth behavior at weld nugget zone (WNZ) and heat affected zone (HAZ) in FSWed similar material joints joined by using a bobbin type tool in 5052, 6N01 and 7N01 aluminum alloys were investigated comparing to the base materials (BM). The effect of materials on FCG behavior in different FSWed similar aluminum alloy joints was studied in this chapter.

**Chapter 4** Effect of materials combination in FSWed dissimilar materials joint between 5052 and 6N01 alloys which showed the similar FCG behavior in FSWed similar material joints was studied. Fatigue crack growth behavior in weld nugget zone (WNZ) of FSWed 6N01-5052 dissimilar aluminum alloys joints were investigated comparing to that of the FSWed 5052 and 6N01 similar aluminum alloy joints and the base materials.

**Chapter 5** Effect of materials combination in FSWed dissimilar materials joint between 6N01 and 7N01 alloys which showed different FCG behavior in FSWed similar material joints was studied. Fatigue crack growth behavior in weld nugget zone (WNZ) of FSWed 6N01-7N01 dissimilar aluminum alloys joints were investigated comparing to that of the FSWed 6N01 and 7N01 similar aluminum alloy joints and the base materials.

**Chapter 6** Effect of welding process on FCG behavior, effect of materials on FCG behavior in different FSWed similar aluminum alloys joints, effect of materials combination on FCG behavior in FSWed dissimilar aluminum alloys joints, general conclusions and recommendations for further work have been discussed and summarized.

## 1.6 References


[1] T. Luijendijk, J. Mat. Proc. Tech. 103 (2000) 29-35.

[2] R.S. Mishra and Z.Y. Ma, Mater. Sci. Eng. R 50 (2005) 1-78.

[3] W.M. Thomas, E.D. Nicholas, J.C. Needham, M.G. Murch, P. Templesmith, C.J. Dawes, G.B. Patent Application No. 9125978.8 (December 1991).

[4] C. Dawes, W. Thomas, TWI Bulletin 6, November/December 1995, p. 124).

[5] C.G. Rhodes, M.W. Mahoney, W.H. Bingel, R.A. Spurling, C.C. Bampton, Scripta Mater. 36 (1997) 69.

[6] G. Liu, L.E. Murr, C.S. Niou, J.C. McClure, F.R. Vega, Scripta Mater. 37 (1997) 355.

[7] K.V. Jata, S.L. Semiatin, Scripta Mater. 43 (2000) 743.

[8] S. Benavides, Y. Li, L.E. Murr, D. Brown, J.C. McClure, Scripta Mater. 41 (1999) 809.

[9] L.E. Murr, Y. Li, R.D. Flores, E.A. Trillo, Mater. Res. Innovat. 2 (1998) 150.

[10] Y. Li, E.A. Trillo, L.E. Murr, J. Mater. Sci. Lett. 19 (2000) 1047.

[11] Y. Li, L.E. Murr, J.C. McClure, Mater. Sci. Eng. A 271 (1999) 213.

[12] A.L. Biro, B.F. Chenelle and D.A. Lados, Metall. Mater. Trans. B, 43A, 2012, pp. 1622-1637.

[13] V. Fahimpour, S.K. Sadrnezhaad and F. Karimzadeh, Metall. Mater. Trans. A, 44A, 2013, pp. 2187-2195.

[14] M. Ericsson and R. Sandstrom, Inter. Jour. Fatig. 25 (2003) 1379-1387.

[15] Z.Y. Ma, R.S. Mishra, M.W. Mahoney, Acta Mater. 50 (2002) 4419.

[16] M.W. Mahoney, C.G. Rhodes, J.G. Flintoff, R.A. Spurling, W.H. Bingel, Metall. Mater. Trans. A 29 (1998) 1955.

[17] W. Tang, X. Guo, J.C. McClure, L.E. Murr, J. Mater. Process. Manufact. Sci. 7 (1998) 163.
[18] Y.J. Kwon, N. Saito, I. Shigematsu, J. Mater. Sci. Lett. 21 (2002) 1473.
[19] B. Heinz, B. Skrotzki, Metall. Mater. Trans. B 33 (6) (2002) 489.
[20] L.E. Murr, G. Liu, J.C. McClure, J. Mater. Mater. Lett. 16 (1997) 1081.
[21] G.S. Frankel, Z. Xia, Corrosion 55 (1999) 139.
[22] Y.S. Sato, S.H.C. Park, H. Kokawa, Metall. Mater. Trans. A 32 (2001) 3023.
[23] S.H. Kazi, L.E. Murr, in: K.V. Jata, M.W. Mahoney, R.S. Mishra, S.L. Semiatin, D.P. Filed (Eds.), Friction Stir Welding and Processing, TMS, Warrendale, PA, USA, 2001, p. 139.
[24] H.G. Salem, A.P. Reynolds, J.S. Lyons, Scripta Mater. 46 (2002) 337.
[25] R. Braun, L. Litynska-Dobrzynska, Mater. Sci. Forum 396–402 (2002) 1531.
[26] A.F. Norman, I. Brough, P.B. Prangnell, Mater. Sci. Forum 331–337 (2000) 1713.
[27] K.A.A. Hassan, A.F. Norman, P.B. Prangnell, Mater. Sci. Forum 396–402 (2002) 1549.
[28] J.Q. Su, T.W. Nelson, R.S. Mishra, M.W. Mahoney, Acta Mater. 51 (2003) 713.
[29] Z.Y. Ma, R.S. Mishra, M.W. Manohey, R. Grimes, Mater. Sci. Eng. A 351 (2003) 148.
[30] I. Charit, R.S. Mishra, Mater. Sci. Eng. A 359 (2003) 290.
[31] I. Charit, R.S. Mishra, M.W. Mahoney, Scripta Mater. 47 (2002) 631.
[32] I. Charit, Z.Y. Ma, R.S. Mishra, in: Z. Jin, A. Beaudoin, T.A. Bieler, B. Radhakrishnan (Eds.), Hot Deformation of Aluminum Alloys III, TMS, 2003, pp. 331–342.
[33] P.S. Pao, E. Lee, C.R. Feng, H.N. Jones, D.W. Moon, in: K.V. Jata, M.W. Mahoney, R.S. Mishra, S.L. Semiatin, T. Lienert (Eds.), Friction Stir Welding and Processing II, TMS, Warrendale, PA, USA, 2003, p. 113.
[34] Y.J. Kwon, I. Shigematsu, N. Saito, Mater. Trans. 44 (2003) 1343.
[35] Y.J. Kwon, I. Shigematsu, N. Saito, Scripta Mater. 49 (2003) 785.
[36] Y.S. Sato, H. Kokawa, M. Enmoto, S. Jogan, Metall. Mater. Trans. A 30 (1999) 2429.
[37] K.V. Jata, K.K. Sankaran, J.J. Ruschau, Metall. Mater. Trans. A 31 (2000) 2181.
[38] M. James, M. Mahoney, in: Proceedings of the First International Symposium on Friction Stir Welding, Thousand Oaks, CA, USA, June 14–16, 1999.
[39] Y.S. Sato, M. Urata, H. Kokawa, Metall. Mater. Trans. A 33 (2002) 625.

[40] F. .J. Humphreys,M. Hotherly, Recrystallization and Related Annealing Phenomena, Pergamon Press, New York, 1995

[41] L.E. Murr, G. Liu, J.C. McClure, J. Mater. Sci. 33 (1998) 1243.

[42] J.Q. Su, T.W. Nelson, R.S. Mishra, M.W. Mahoney, Acta Mater. 51 (2003) 713.

[43] S. Suresh, Fatigue of Materials, 2nd edition, Cambridge University Press, 1998.

[44] M. Janssen, J. Zuidema and R. Wanhill, Fracture Mechanics, 2nd edition, Spon Press, 2004.

[45] G. Biallas, R. Braun, C.D. Donne, G. Staniek,W.A. Kaysser, in: Proceedings of the First International Symposium on Friction Stir Welding, Thousand Oaks, CA, USA, June 14–16, 1999.

[46] P.S. Pao, E. Lee, C.R. Feng, H.N. Jones, D.W. Moon, in: K.V. Jata, M.W. Mahoney, R.S. Mishra, S.L. Semiatin, T.
Lienert (Eds.), Friction Stir Welding and Processing II, TMS, Warrendale, PA, USA, 2003, p. 113.

[47] H. Hori, S. Makita, H. Hino, in: Proceedings of the First International Symposium on Friction Stir Welding, Thousand Oaks, CA, USA, June 14–16, 1999.

[48] M. Kumagai, S. Tanaka, in: Proceedings of the First International Symposium on Friction Stir Welding, Thousand Oaks, CA, USA, June 14–16, 1999.

[49] G. Bussu, P.E. Irving, in: Proceedings of the First International Symposium on Friction Stir Welding, Thousand Oaks, CA, USA, June 14–16, 1999.

[50] J.Z. Zhang, R. Pedwell, H. Davies, in: Proceedings of the Second International Symposium on Friction Stir Welding, Gothenburg, Sweden, June 2000.

[51] M. Erisson, R. Sandstrom, J. Hagstrom, in: Proceedings of the Second International Symposium on Friction Stir Welding, Gothenburg, Sweden, June 2000.

[52] N. Jayaraman, P. Prevey, M. Mahoney, in: K.V. Jata, M.W. Mahoney, R.S. Mishra, S.L. Semiatin, T. Lienert (Eds.), Friction Stir Welding and Processing II, TMS, 2003, p. 259.

[53] K.V. Jata, K.K. Sankaran, J.J. Ruschau, Metall. Mater. Trans. A 31 (2000) 2181.

[54] C.D. Donne, G. Biallas, T. Ghidini, G. Raimbeaux, in: Proceedings of the Second International Symposium on Friction Stir Welding, Gothenburg, Sweden, June 26–28, 2000.

[55] P.S. Pao, S.J. Gill, C.R. Feng, K.K. Sankaran, Scripta Mater. 45 (2001) 605.

[56] R. Braun, G. Biallas, C.D. Donne, G. Staniek, in: P.J. Winkler (Ed.), Materials for Transportation Technology EUROMAT'99, vol. 1, Wiley/VCH, 1999, pp. 150–155.

[57] G. Bussu and P.E. Irving, Int. J. Fatigue 25 (2003) 77.

[58] S. Kim, C.G. Lee and S.J. Kim, Mat. Sci. Eng. A. 478 (2008) 56-64.

[59] C. Zhou, X. Yang and G. Luan, J. Mater. Sci. 41 (2006) 2771-2777.

[60] A. Steuwer et al., Materials Science and Engineering A 441 (2006) 187–196].

[61] www.twi.co.uk

# Chapter 2

# Fatigue crack growth behavior of FSWed 5052 aluminum alloy joint joined with a bobbin type tool comparison with single-passed and double-passed conventional FSWed joint

Effect of FSW processes on FCG behavior of FSWed joints was studied in this chapter in 5052 aluminum alloy. Fatigue crack growth behavior at weld nugget zone (WNZ) and heat affected zone (HAZ) in the joints joined by using a bobbin type tool was investigated by comparing to those in the joints joined by using a conventional tool with single-passed and double-passed FSW processes. Friction stir welding process with the bobbin type tool introduced higher heat input compared to FSW processes with the single-pass and double-pass. Different FCG behavior was found in the joints joined with different FSW processing. Fatigue crack growth resistance of WNZ and HAZ in FSWed joint with single-passed process by using a conventional tool was higher compared to those observed in the FSWed joint with double-passed process by using a conventional tool and a bobbin type tool. However, the differences in FCG curves due to different FSW processes and positions in FSWed joints were arranged into a single curve when crack closure effect was taken into account. Grain size in the WNZ was dominant on threshold stress intensity factor range. Intrinsic FCG resistance of the FSWed joints were the similar regardless of FSW process.

## 2.1 Introduction

Friction stir welding (FSW) is known as a solid state joining process and has been widely applied in currently to join high strength aluminum alloys, dissimilar materials and other materials to overcome the difficulty in conventional fusion welding [1-3]. In previous study, the effect of welding process to join aluminum alloys was investigated. M. Ericsson and R. Sandstrom (2003) studied the influence of welding speed on fatigue of the joint joined by FSW comparison with the joints joined by MIG and TIG [4]. V. Fahimpour et al. (2013) investigated the microstructure and mechanical property change during FSW and GTAW of 6001 aluminum alloy [5]. The results of those studies showed that FSW obtained higher in tensile and fatigue properties than that of conventional fusion welding processes. Although, previous works had been studied to compare the benefit of different welding processes between FSW and conventional fusion welding. However, investigation of the difference within FSW process itself by different FSW tool and FSW process were limited.

Solid state joining of FSW process can be achieved by localized friction heating and deformation of material by mechanical stirring around the FSW tool. These thermo-mechanical processing are mainly affected by welding parameters and also tool type to generate heat input and deform the material during joining process. The effect of FSW parameters [6-10] and heat input [11-12] on peak welding temperature, microstructure, hardness distribution and tensile properties were also reported in previous studies. H. Fujii et al. (2006) reported that FSW/FSP at higher ratio of tool rotation rate/travelling speed or higher tool rotation rate resulted in an increase in both degree of deformation and peak temperature [6]. V. Dixit et al. (2007) showed the results that increase in heat input index (HI) values appeared to coarsen the grain structures in the nugget region [12]. At low HI, the area fraction (thus, volume fraction) of the precipitates is large, which appeared to decrease at higher HI. Moreover, coarsening of second phase particles was also observed at higher HI.

R.D. Fu et al. (2013) and V. Dixit et al. (2007) evaluated the heat input which depend on tool rotation speed and travelling speed in their study by calculation the pseudo heat index (HI) value to represent heat input per unit length which related to peak temperature as proposed as following equation [11-13] :

$$HI = \frac{\omega^2}{\nu \times 10^4} \quad (1)$$

Then peak temperature was calculated by:

$$\frac{T}{T_m} = K(HI)^A \quad (2)$$

Where HI = pseudo heat index (HI) ($min^{-1}$ $cm^{-1}$), ω = rotating speed (rpm), ν = traveling speed (mm/min), $T_m$ = melting temperature, A = constant that was reported in range of 0.04 to 0.06 and K = constant is between 0.65 and 0.75. The maximum temperature have been observed during FSW of various aluminum alloys is found to be between $0.6T_m$ and $0.9T_m$ which is within the hot working temperature range for those aluminum alloys [1].

In this work, the difference FSW tool and FSW processes were applied to join 5052 aluminum alloy plates by using bobbin type tool comparing with single-passed and double-passed by using conventional FSW tool. These FSWed joints from different FSW processes were different in heat input. FSWed joint joined by using a bobbin type tool which friction heat generated from both sides of welded plates was expected to higher heat input compared to single-passed and double-passed conventional FSWed joints.

Many advantages of 5052 aluminum alloy such as good formability, good corrosion resistance and good weldability has been reported. Applications of those were used in pressure vessels, tank fitting, boat hulls, car body application and aircraft fuel and oil lines [14-17]. In previous studies, Y.S. Sato et al. (2004) has been evaluated the post-weld formability of FSWed of 5052 for car body applications [15] and studied FIB-assisted TEM of an oxide array in the root of a FSWed 5052 aluminum alloy [18]. Z. Zhang et al. (2011) investigated the effect of welding parameters on microstructure and mechanical properties of friction stir spot welded 5052 aluminum alloys [16]. N. T. Kumbhar et al. (2011) investigated microstructure and microtextural of FSWed 5052 aluminum alloy [19].

In the present work, FSWed 5052 aluminum alloy joint was focused and investigated the FCG behavior in three different kind of FSW processes which different in heat input. The results from this study will give us information and understanding the effect of FSW process on FCG behavior and obtained the beneficial information for material joining process selection.

## 2.2 Experimental Procedure

Rolled 5052 aluminum alloy plates were used for joining in this study and 3D microstructure of these base materials was shown in Fig 2.1. Plates of these alloy with thickness of 6 mm were welded parallel to the rolling direction by FSW using a bobbin type tool and conventional FSW tool by applying single-passed and double-passed which

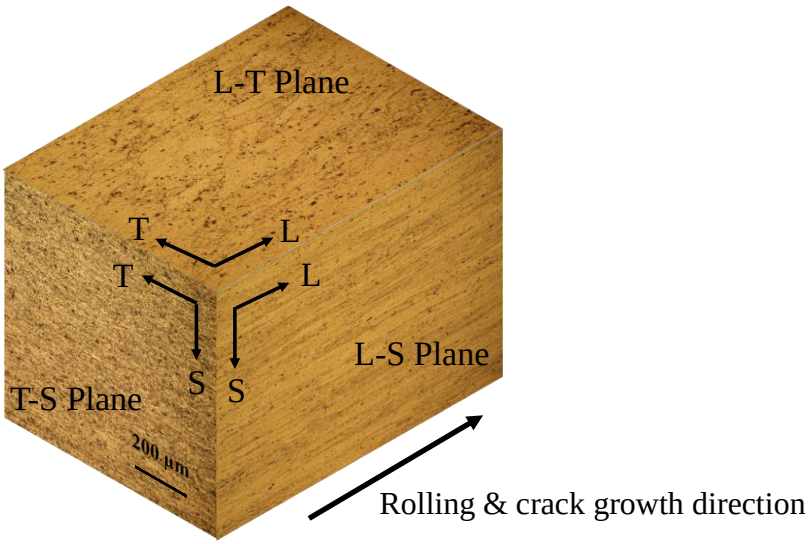


Fig. 2.1 Microstructures of 5052 base material in 3 dimensional planes.

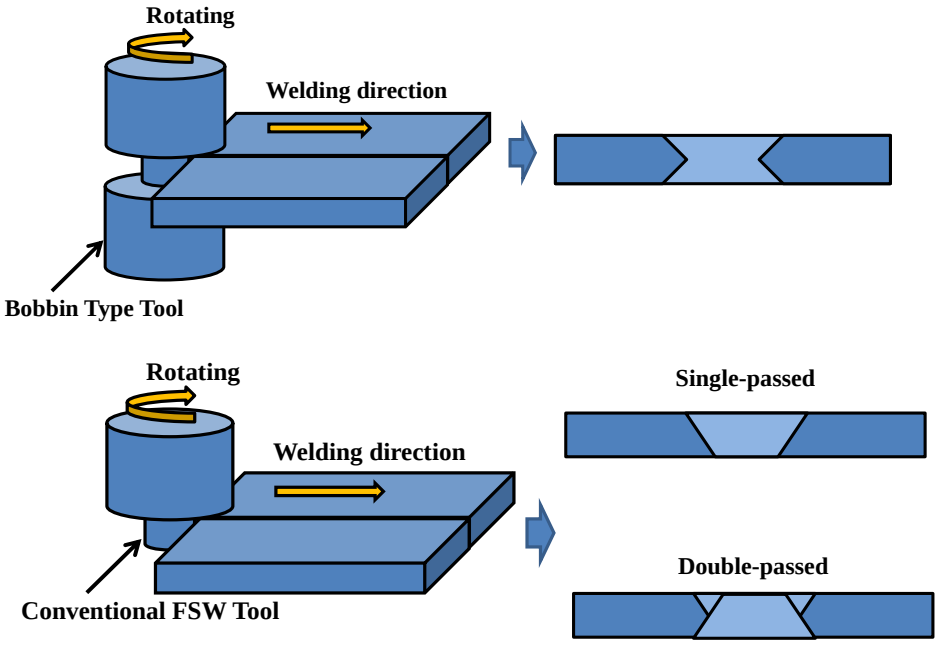


Fig. 2.2 Schematics illustration of FSW process by using bobbin type tool and conventional tool.

illustrated as schematic processes in Fig 2.2. The bobbin type tool with shoulder diameter of 20 mm has a pin with diameter of 12 mm and distance between the shoulders is 5.8 mm. The conventional FSW tool with shoulder diameter of 17 mm for single-passed and 15 mm for double-passed were used. Welding conditions were selected according to result of a trial test to obtain appropriate conditions. Tool rotation speed and traveling speed in FSW by bobbin type tool was 300 rpm with 200 mm/min, by conventional tool single-passed was 500 rpm with 400 mm/min, by conventional tool double-passed was 300 rpm with 200

mm/min. The pseudo heat input index (HI) of FSWed joints joined by different FSW tools and FSW processes which evaluated from welding parameters in equation (1) were shown in Table 2.1. A chemical composition of 5052 base material was shown in Table 2.2. Table 2.3 shows tensile properties of the base materials in direction perpendicular to rolling direction and of the FSWed joints in direction perpendicular to the welding line. Gage lengths of the tensile specimens were 50 mm for the base metal and the joints.

Compact-tension (CT) specimen following ASTM E 647-08 [20] with a thickness of 4 mm and a width of 32 mm were cut from base materials and the FSWed plates as shown in Fig 2.3. Fatigue crack growth direction was parallel to rolling direction in the base material and welding direction in the joints. In case of the FSWed joint specimen, fatigue pre-crack was introduced at the weld center line in WNZ and at the lowest hardness position in HAZ. Actual locations of the pre-crack introduced in HAZ were 11 mm far from weld center line (WCL) for FSWed joint joined by bobbin type tool and 5 mm far from the WCL for FSWed joint joined by conventional FSW tool for both single-passed and double passed.

Table 2.1 Welding parameters and pseudo heat input index of FSWed 5052 joints.

| Specimen | Rotating speed (rpm) | Traveling speed (mm/min) | Heat input index (HI) $(min.cm)^{-1}$ |
|---|---|---|---|
| 5052 FSW (Bobbin type tool) | 300 | 200 | 1.800[*1] |
| 5052 FSW (Conventional FSW tool: Single-passed) | 500 | 400 | 0.625 |
| 5052 FSW (Conventional FSW tool: Double-passed) | 300 | 200 | 0.900[*2] |

*1: Two-sides of shoulder simultaneous rotation for generating friction heat
*2: Two-times of shoulder rotation for generating friction heat

Table 2.2 Chemical composition of base metal 5052 aluminum alloy used (Wt%).

| Alloy | Si | Mg | Zn | Fe | Mn | Cu | Ti | Cr | Zr | V |
|---|---|---|---|---|---|---|---|---|---|---|
| 5052 | 0.10 | 2.53 | 0.01 | 0.29 | 0.04 | 0.03 | 0.02 | 0.19 | - | - |

Table 2.3 Tensile properties of base materials and FSWed 5052 joints.

| Specimen | 0.2% Proof Strength (MPa) | Tensile Strength (MPa) | Elongation (%) |
|---|---|---|---|
| 5052 BM | 157 | 229 | 16.20 |
| 5052 FSW (Bobbin type tool) | 102 | 202 | 13.70 |
| 5052 FSW (Conventional FSW tool: Single-passed) | 130 | 218 | 11.20 |
| 5052 FSW (Conventional FSW tool: Double-passed) | 132 | 219 | 10.50 |

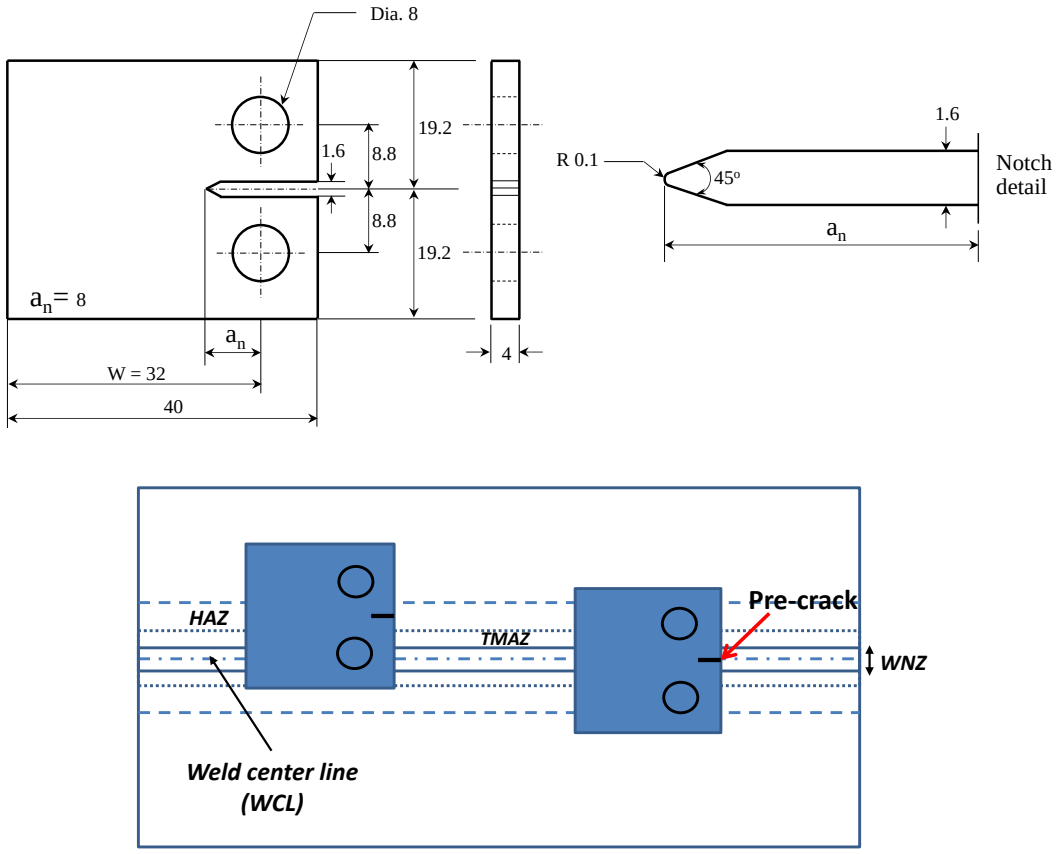


Fig. 2.3 Geometry of CT specimen used and FSWed specimen layout (in mm).

Fatigue crack growth test was conducted by using an electro servo-hydraulic fatigue testing machine under constant stress amplitude condition according to ASTM E 647-08 [20] in laboratory air. Fatigue loading with stress ratio of 0.1 and frequency of 20 Hz was applied with sinusoidal wave form. Crack length was measured in both sides of the specimen by using traveling microscopes during the test. Stress intensity factor range ($\Delta K$) for CT specimen was calculated according to ASTM E 647-08 [20]. In order to investigate crack closure behavior, cyclic load-strain curve was measured under frequency of 2 Hz during the test by using a strain gage with gage length of 2 mm attached at the back face of the specimen. Crack opening load to calculate stress intensity factor at crack opening ($K_{op}$) was determined by unloading elastic compliance method. Effective stress intensity factor range, $\Delta K_{eff}$ was calculated as $\Delta K_{eff} = K_{max} - K_{op}$, where $K_{max}$ is stress intensity factor for the maximum applied stress. Fracture surfaces of FCG test specimens were observed by using a scanning electron microscope after the test.

## 2.3 Results and Discussions

### 2.3.1 Weld structures and hardness distribution

Fig 2.4 shows the welded structures in the cross section perpendicular to the welding direction. Welded structures of FSWed 5052 aluminum alloy joints joined by using a bobbin type tool and conventional FSW tool are classified into three different regions, WNZ, HAZ and thermo-mechanically affected zone (TMAZ). Weld regions were observed as symmetry in upper and lower sides of the joints that joined by using a bobbin type tool. Different material flow pattern in welded region was observed among in the different FSW processes of single-passed, double-passed conventional FSWed and bobbin type FSWed. The interface between the WNZ and the BM is more relatively diffused on the retreating side of the tool, but quite sharp on the advancing side of the tool [21].

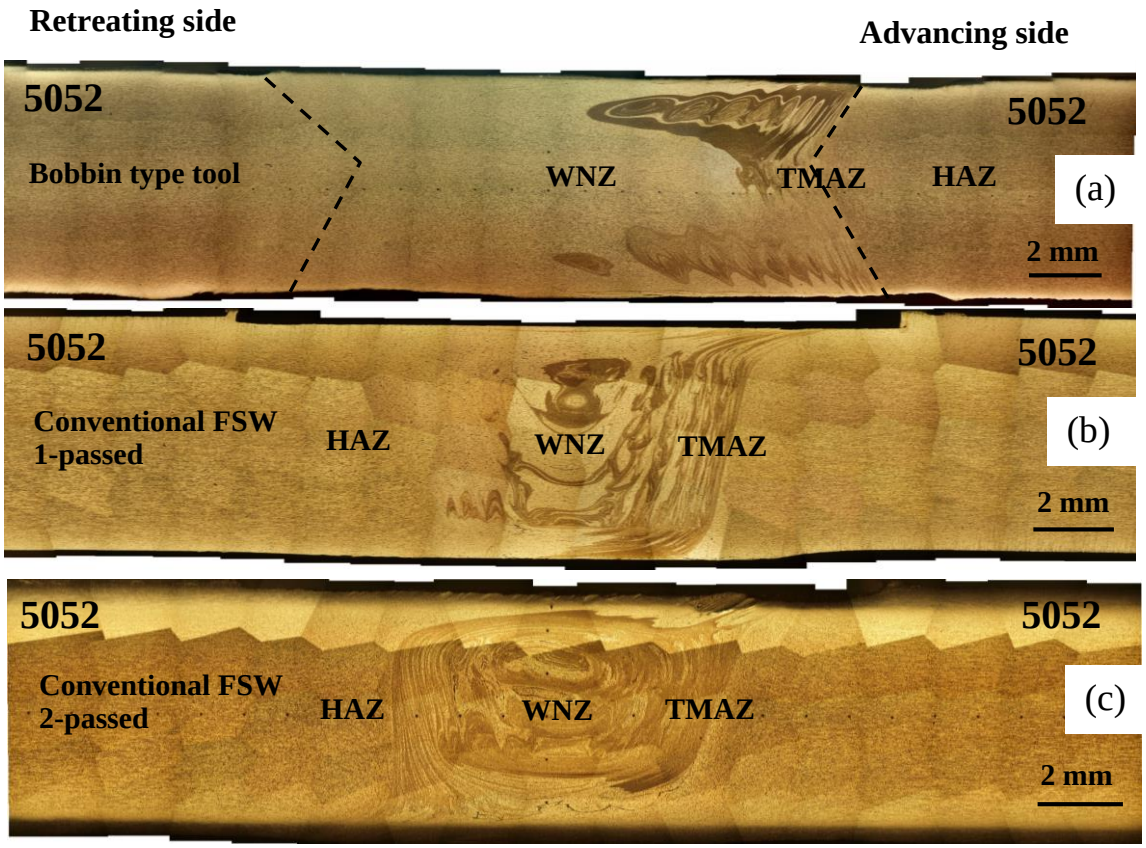


Fig. 2.4 Welded structure in transverse cross-section of FSWed 5052 joints joined by (a) bobbin type tool, (b) conventional FSW tool: single-passed and (c) conventional FSW tool: double-passed.

Microstructures of the BM, the WNZ and the HAZ in different FSW process were shown in Fig 2.5, 2.6 and 2.7 respectively. The microstructure of the BM and the HAZ was almost similar as shown in Fig 2.5 and Fig 2.7. Dynamic recrystallized (DRX) grains size in the WNZ of single-passed and double-passed conventional FSWed was significantly smaller than FSWed joint joined by using a bobbin type tool as shown in Fig 2.6. Lower heat input FSWed joint was smaller in DRX grain size. Previous studies [7-10] have been reported that FSW/FSP parameters affected on DRX grain size by decreasing the ratio of tool rotation rate/traverse speed or decreasing tool rotation rate at a constant tool traverse speed can be reduced DRX grain size. On the other hand, increasing peak temperature of FSW/FSP thermal cycle leads to generate the coarse recrystallized grains, and also results in remarkable grain growth. Moreover, DRX grain size in the WNZ has a nearly linear relationship with the peak temperature regardless of backing plates used also reported by P. Upadhyay and A.P. Reynolds (2012) [22]. They proposed that backing plate diffusivity has very important role affected to the peak stir zone temperature. For considered the plate gage, thermal and microstructural through thickness homogeneity can be achieved by the use of low diffusivity backing plate material. In the present work, bobbin type tool has no backing plate; therefore, heat input on both sides of welded plate from friction heating of the tool was resulted in high peak temperature in stir zone than that of single-passed and double-passed conventional FSWed as expected.

Precipitate dissolution and coarsening have also been reported in previous study. Liu et al. (1997) investigated microstructure of FSWed 6061Al-T6. They reported that the homogeneously distributed precipitates are generally smaller in the BM than in the nugget zone. However, there were far fewer large precipitates in the nugget zone than in the BM [23]. Sato et al. (1999) [24] examined microstructural evolution of a 6063Al-T5, Heinz and Skrotzki (2002) [25] investigated microstructure of FSW 6013Al-T6 and 6013Al-T4, Jata et al. (2000) [26] observed microstructure of FSW 7075Al-T7451 and they reported that did not observed precipitated within the nugget zone. Those results indicated that completely dissolution of the precipitates into aluminum matrix during FSW. Precipitates dissolution and coarsening phenomena in the WNZ and the HAZ did not investigate in this present work. However, from the previous study discussed above, heat input during FSW process might be directly affected on dissolution of strengthening particles and DRX grains size in the WNZ.

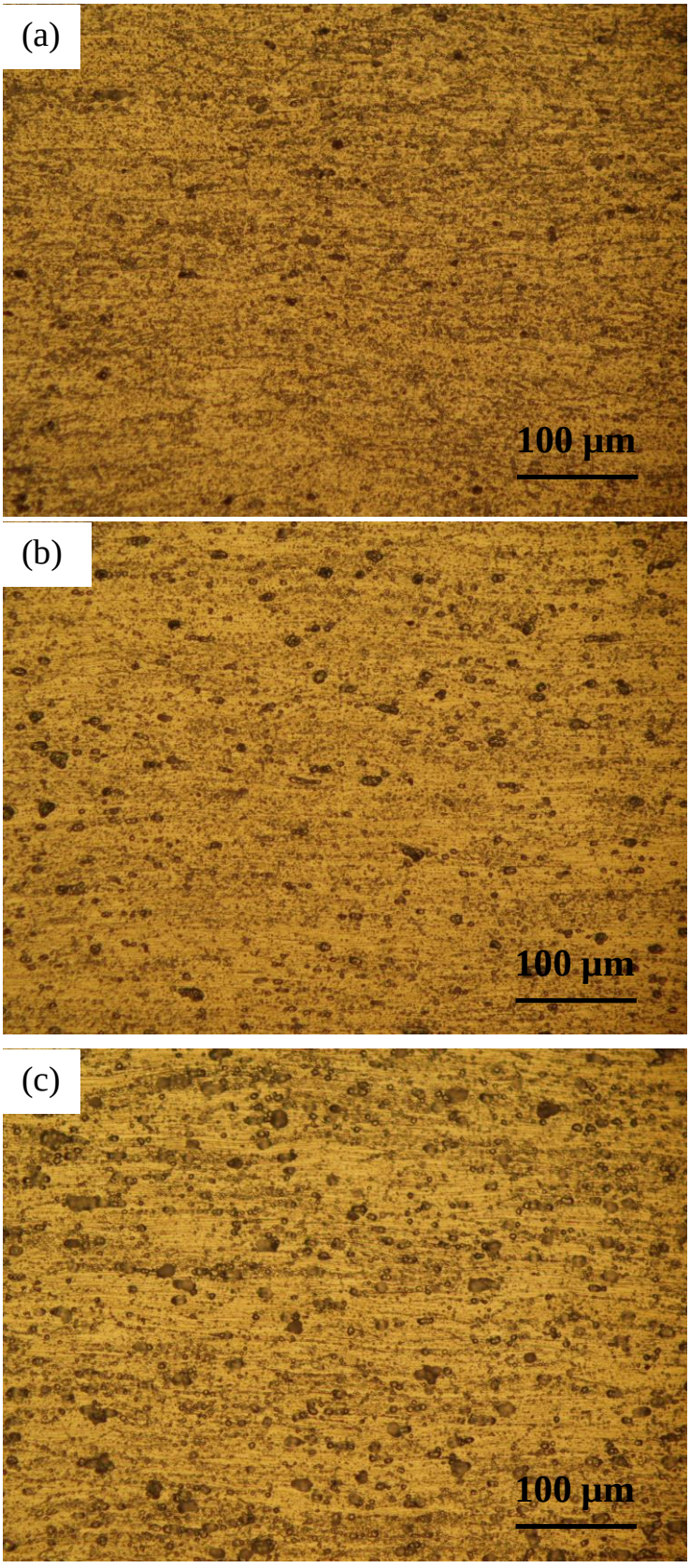


Fig. 2.5 Microstructures of 5052 base metal region in FSWed joints (a) bobbin type tool, (b) conventional FSW tool: single-passed and (c) conventional FSW tool: double-passed.

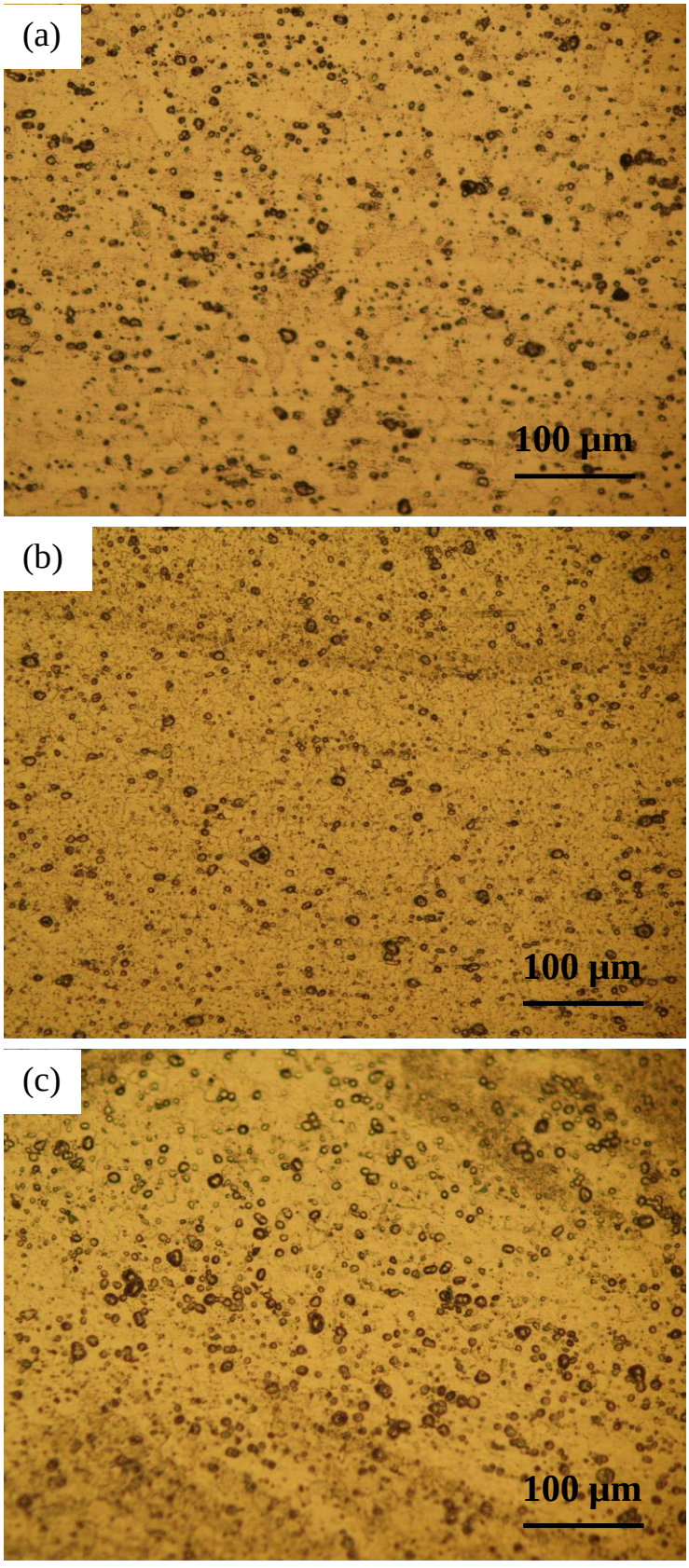


Fig. 2.6 Microstructures of WNZ in FSWed 5052 joints joined by (a) bobbin type tool, (b) conventional FSW tool: single-passed and (c) conventional FSW tool: double-passed.

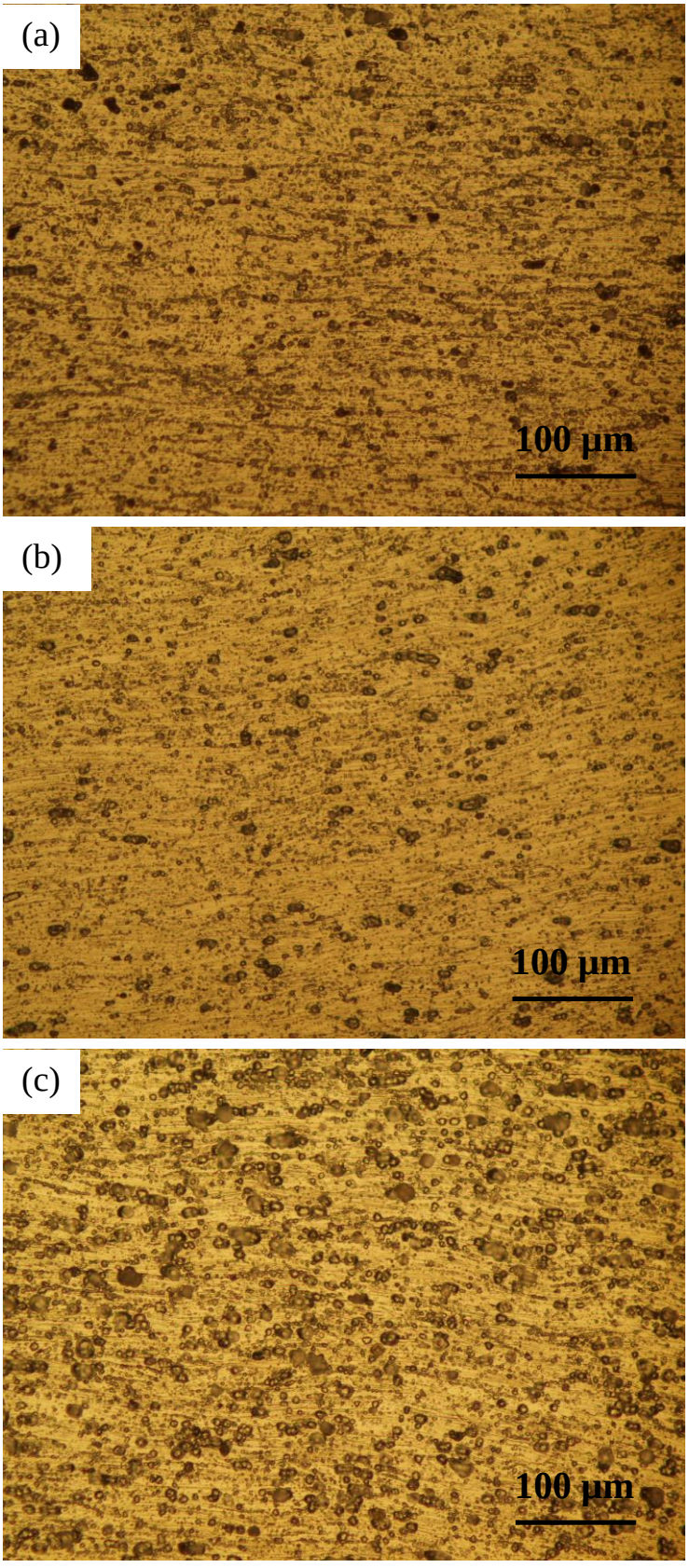


Fig. 2.7 Microstructures of HAZ in FSWed 5052 joints joined by (a) bobbin type tool, (b) conventional FSW tool: single-passed and (c) conventional FSW tool: double-passed.

Higher heat input might expect resulting in more dissolution of strengthening particles and larger DRX grains size in WNZ. All FSWed joints from different FSW processes in this study showed lower in yield and tensile strength compared to the base materials as seen in Table 2.3. Single-passed and double-passed conventional FSWed was higher yield and tensile strength than FSWed joint joined by using a bobbin type tool.

Hardness distributions of FSWed joints at mid-thickness in the cross section perpendicular to the welding direction are shown in Fig 2.8. Microvickers hardness test was carried out with applied load of 200 gf and holding time of 15 s. Hardness in welded region was lower than that of the base material in all FSWed joints. FSWed joint joined by using conventional FSW tool in single-passed showed higher hardness compared to FSWed joints joined by conventional FSW tool in double-passed and bobbin type tool respectively. R.D. Fu et al. (2013) showed the results that welding heat input has obvious effect on the hardness in stir zone [11]. They mentioned that the variation in the strengthening-phase particles plays a more important role than does grain size in the SZ for

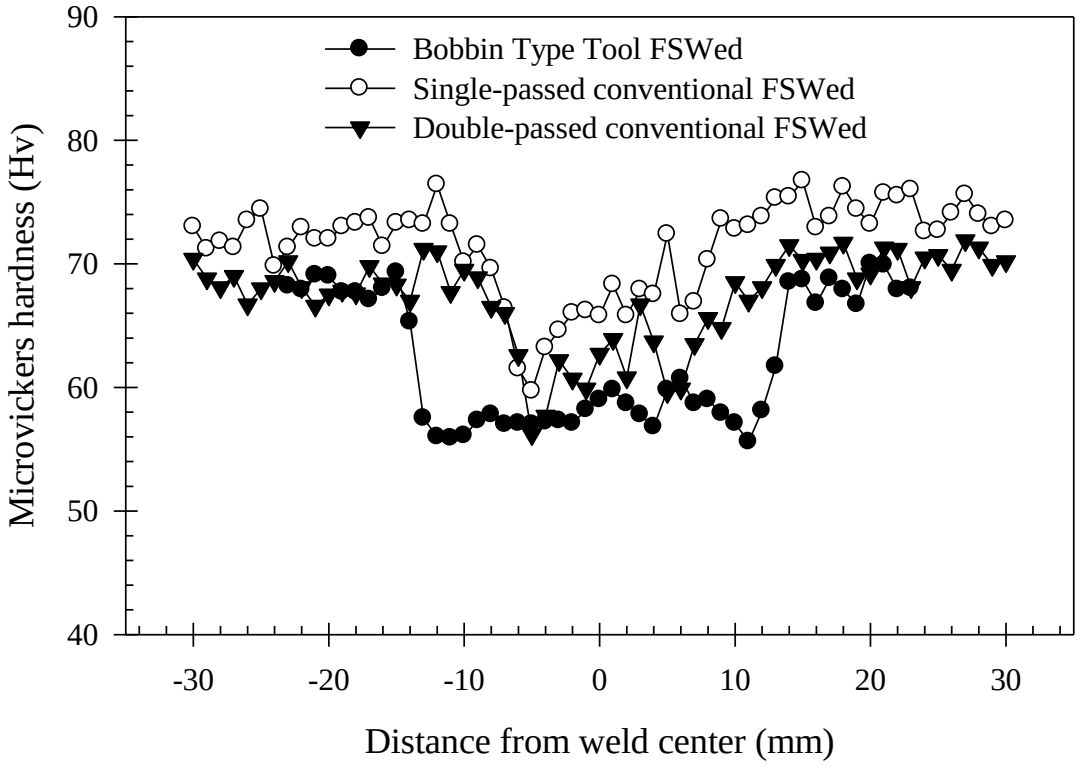


Fig. 2.8 Hardness distribution at mid-thickness position of FSWed 5052 joints joined by bobbin type tool and single-passed and double-passed by conventional FSW tool.

the improvement of hardness. Y.S. Sato et al. (2001) studied in microstructural factor governing hardness in FSW of solid-solution hardened Al-alloys. They mentioned that hardness profile in FSWed of 5083 Al alloy could not be explained by the Hall-Petch relationship, but rather by Orowan hardening [27]. The results of these study suggested that the hardness profile mainly affected by the distribution of small particles in FSW of aluminum alloys containing many such particles. In this study, FSWed joint joined by using a bobbin type tool which higher heat input was lower hardness and wider weld region compared to single-passed and double-passed conventional FSWed. The lowest hardness was located in HAZ for the all FSWed joints at 11 mm for bobbin type tool and 5 mm from weld center line for single-passed and double passed conventional FSWed respectively. Higher heat input affected to wider welded region and lower hardness value.

### 2.3.2 Fatigue Crack Growth Behavior

Figure 2.9 showed fatigue crack growth curves of WNZ and HAZ in different FSW processes comparing with the BM. The difference of FCG behavior was observed among the different FSW processes that joined by using bobbin type tool and conventional FSW tool by applying single and double-passed.

In case of FSWed joint joined by using a bobbin type tool as shown in Fig 2.10, FCG resistance of the WNZ was lower than that of the BM and the HAZ at near-threshold region. At high $\Delta K$ region, FCG resistance of the WNZ was similar to the both of BM and HAZ. In case of single-passed conventional FSWed as shown in Fig 2.11, FCG resistance of the WNZ was higher than that of the BM but lower than the HAZ at near-threshold region. In high $\Delta K$ region, FCG resistance of the WNZ of single-passed conventional FSWed was similar to the both of BM and HAZ. In case of double-passed conventional FSWed as shown in Fig 2.12, FCG resistance of the WNZ was similar to the BM and lower than that of the HAZ at near-threshold region. In high $\Delta K$ region, FCG resistance of the BM and the HAZ in double-passed conventional FSWed was almost the similar, but the WNZ showed slightly lower FCG resistance compared to the BM and the HAZ.

In order to investigate the effect of FSW processes which induced the different amount of heat input generated during FSW process on fatigue crack growth behavior, FCG resistance in the WNZ and the HAZ were plot among of bobbin type FSWed, single-passed and double-passed conventional FSW as shown in Fig 2.13 and Fig 2.14 respectively. Bobbin type FSWed was lower FCG resistance compared to double-passed

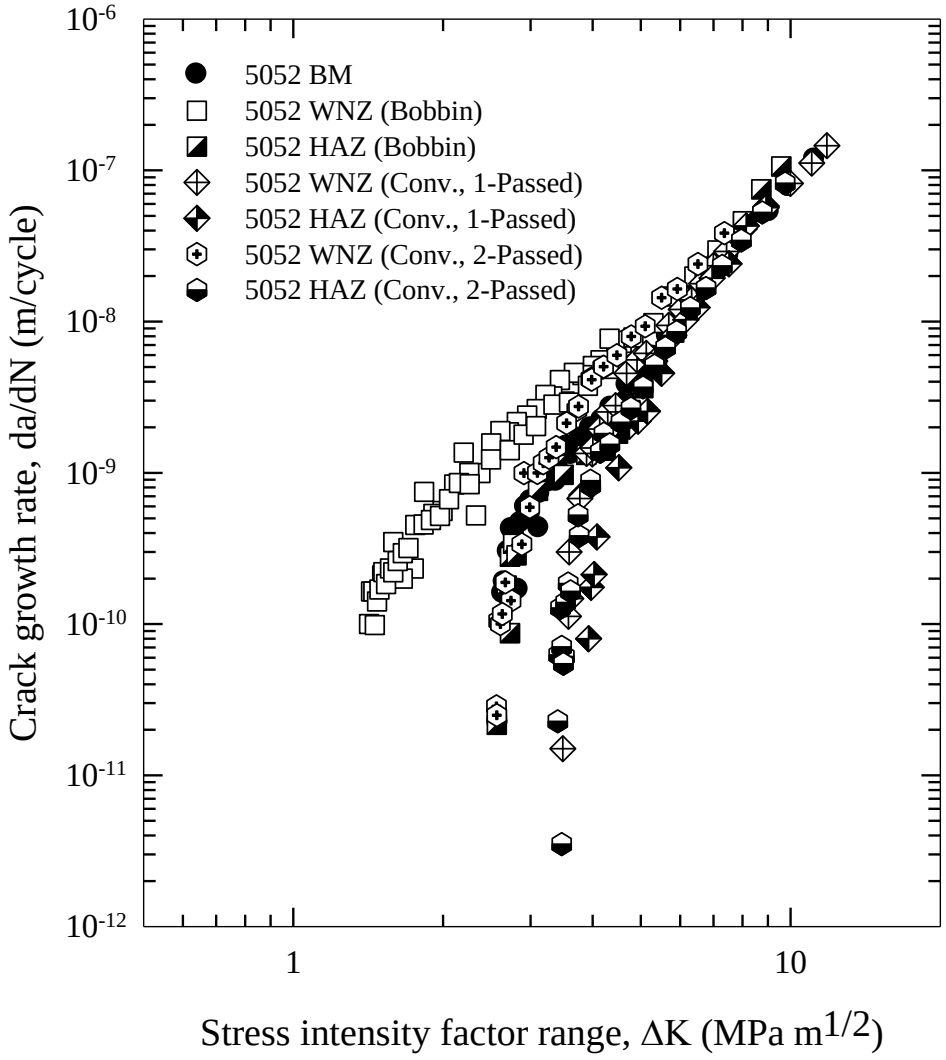


Fig. 2.9 Fatigue crack growth curves of FSWed 5052 joints joined by bobbin type tool and single-passed and double-passed by conventional FSW tool.

and single-passed conventional FSWed in both of the WNZ as shown in Fig 2.13 and the HAZ as shown in Fig 2.14. Higher heat input during FSW processing was lowering FCG resistance. It can be expected that higher heat input was more deteriorated microstructure, mechanical properties as discussed in earlier and also reduced in FCG resistance. Figure 2.13 showed the comparison of FCG resistance in different FSW processes in the WNZ. At low ΔK region, FCG resistance of single-passed conventional FSWed showed higher compared to the BM, double-passed conventional FSWed was identical to the BM and FSWed joint joined by using bobbin type tool showed lower than the BM.

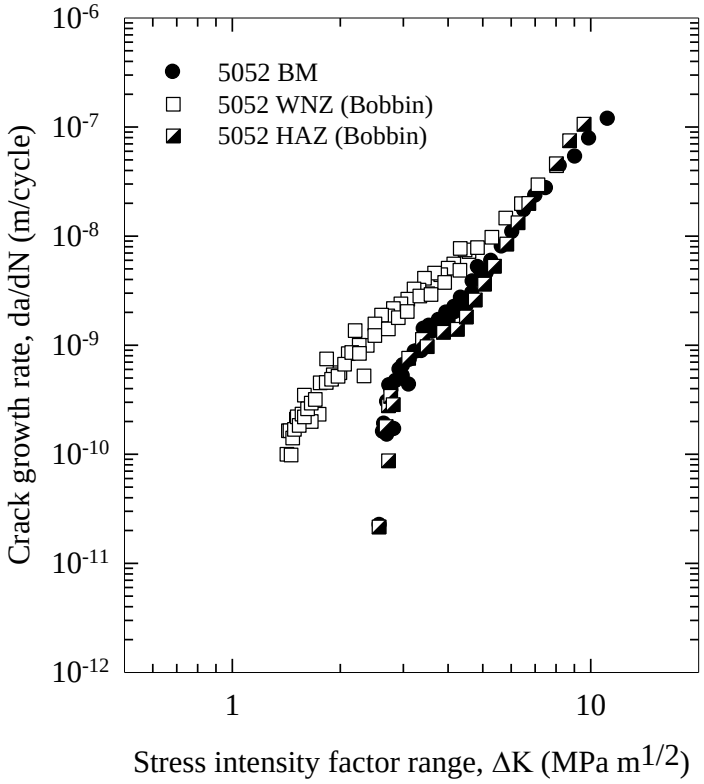


Fig. 2.10 FCG curves of FSWed 5052 joints joined by bobbin type tool.

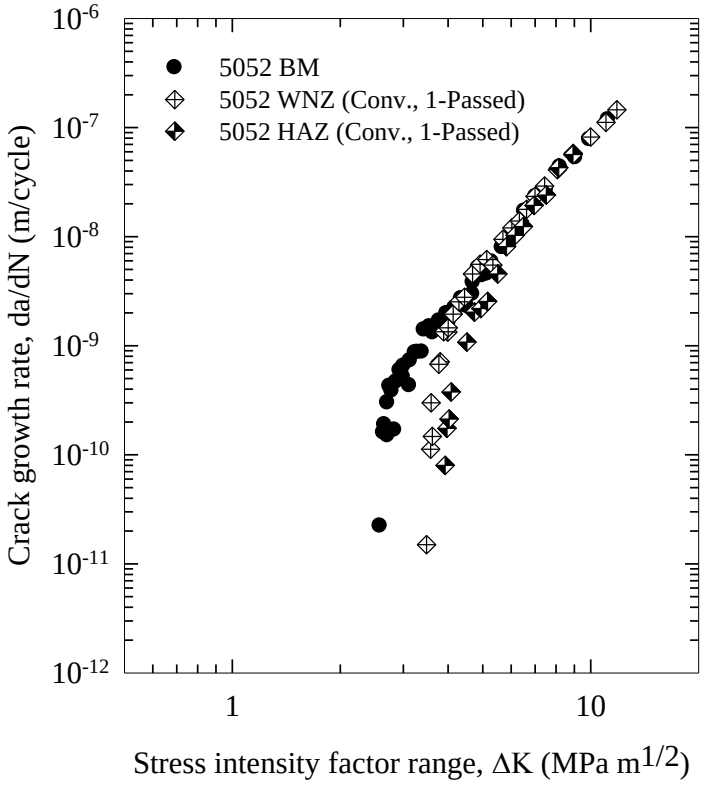


Fig. 2.11 FCG curves of FSWed 5052 joints joined by conventional FSW tool in single-passed.

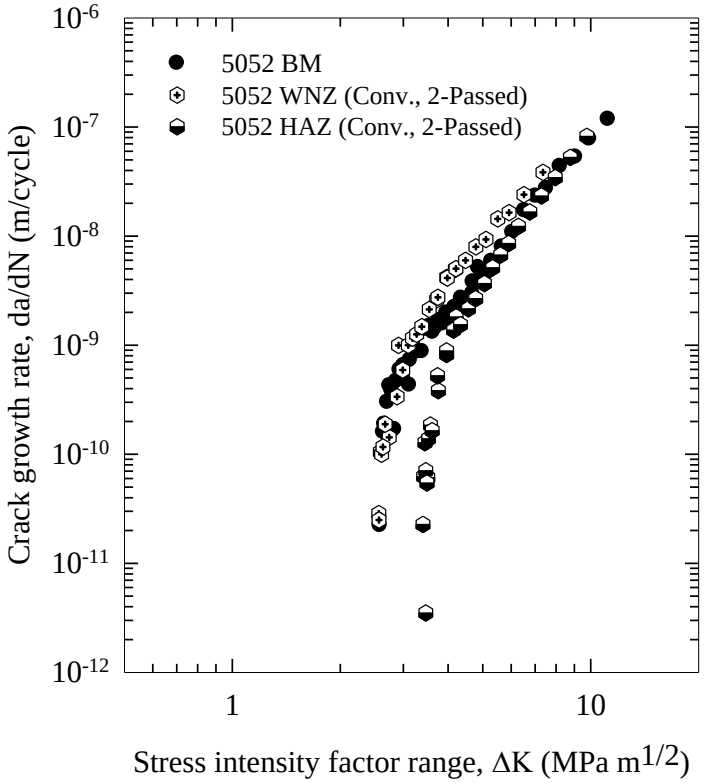


Fig. 2.12 FCG curves of FSWed 5052 joints joined by conventional FSW tool in double-passed.

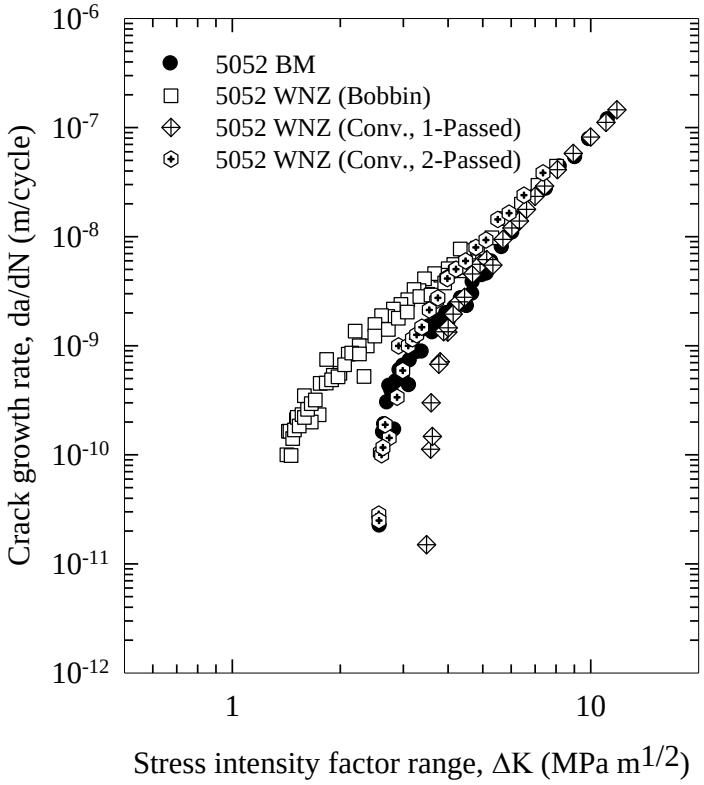


Fig. 2.13 Comparison of FSW processes on FCG curves for WNZ.

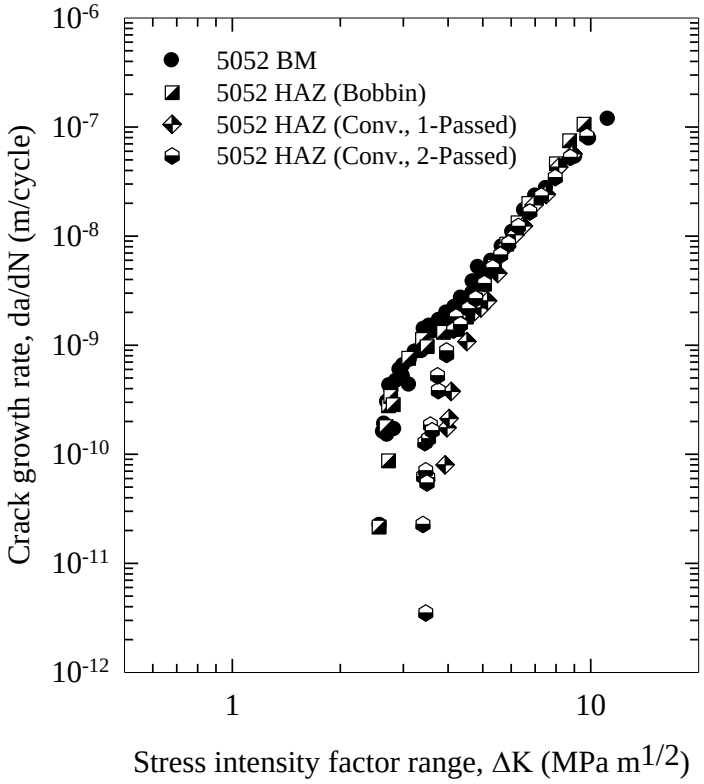


Fig. 2.14 Comparison of FSW processes on FCG curves for HAZ.

In high ΔK region, FCG resistance of WNZ in all FSW processes was almost the similar when ΔK higher than 5 MPa.$m^{1/2}$ at CGR of around $8x10^{-9}$ m/cycle. Figure 2.14 showed the comparison of FCG resistance in different FSW processes in the HAZ. FCG resistance in the HAZ of all FSW processes showed higher than in the WNZ. At low ΔK region, in the HAZ of single-passed and double-passed conventional FSWed showed higher FCG resistance compared to the BM and FSWed joint joined by using a bobbin type tool. While FCG resistance in the HAZ of FSWed joint joined by using a bobbin type tool was identical to the BM at near-threshold region. In high ΔK region, FCG resistance of the HAZ in all FSW processes was almost the similar when ΔK higher than 5 MPa.$m^{1/2}$ at CGR of around $2x10^{-9}$ m/cycle. As a result, lower heat input in FSW process induced higher FCG resistance of FSWed joints in both of the WNZ and the HAZ.

### 2.3.3 Residual stresses investigation

In generally, residual stresses produced in FSW process was very little compared to conventional fusion welding. However, in previous study, many researchers investigated the effect of residual stresses on fatigue crack growth behavior. It is showed that the tensile residual stress induced to increase effective stress intensity factor range and increase driving force for crack propagation. In contrast, the compressive residual stress induced to reduce effective stress intensity factor and reduce driving force for crack propagation. They suggested that residual stresses significantly affected on fatigue crack growth behavior of FSWed joints. In this work, residual stresses were measured on CT specimen before fatigue crack growth tests in relation with distance from weld center line for WNZ samples by using X-ray diffractmeter and the results shown in Fig 2.15. In this study, the CT specimens are prepared from the large plate and residual stress might be fewer remains in testing specimens. Moreover, the residual tresses measurement results in all FSWed joints obtained in this study showed very small amount of residual stresses value. Therefore, it can be suggested that residual stresses effect in this study is negligible.

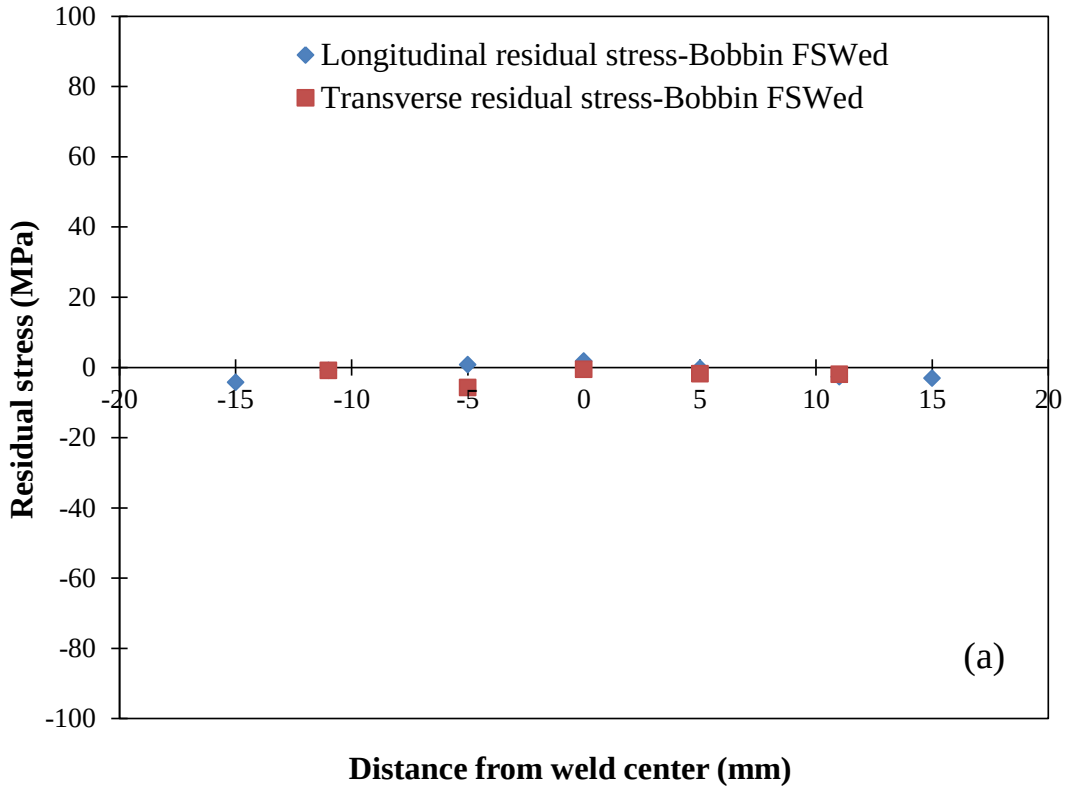

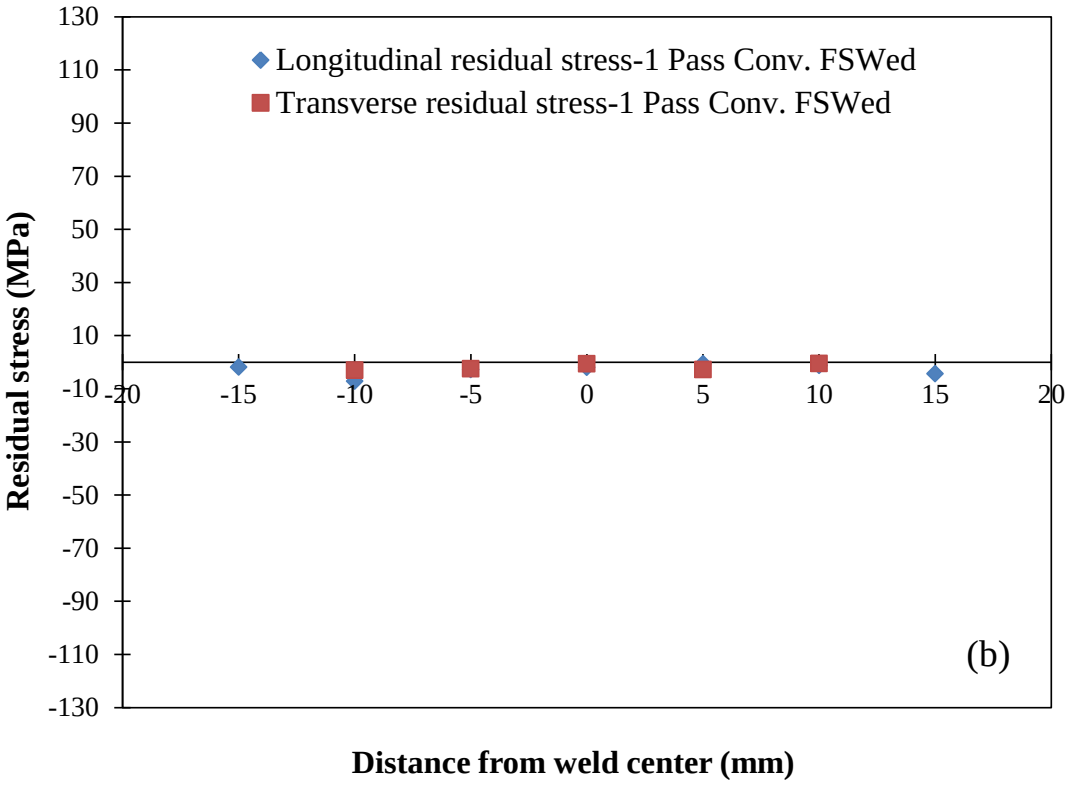


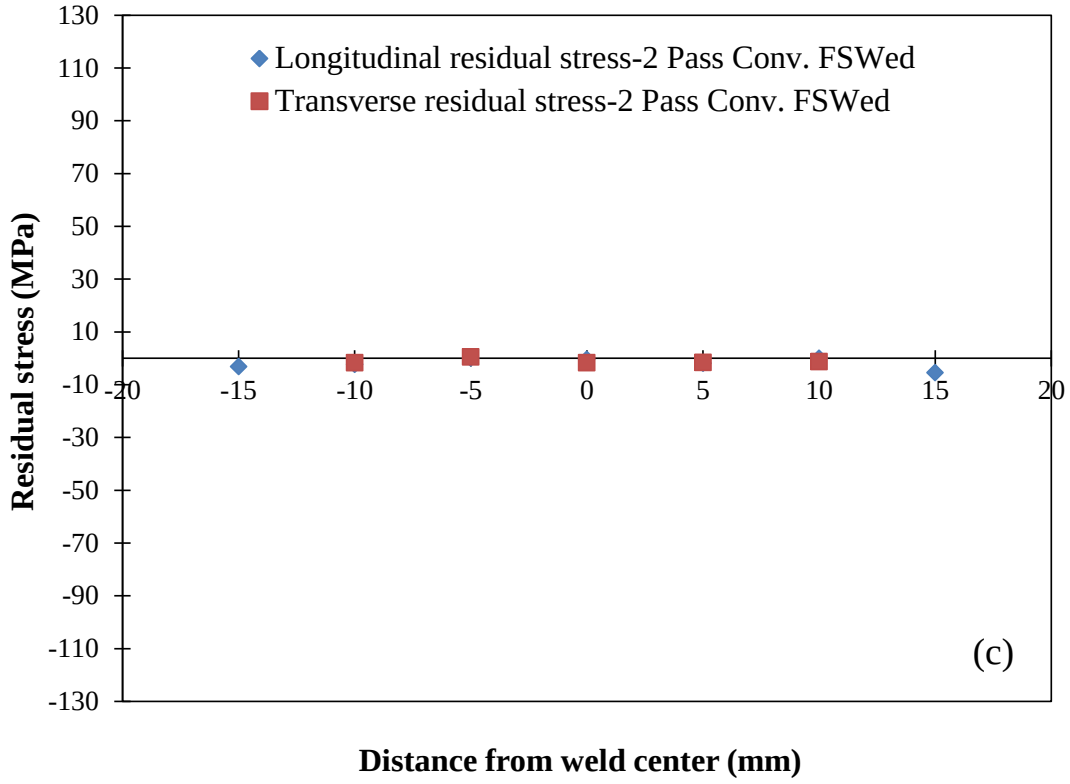


Fig. 2.15 Residual stresses distribution in relation with distance from weld center line for (a) bobbin type FSW, (b) single-passed conventional FSW and (c) double-passed conventional FSW.

### 2.3.4 Fracture surfaces

Fracture surfaces of the BM, the WNZ and the HAZ in both of at near-threshold region and at high ΔK region was shown in Fig 2.16, 2.17 and 2.18 respectively. Fracture surfaces of the BM and the HAZ in different FSW processes in both of at near-threshold region and at high ΔK region were observed transgranular fracture mode as shown in Fig 2.16 and Fig 2.18. Figure 2.17 showed the fracture surfaces of the WNZ in different FSW process. In case of WNZ, transgranular fracture was observed at near-threshold region of

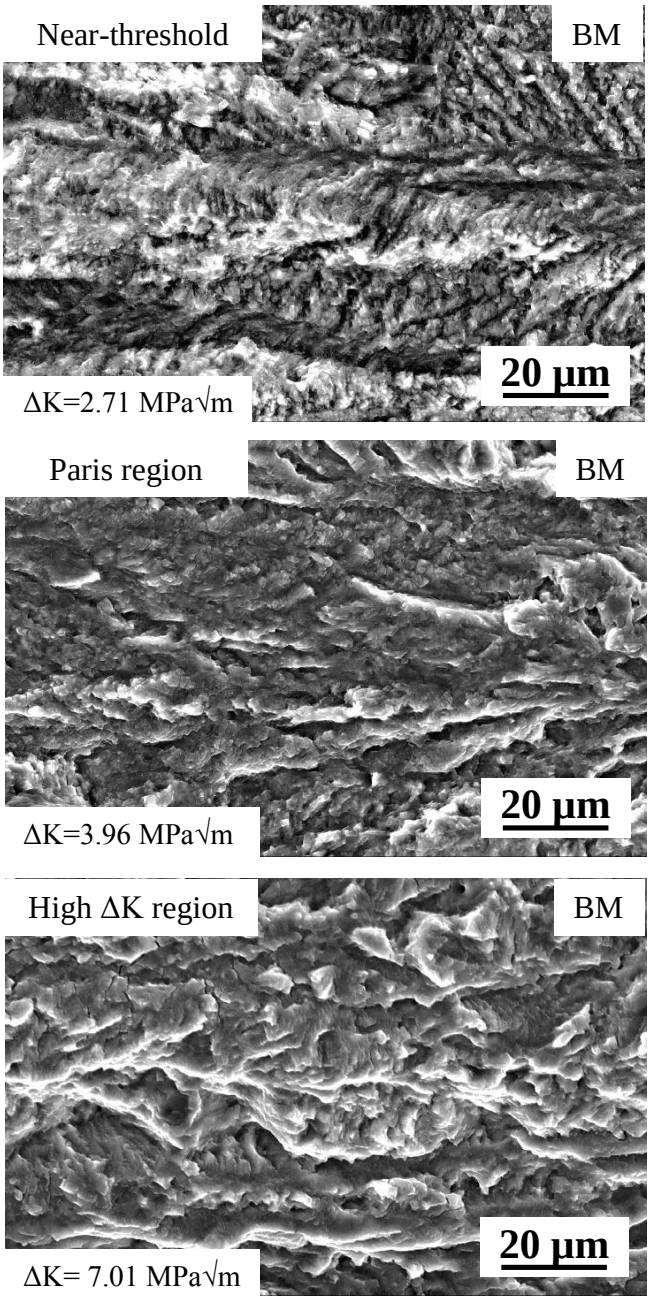


Fig. 2.16 Fracture surfaces of 5052 base material at low ΔK and high ΔK region.

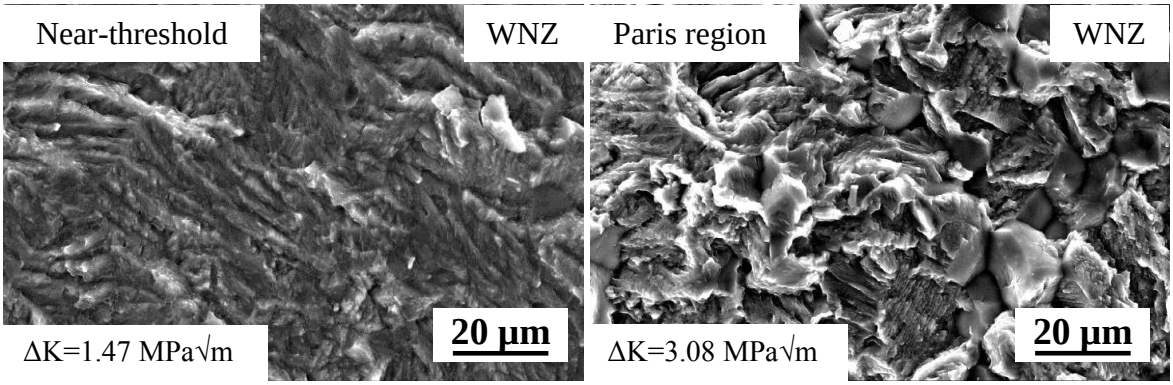


(a) Bobbin type tool.

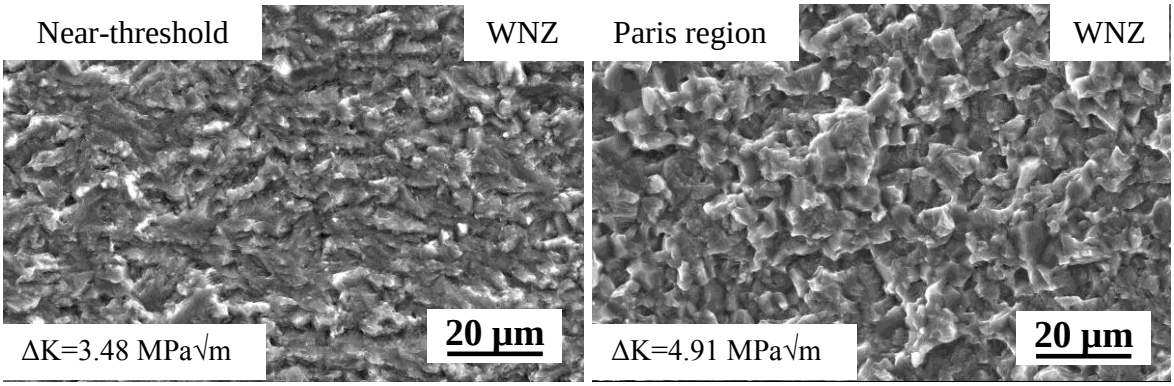


(b) Conventional FSW tool: Single-passed.

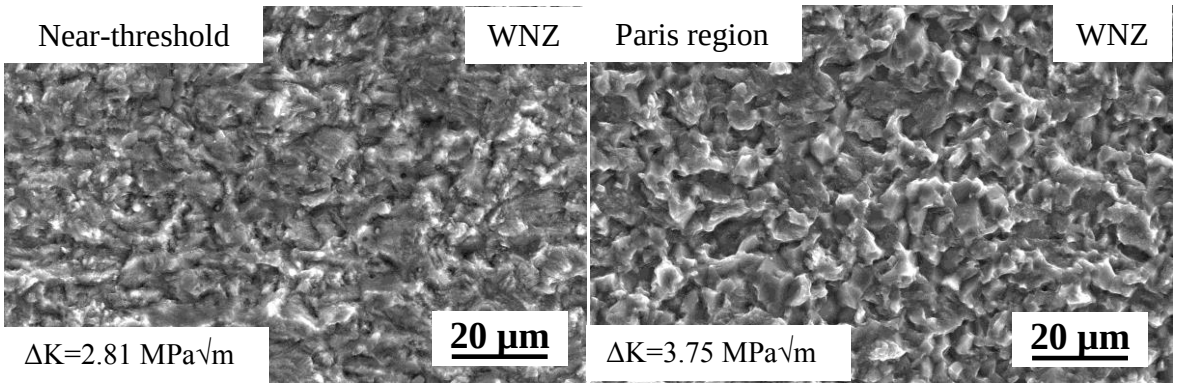


(c) Conventional FSW tool: Double-passed.

Fig. 2.17 Fracture surfaces of WNZ in FSWed 5052 joints joined by (a) bobbin type tool, (b) conventional FSW tool: single-passed and (c) conventional FSW tool: double-passed at low ΔK and high ΔK region.

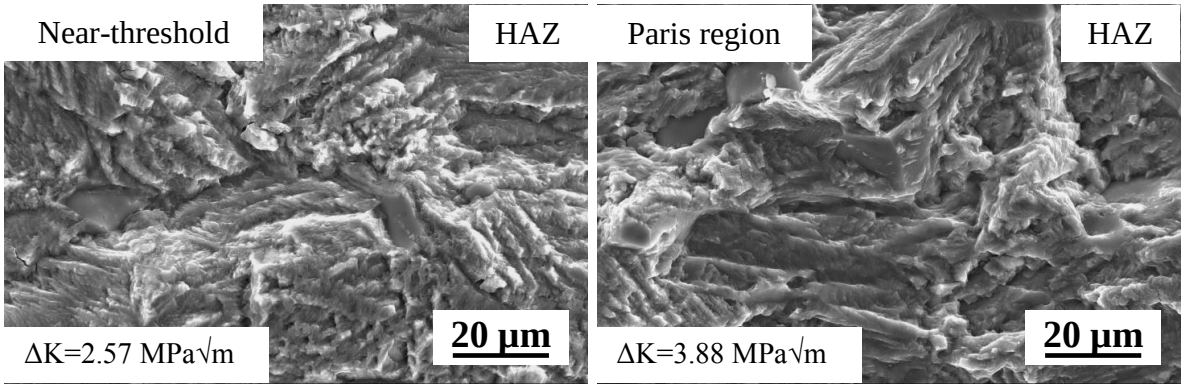


(a) Bobbin type tool.

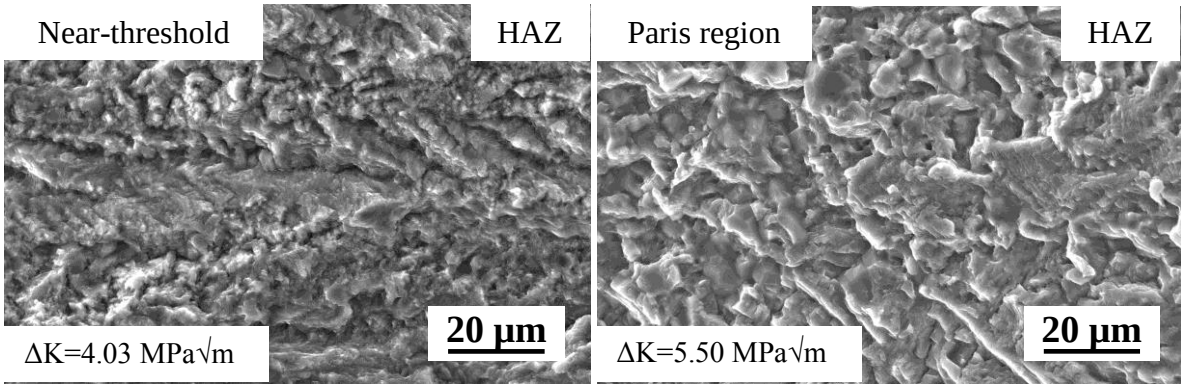


(b) Conventional FSW tool: Single-passed.

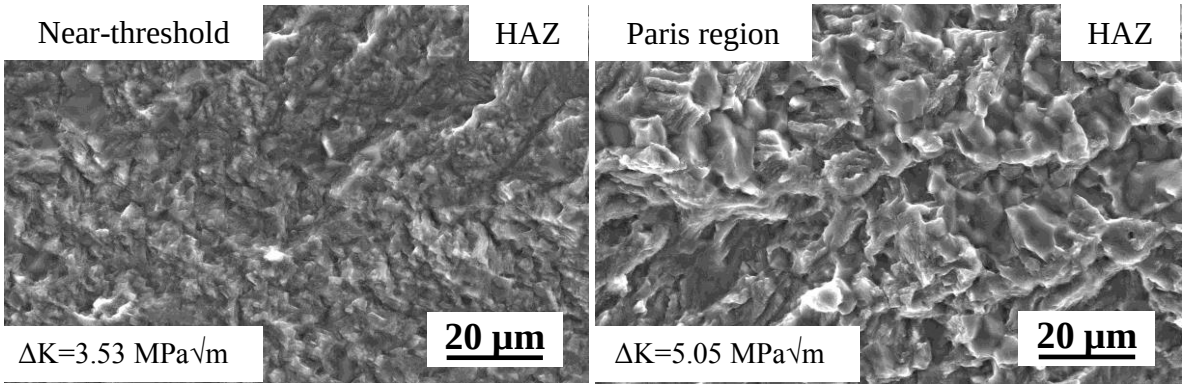


(c) Conventional FSW tool: Double-passed.

Fig. 2.18 Fracture surfaces of HAZ in FSWed 5052 joints joined by (a) bobbin type tool, (b) conventional FSW tool: single-passed and (c) conventional FSW tool: double-passed at low ΔK and high ΔK region.

bobbin type FSWed, single-passed and double-passed conventional FSWed. In high ΔK region, mixed mode fracture (intergranular + transgranular) was observed in the WNZ of all FSWed joints in different FSW processes. It can be observed from intergranular fracture in the WNZ at high ΔK region that DRX grains of bobbin type FSWed which higher heat input was significant larger grain size compared to single-passed and double-passed conventional FSWed. From the result, different FSW processes showed the similar fracture mechanism even if heat input and microstructure in welded region were difference. It can be mentioned that the difference in FCG behavior of different FSW processes might not be due to fracture mechanism.

### 2.3.5 Effect of grain size and hardness on threshold stress intensity factor

In generally, relationship between yield stress or hardness and grain size is well agreement in accordance to Hall-Petch relation as below equations;

$$\sigma_{ys} = \sigma_{y0} + \frac{k_y}{\sqrt{d}}$$

$$H_v = H_{v0} + \frac{K_H}{\sqrt{d}}$$

where $\sigma_{ys}$ is yield stress, $H_v$ is Vickers hardness, $d$ is grain size and $\sigma_{y0}$, $H_{v0}$, $k_y$ and $k_H$ are material constants given in Hall-Petch relation.

In according to Hall-Petch relation, smaller grain size materials should show higher in hardness and yield strength for grain boundary strengthening. In contrast, the FSW microstructure obtained in this study, smaller grain size of fine-equiaxed dynamic recrystallized grains in the WNZ showed lower hardness and yield strength compared to the larger elongated grains in base material. Moreover, lower hardness and yield strength was obtained in the HAZ of FSW microstructure which similar grain size with the base material.

The effect of grain size and yield stress on threshold stress intensity factor range has been reported in previous study [28] which materials used in previous study showed Hall-Petch relation between grain size and yield stress. In this study, the FSW materials which showed contradiction trend with Hall-Petch relation will discussed on the effect of grain size and hardness on threshold stress intensity factor range.

Figure 2.19 shows the relationship between hardness and grain size. The results of FSW materials in different FSW processes showed clearly contradiction trend with Hall-Petch relation which smaller grain size in WNZ was lower in hardness. As a consequence, relationship between grain size, hardness and threshold stress intensity factor range were shown in Fig 2.20, 2.21 and Table 2.4 respectively for investigation the effect of grain size and hardness on threshold stress intensity factor range.

In case of bobbin type FSW, larger grain size has higher threshold stress intensity factor range which similar to general trend with other materials studied as shown in Fig. 2.20. However, in the relation between hardness and threshold stress intensity factor range for bobbin type FSW shown in Fig. 2.21, the result in this study did not show significant trend. Previous study indicated that the lower yield stress or lower hardness materials showed higher threshold stress intensity factor range.

In case of welded structures in conventional FSW for both of single-passed and double-passed, the HAZ that larger grain size than the WNZ showed higher threshold stress intensity factor range which similar to general trend with other materials studied as shown in Fig. 2.20. However, the relation between hardness and threshold stress intensity factor for conventional FSW shown in Fig. 2.21, the result in this study did not show significant trend between hardness and threshold stress intensity factor as observed in bobbin type FSW.

As a result, the different FSW processes showed similar trend in the effect of grain size and hardness on threshold stress intensity factor range. In relation between grain size and threshold stress intensity factor range showed that larger grain size was resulted in higher threshold stress intensity factor range. However, the relation between hardness and threshold stress intensity factor did not show significant trend. It can be mentioned that the grain size was a factor to controlling the threshold stress intensity factor range in this study.

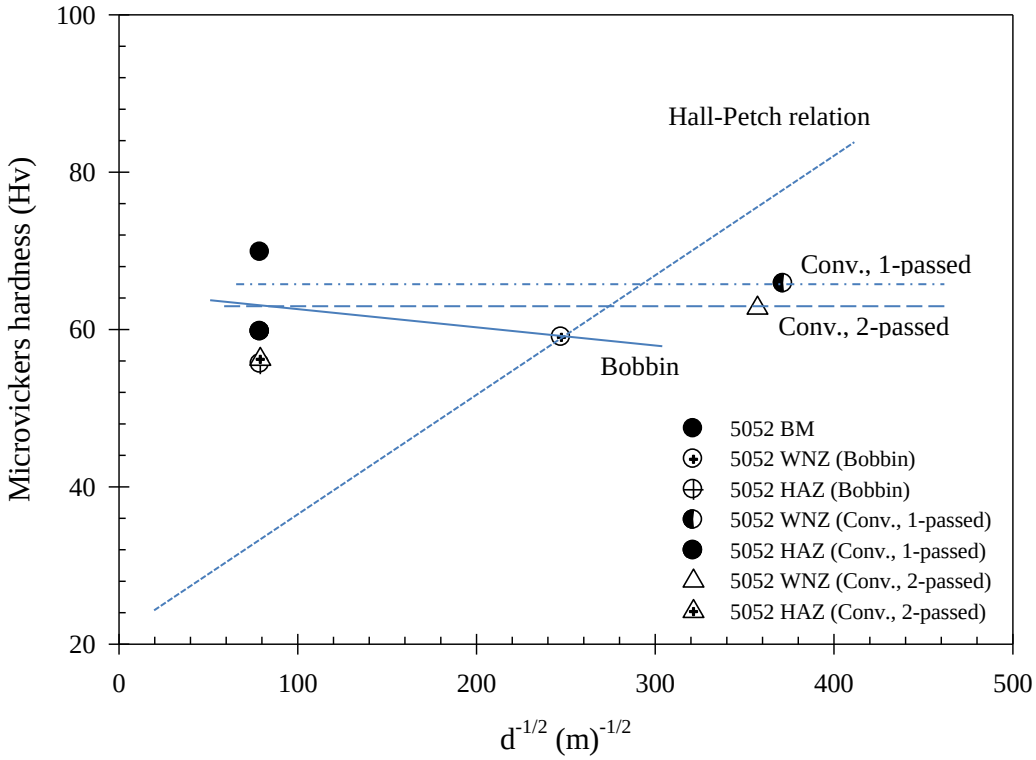


Fig. 2.19 Relation between microvickers hardness and grain size.

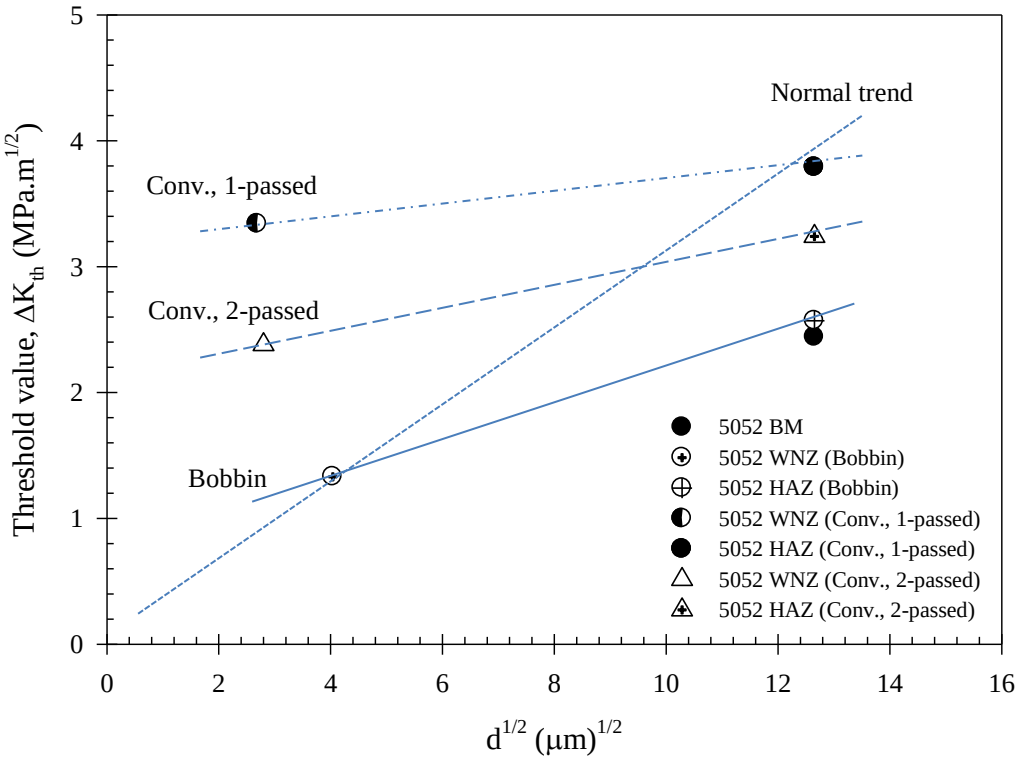


Fig. 2.20 Relation between threshold stress intensity factor range and grain size.

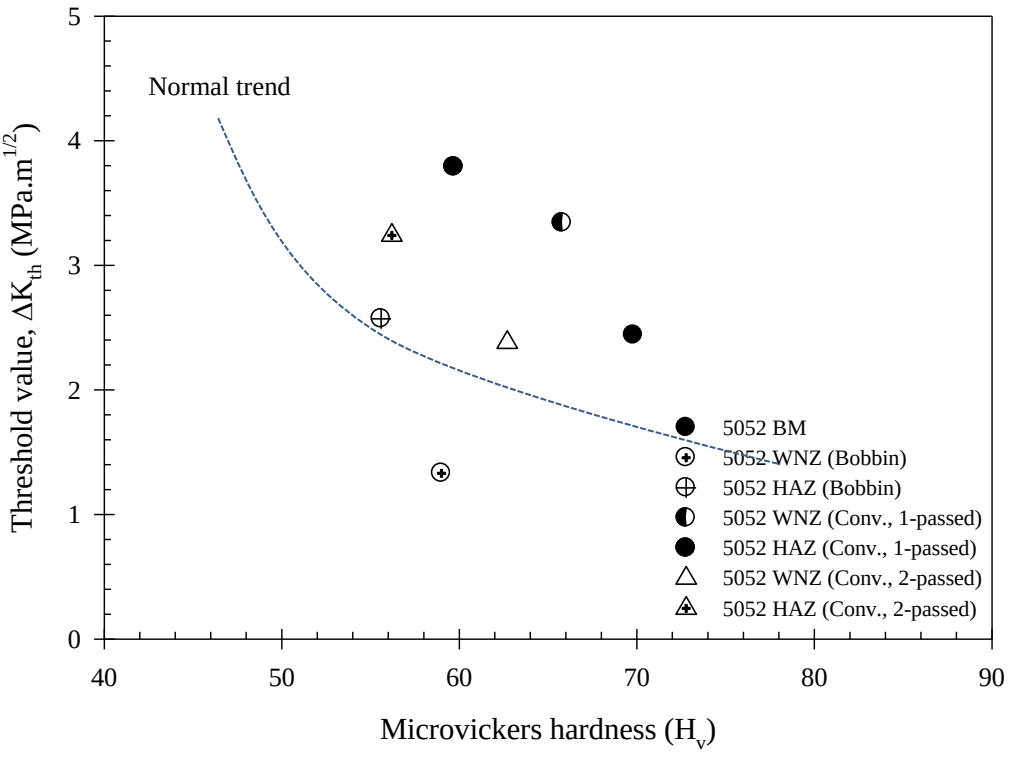


Fig. 2.21 Relation between threshold stress intensity factor range and microvickers hardness.

Table 2.4 Relationship between $\Delta K_{th}$, hardness and grain size.

| Materials | $\Delta K_{th}$ (MPa√m) | Hardness (Hv) | Observed Grain Size (μm) | $\Delta K_T$ (MPa√m) | Estimated Cyclic PZS at $\Delta K_T$ (μm) |
|---|---|---|---|---|---|
| 5052 BM | 2.44 | 69.8 | 160.00 | 2.78 | 11.15 |
| 5052 WNZ (Bobbin) | 1.33 | 59.0 | 16.32 | 1.62 | 9.25 |
| 5052 HAZ (Bobbin) | 2.57 | 55.6 | 160.00 | 2.77 | 26.91 |
| 5052 WNZ (Conv., 1-Passed) | 3.34 | 65.8 | 7.27 | 3.89 | 32.74 |
| 5052 HAZ (Conv., 1-Passed) | 3.79 | 59.7 | 160.00 | 4.51 | 42.81 |
| 5052 WNZ (Conv., 2-Passed) | 2.38 | 62.7 | 7.84 | 3.18 | 20.16 |
| 5052 HAZ (Conv., 2-Passed) | 3.24 | 56.2 | 160.00 | 3.74 | 29.36 |

### 2.3.6 Effect of microstructural dimension on fatigue crack growth characteristic

As considered on microstructural dimension, fatigue crack growth behavior in near-threshold region and Paris region can be described in different mechanisms. The transition behavior between near-threshold and Paris region was explained by the correlation of microstructural dimension and plastic zone size ahead the crack tip during crack propagation. At near-threshold region, the region that cyclic plastic zone size (CPZS) during crack propagation was less than microstructural dimensions or grain size which so called microstructural sensitive due to limited number of slip systems only one or few slip planes which are operative at crack tip at low level of stress intensity factor range. Microstructural boundaries act as barrier to restrict or retard the slip spreading across to the adjacent grains. Crack path was deflected at grain boundaries and degree of deflection or roughness is comparable to grain size. Larger grain sizes tend to higher FCG resistance due to large deflection and increase in surface roughness which causes to increase in crack closure due to crack faces contact. In according to mismatching of rough crack faces, the Mode I (opening mode) and Mode II (sliding mode) crack growth are in cooperated in this region [29]. Previous studies [29-32] suggested that fine or small grain size is less resistance to FCG compared to large grain size at near-threshold region. In Paris region, the region that CPZS during crack propagation larger than grain size, the high local stress concentrations induced slip on several sets of crystal planes in each grain and also slip spreads across barriers like grain boundaries. The plastic deformation is therefore homogeneous and the fatigue crack propagates by a continuum mechanism.

In near-threshold region, increasing in grain size or decreasing in yield strength of materials generally results in a marked reducing near-threshold FCG rate and increasing threshold value, $\Delta K_{th}$. In this study, in case of the HAZ in all FSW processes, which similar grain size with the base material but lower in yield strength showed lower near-threshold FCG rate and higher threshold value, $\Delta K_{th}$ comparing with the base material. In case of the WNZ of bobbin type FSWed, even if lower in yield strength/hardness but smaller grain size showed higher near-threshold FCG rate and lower $\Delta K_{th}$ compared to the base materials as discussed in earlier. In case of bobbin type FSW material, the $\Delta K_{th}$ was more significantly controlled by grain size. In case of conventional FSWed, the WNZ which smaller grain size showed higher near-threshold FCG rate and lower $\Delta K_{th}$ comparing with the HAZ. However, the WNZ of conventional FSWed showed higher $\Delta K_{th}$ comparing with the BM. As discussed in earlier, in case of welded structures in

conventional FSWed, the threshold stress intensity factor was controlled by grain size. At near-threshold region, transgranular fracture mechanism was observed in this fatigue crack growth region in all cases of the BM, the WNZ and the HAZ in all FSW processes. It might be explained that due to the PZS ahead the crack tip during crack propagate in this region was less than the grain size and slip cannot spread encompassed the adjacent grains and then resulted in transgranular fracture occurred.

In Paris region, the fracture surfaces of the BM and the HAZ was observed transgranular fracture mechanism. In contrast, when the PZS during crack propagation in this region larger than the grain size, the fine-equiaxed DRX grains of WNZ in all FSW processes changed in fracture mechanism from transgranular as observed at near-threshold region to mixed mode (intergranular + transgranular) at Paris region. Moreover, intergranular crack growth observed only at higher ΔK levels when the PZS ahead the crack tip expected in order of or larger than the grain size of DRX grains in WNZ. However, when the PZS is smaller than the grain size, the slip cannot encompass or across the grain boundaries and then resulted in transgranular fracture.

In this study, the transition behavior did not well match when correlated between grain size and plastic zone size at the transition stress intensity factor range, $\Delta K_T$ as shown in Table 2.4. It might be suggested that not only grain size influenced the correlation in transition behavior in this study but also other microstructural dimensions would be a factor to correlate transition behavior such as dispersoid spacing, sub-grain size and etc.

### 2.3.7 Crack closure

In order to evaluate the influence of crack closure, FCG curves of different FSW processes in the both of WNZ and HAZ comparing with the BM were investigated by using effective stress intensity factor range, $\Delta K_{eff}$ as shown in Fig 2.22.

The difference in FCG resistance of different FSW processes and weld regions with comparing to the BM in crack growth curve arranged by effective stress intensity factor range, $\Delta K_{eff}$ showes in Fig 2.22. The FCG curves of WNZs and HAZs was well coincided into single curve when the curves were arranged by effective stress intensity factor range, $\Delta K_{eff}$. It can be mentioned that the difference in FCG resistance of the WNZs and the HAZs in different FSW processes were mainly due to different in crack closure. However, the BM can be arranged well by $\Delta K_{eff}$ only at high-ΔK region but at near-threshold region

was lower FCG resistance and lower $\Delta K_{th}$. Higher hardness and yield strength in the BM comparing with WNZs and HAZs was observed in this study. Hardness reduction in WNZ and HAZ was reported due to dissolution and coarsening of precipitates occurred during FSW processing [1, 23-26]. Previous study [28] reported that the materials which higher hardness and yield strength showed lower threshold stress intensity factor range. However, in this study, hardness and $\Delta K_{th}$ did not show correlation trend. It can be speculated that the FSWed materials was changed in microstructure characteristics form the BM that might be result in slightly different in $\Delta K_{th}$ even when arranged by $\Delta K_{eff}$ as shown in Fig. 2.22. Crack closure level in the WNZ and the HAZ of single-passed conventional FSWed was observed higher than double-passed conventional FSWed and FSWed joint joined by using a bobbin type tool as shown in Fig. 2.23 and Fig. 2.24 respectively. Lower heat input FSW process showed higher in crack closure level. The effect of FSW process on crack closure level was significantly pronounced in the WNZ compared to the HAZ. However, the HAZ shows higher crack closure level than that observed in the WNZ.

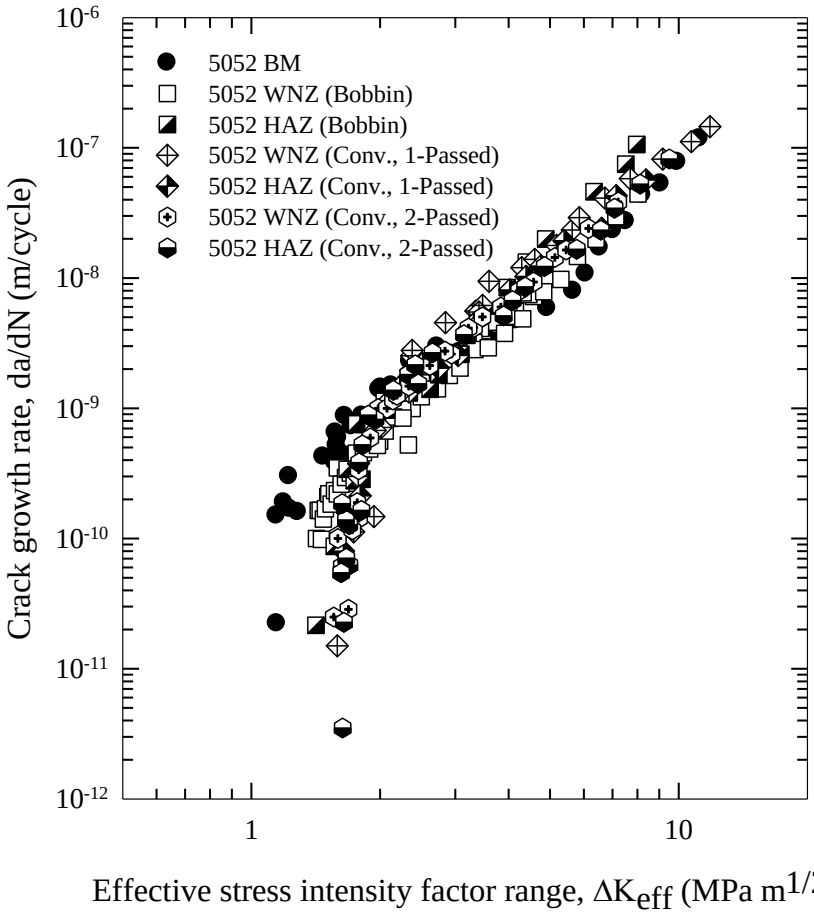


Fig. 2.22 Crack growth rate versus effective stress intensity factor range of FSWed 5052 joint joined by bobbin type tool and single-passed and double-passed by conventional FSW tool.

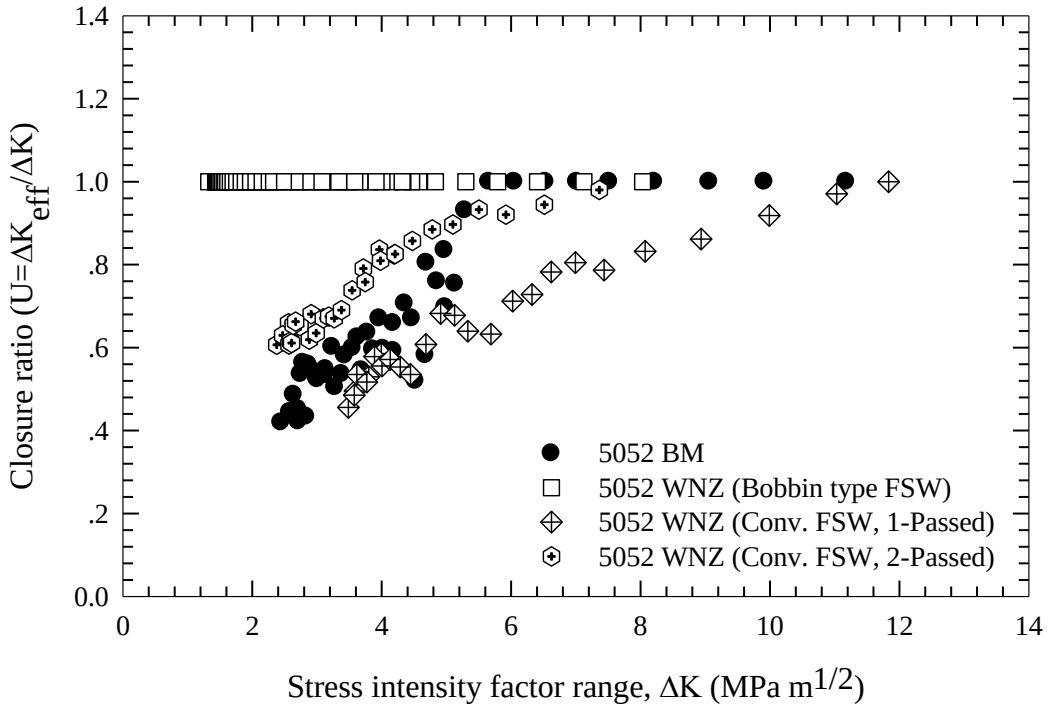


Fig. 2.23 Comparison of FSW processes on relationship between crack closure ratio and stress intensity factor for WNZ.

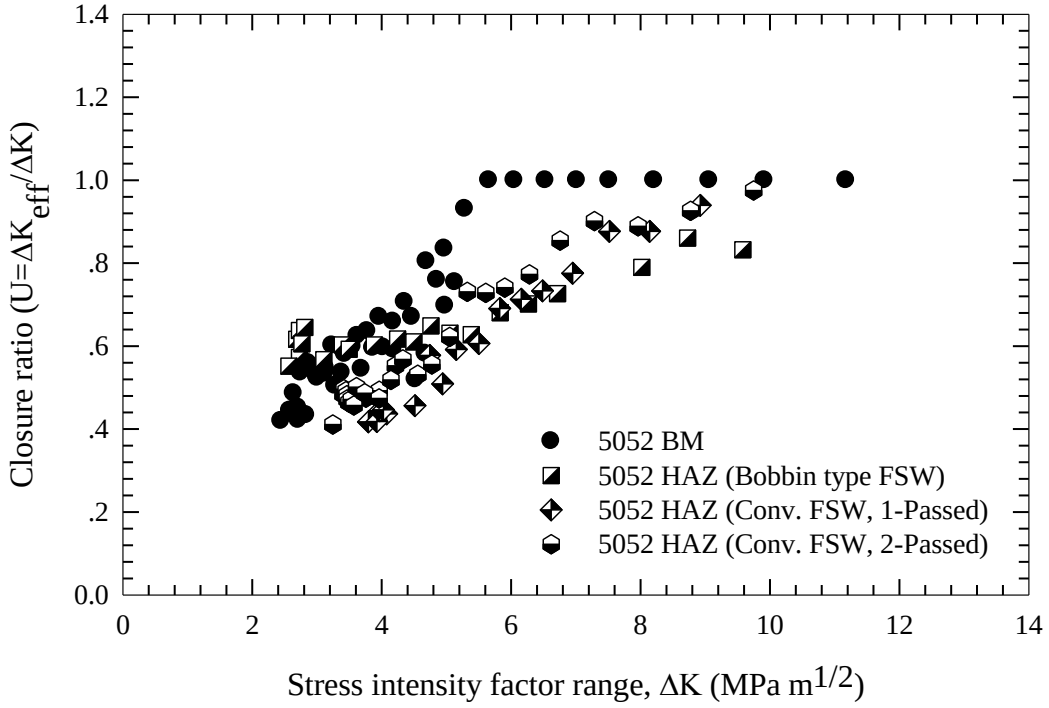


Fig. 2.24 Comparison of FSW processes on relationship between crack closure ratio and stress intensity factor for HAZ.

## 2.4 Conclusions

(1) Heat input during FSW process of single-passed conventional FSW was lower than double-passed conventional FSW and bobbin type FSW respectively.

(2) Weld microstructure in FSWed joints joined by using a bobbin type tool was produced as symmetry between upper and lower sides in thickness direction of the joints. Different in material flow pattern in weld regions due to stirring action of the tools have been observed among of three different kinds of FSW processes.

(3) Tensile properties and hardness distribution in welded region was lower than base materials in all FSW processes. Regardless of the joint joined by conventional FSW tool with lower heat input showed higher tensile properties compared to FSWed joint joined by using a bobbin type tool. Hardness distribution in welded regions of single-passed conventional FSWed was higher than that of double-passed conventional FSWed and FSWed joint joined by using a bobbin type tool respectively. The lowest hardness was located in the HAZ in all FSWed joints. Single-passed conventional FSWed show hardness profile shape differs from double-passed conventional FSWed and FSWed joint joined by using a bobbin type tool which observed as “W-shape like profile”.

(4) Dynamic recrystallized grain size in the WNZ of conventional FSWed which lower heat input during FSW process was smaller than that observed in FSWed joint joined by using a bobbin type tool.

(5) Different FSW process and heat input show different in FCG behavior. Lower heat input in single-passed conventional FSWed showed higher FCG resistance compared to FCG resistance of double-passed conventional FSWed and FSWed joint joined by using a bobbin type tool respectively in the both of WNZ and HAZ.

(6) In case of FSWed joint joined by using a bobbin type tool, FCG resistance of the WNZ was lower than that of the BM and the HAZ at near-threshold region. At high $\Delta K$ region, WNZ was almost the similar FCG resistance to the both BM and HAZ. In case of single-passed conventional FSWed, FCG resistance of the WNZ was higher than that of the BM but lower FCG resistance than the HAZ at near-threshold region. At high $\Delta K$ region, the WNZ of single-passed conventional FSWed was the similar FCG resistance to the both BM and HAZ. In case of double-passed conventional FSWed, FCG resistance of the WNZ was similar to the BM and lower than that of the HAZ at near-threshold region. In high $\Delta K$ region, FCG resistance of the BM and the HAZ in double-passed conventional FSWed was

almost the similar, but in the WNZ showed slightly lower FCG resistance compared to the BM and the HAZ.

(7) In FSWed materials, grain size is a main factor to control the threshold stress intensity factor range.

(8) FCG curves obtained in different welded regions and different FSW processes were coincided into a single curve when the curves were arranged by $\Delta K_{eff}$. It can be mentioned that the difference in FCG behavior in different welded region and different in FSW processes is mainly due to difference in crack closure behavior even if there are different in heat input generated during the FSW process.

## 2.5 References


[1] R.S. Mishra and Z.Y. Ma, Mat. Sci. Eng. R. 50 (2005) 1-78.

[2] L.E. Murr, J. Mat. Eng. Perform. 19 (2010) 1071-1089.

[3] A.L. Biro, B.F. Chenelle and D.A. Lados, Met. Mat. Tran. B. 43B (2012) 1622-1636.

[4] M. Ericsson and R. Sandstrom, Int. J. Fat. 25 (2003) 1379-1387.

[5] V. Fahimpour, S.K. Sadrnezhaad and F. Karimzadeh, Met. Mat. Trans. A. 44A (2013) 2187-2195.

[6] H. Fujii, L. Cui, M. Maeda and K. Nogi, Mat. Sci. Eng. A. 419 (2006) 25-31.

[7] Y. Li, L.E. Murr and J.C. McClure, Mat. Sci. Eng. A. 271 (1999) 213.

[8] Z. Y. Ma, R.S. Mishra and M.W. Mahoney, Acta Mater. 50 (2002) 4419.

[9] Y.J. Kwon, N. Saito and I. Shigematsu, J. Mater. Sci. Lett. 21 (2002) 1473.

[10] Y.S. Sato, M. Urata and H. Kokawa, Met. Mat. Trans. A. 33A (2002) 625.

[11] R.D. Fu, J. F. Zhang, Y. J. Li, J. Kang, H. J. Liu and F.C. Zhang, Mat. Sci. Eng. A. 559 (2013) 319-324.

[12] V. Dixit, R. S. Mishra, R.J. Lederich and R. Talwar, Sci. Technol. Weld. Joining 12 (4) (2007) 334-339.

[13] W.J. Arbegast, in: Proceedings of the Hot Deformation of Aluminum Alloys III, San Diego, 2003, pp. 313-319.

[14] Aluminum: Properties and Physical Metallurgy, Edited by J.E. Hatch, ASM, 1984.

[15] Y.S. Sato, Y. Sugiura, Y. Shoji, S.H.C. Park, H. Kokawa and K. Ikeda, Mat. Sci. Eng. A. 369 (2004) 138-143.

[16] Z. Zhang, X. Yang, J. Zhang, G. Zhou, X. Xu and B. Zou, Materials and Design 32 (2011) 4461-4470.

[17] S.H. Avner, Introduction to Physical Metallurgy, 2nd edition, McGraw-Hill, 1974.

[18] Y.S. Sato, F. Yamashita, Y. Sugiura, S.H.C. Park, H. Kokawa, Scripta Materialia 50 (2004) 365-369.

[19] N.T. Kumbhar, S.K. Sahoo, I. Samajdar, G.K. Dey and K. Bhanumurthy, Materials and Design 32 (2011) 1657-1666.

[20] ASTM E 647-08, Annual Book of ASTM standards, 2008.

[21] M. James and M. Mahoney, in: Proceedings of the First International Symposium on Friction Stir Welding, Thousand Oaks, CA, USA, June 14-16, 1999.

[22] P. Upadhyay and A.P. Reynolds, Mat. Sci. Eng. A. 558 (2012) 394-402.

[23] G. Liu, L.E. Murr, C.S. Niou, J.C. McClureand F.R. Vega, Scripta Materialia 37 (1997) 355.

[24] Y.S. Sato, H. Kokawa, M. Enmoto and S. Jogan, Met. Mat. Trans. A. 30 (1999) 2429.

[25] B. Heinz and B. Skrotzki, Metall. Mater. Trans. B. 33 (6) (2002) 489.

[26] K.V. Jata, K.K. Sankaran and J.J. Ruschau, Met. Mat. Trans. A. 31 (2000) 2181.

[27] Y.S. Sato, S.H.C. Park and H. Kokawa, Met. Mat. Trans. A. 32A (2001) 3033-3041.

[28] Y. Mutoh and V.M. Radhakrishnan, J. Eng. Mat. Tech., 108 (1986) 174-178.

[29] S. Suresh, Fatigue of Materials, 2nd edition, Cambridge University Press, 1998.

[30] K. Minakawa, G. Levan and A.J. McEvily, Met. Mat. Trans. A, 17 (1986) 1787-1795.

[31] R.D. Carter, E.W. Lee, E.A. Starke, Jr. and C.J. Beevers, Met. Trans. A, 15 (1984) 555-563.

[32] M. Janssen, J. Zuidema and R. Wanhill, Fracture Mechanics, 2nd edition, Spon Press, 2002.

# Chapter 3

# Fatigue crack growth behavior of FSWed 5052, 6N01 and 7N01 similar aluminum alloy joints joined with a bobbin type tool

Fatigue crack growth behavior at WNZ and HAZ in FSWed similar material joints joined by using a bobbin type tool in 5052, 6N01 and 7N01 aluminum alloys were investigated and compared to that of the BM. Different FCG behavior was found in FSWed joints with different aluminum alloys. The results showed that difference in FCG resistance was significantly observed in near threshold region, FCG resistance in WNZ of FSWed 5052 and 6N01 joints was lower than that in the BM and the HAZ. In contrast, FCG resistance in WNZ of FSWed 7N01 joint was higher than that in the BM and the HAZ. Difference in FCG behavior at different weld region was mainly due to difference in crack closure behavior in the FSWed joints. Grain size in the WNZ was dominant on threshold stress intensity factor range.

## 3.1 Introduction

Friction stir welding (FSW) is known as a solid state joining process and has been widely applied in currently to join high strength aluminum alloys, dissimilar materials and other materials to overcome the difficulty in conventional fusion welding [1,2,3]. In FSW process, rotating tool is inserted into butt-edges of two plates and induces plastic deformation with material flowing then results in joining the plates together along the tool travelling. According to joining process of FSW, materials can be joined in solid state due to mechanical stirring by the rotating tool without the melting. In the most of previous studies, FSW was carried out by penetrating a rotating tool from one side. In this case, microstructure obtained in welded area is un-symmetry in the thickness direction and it could be difficult to joint thicker plates in one process. On the other hand, using bobbin type tool can show new advantages which will be different from conventional FSW such as suppressing formation of root flaws, low distortion of welded plate, symmetry welded structures and able to join a thick plate in single process.

Fatigue crack growth (FCG) behaviors of FSWed joints joined by using a conventional tool have been reported previously. For example, G. Bussu and P.E. Irving indicated that FCG behavior in FSWed 2024-T351 joint was sensitive to both direction and position of crack propagating [4]. It was also suggested that FCG behavior of FSWed joints was strongly affected by the weld residual stress and microstructure, but was not much affected by change in hardness. K.V. Jata et al. investigated FCG behavior in FSWed 7050-T7451 joints and showed that decrease in FCG resistance in WNZ was due to intergranular failure. They also suggested that effect of residual stresses was more dominant on increase in FCG resistance of HAZ compared to that of the microstructure improving [5]. T.H. Tra et al. studied FCG behavior in FSWed AA6063-T5 joint and found that the different FCG resistance was caused by microstructural effects around the welded zone [6]. While the residual stress was remarkable in the shoulder limit areas but had a minor effect on the FCG behavior. There are very few works to study FCG behavior of FSWed joint taking crack closure behavior into account. S. Kim et al. reported that FCG resistance in WNZ of FSWed 5083-H32 and 6061-T651 joints were higher than FCG resistance in the BM. It was suggested that compressive residual stress in WNZ decreased effective stress intensity factor range, $\Delta K_{eff}$ and resulted in reduction of FCG rate [7]. There are also other reports on FCG behavior of FSWed joint, however, it might be difficult to systematically understand effect of each factor which possibly affects on FCG behavior.

In this study, different aluminum alloys plates, such as 5052, 6N01 and 7N01 aluminum alloys were joined by using a bobbin type tool. Fatigue crack growth (FCG) tests were carried out with crack closure measurement at WNZ, HAZ and BM of the FSWed joints to investigate the FCG behavior in different welded regions for different aluminum alloys.

## 3.2 Experimental Procedure

Rolled 5052, extruded 6N01 and extruded 7N01 aluminum alloy plates were used for joining in this study. Microstructure observations of the materials used will be shown in later. Plates of the alloys with thickness of 6 mm were welded parallel to the rolling/extrusion direction by FSW using a bobbin type tool. The tool with shoulder diameter of 20 mm has a pin with diameter of 12 mm and distance between the shoulders is 5.8 mm. Welding conditions were selected according to result of a trial test to obtain appropriate conditions. Tool rotation speed and traveling speed in FSW for 5052 alloy was 300 rpm with 200 mm/min, for 6N01 alloy was 500 rpm with 400 mm/min, for 7N01 alloy was 300 rpm with 200 mm/min. Chemical compositions of base material aluminum alloys used in this study were shown in Table 3.1. Table 3.2 shows tensile properties of the base materials in direction perpendicular to the rolling/extrusion direction and of the FSWed joints in direction perpendicular to the welding line. Gage lengths of the tensile specimens were 50 mm for the base metal and the joints.

Compact-tension (CT) specimen following ASTM E 647-08 [8] with a thickness of 4 mm and a width of 32 mm were cut from the base materials and the FSWed plates as shown in Fig. 3.1. Fatigue crack growth direction was parallel to the rolling/extrusion direction in the base material and the welding direction in the joints. In case of the FSWed joint specimen, fatigue pre-crack was introduced at the weld center line in WNZ and at the lowest hardness position in HAZ. Actual locations of the pre-crack introduced in HAZ were 11 mm, 15 mm and 23 mm far from the weld center line for FSWed 5052, 6N01 and 7N01 joints, respectively.

Fatigue crack growth test was conducted by using an electro servo-hydraulic fatigue testing machine under constant stress amplitude condition according to ASTM E 647-08 [8] in laboratory air.

Table 3.1 Chemical compositions of base materials aluminum alloys used (Wt%).

| Alloy | Si | Mg | Zn | Fe | Mn | Cu | Ti | Cr | Zr | V |
|---|---|---|---|---|---|---|---|---|---|---|
| 5052 | 0.10 | 2.53 | 0.01 | 0.29 | 0.04 | 0.03 | 0.02 | 0.19 | - | - |
| 6N01 | 0.58 | 0.66 | 0.01 | 0.09 | 0.08 | 0.11 | 0.01 | 0.06 | - | - |
| 7N01 | 0.08 | 1.38 | 4.49 | 0.21 | 0.37 | 0.18 | 0.02 | 0.10 | 0.14 | 0.01 |

Table 3.2 Tensile properties of base materials and FSWed joints.

| Specimen | 0.2% Proof Strength (MPa) | Tensile Strength (MPa) | Elongation (%) |
|---|---|---|---|
| 5052 BM | 157 | 229 | 16.20 |
| 5052 FSW | 102 | 202 | 13.70 |
| 6N01 BM | 256 | 285 | 9.05 |
| 6N01 FSW | 128 | 185 | 8.65 |
| 7N01 BM | 383 | 431 | 14.20 |
| 7N01 FSW | 269 | 308 | 3.45 |

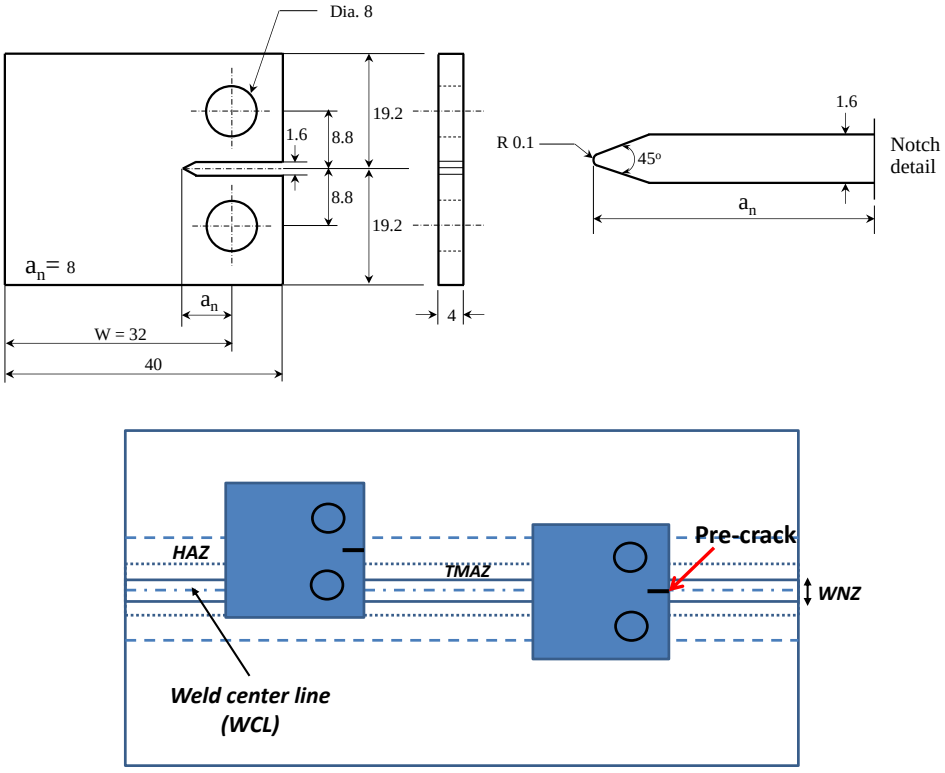


Fig. 3.1 Geometry of CT specimen used and FSWed specimen layout (in mm).

Fatigue loading with stress ratio of 0.1 and frequency of 20 Hz was applied with sinusoidal wave form. Crack length was measured in both sides of the specimen by using

traveling microscopes during the test. Stress intensity factor range (ΔK) for CT specimen was calculated according to ASTM E 647-08 [8]. In order to investigate crack closure behavior, cyclic load-strain curve was measured under frequency of 2 Hz during the test by using a strain gage with gage length of 2 mm attached at the back face of the specimen. Crack opening load to calculate stress intensity factor at crack opening ($K_{op}$) was determined by unloading elastic compliance method. Effective stress intensity factor range, $\Delta K_{eff}$ was calculated as $\Delta K_{eff} = K_{max} - K_{op}$, where $K_{max}$ is stress intensity factor for the maximum applied stress. Fracture surfaces of FCG test specimens were observed by using a scanning electron microscope after the test.

## 3.3 Result and Discussions

### 3.3.1 Weld structure and hardness distribution

Figure 3.2 shows the welded structures in the cross section perpendicular to the welding direction. Welded structures in FSWed 5052, 6N01 and 7N01 aluminum alloy joints are classified into three different regions, WNZ, HAZ and thermo-mechanically affected zone (TMAZ). Those regions were observed as symmetry in upper and lower sides of the joints, because of that the weld regions were formed by using a bobbin type tool. All FSWed joints showed lower in yield and tensile strength comparing to the base metals as seen in Table 3.1. Hardness distributions at mid-thickness in the cross section perpendicular to the welding direction are shown in Fig. 3.3. Microvickers hardness test was carried out with applied load of 200 gf and holding time of 15 s. The similar W-shape profile as shown in Fig. 3.3 was also observed in other reports [9,10,11,12]. Hardness in welded region was lower than that of the base metal in all FSWed joints. FSWed 7N01 joint showed higher hardness value and wider welded region compared to FSWed 6N01and 5052 joints. The lowest hardness was obtained in HAZ for the all joints at 11 mm, 15 mm and 23 mm from weld center line for FSWed 5052, 6N01 and 7N01 joints respectively. WNZ and HAZ were bounded by TMAZ which observed distorted and elongated grains.

Figure 3.4 shows microstructures of the base materials in three planes, WNZ at the weld center line and HAZ at the lowest hardness regions that crack propagated in this study. Elongated grains structure was observed in all base materials which could be due to rolling and extrusion process. 5052 and 6N01 base materials showed the similar large elongated grains microstructure. In case of 5052 and 6N01 base materials, elongation of grains were significantly observed in L-T and L-S planes which parallel to rolling/extrusion direction

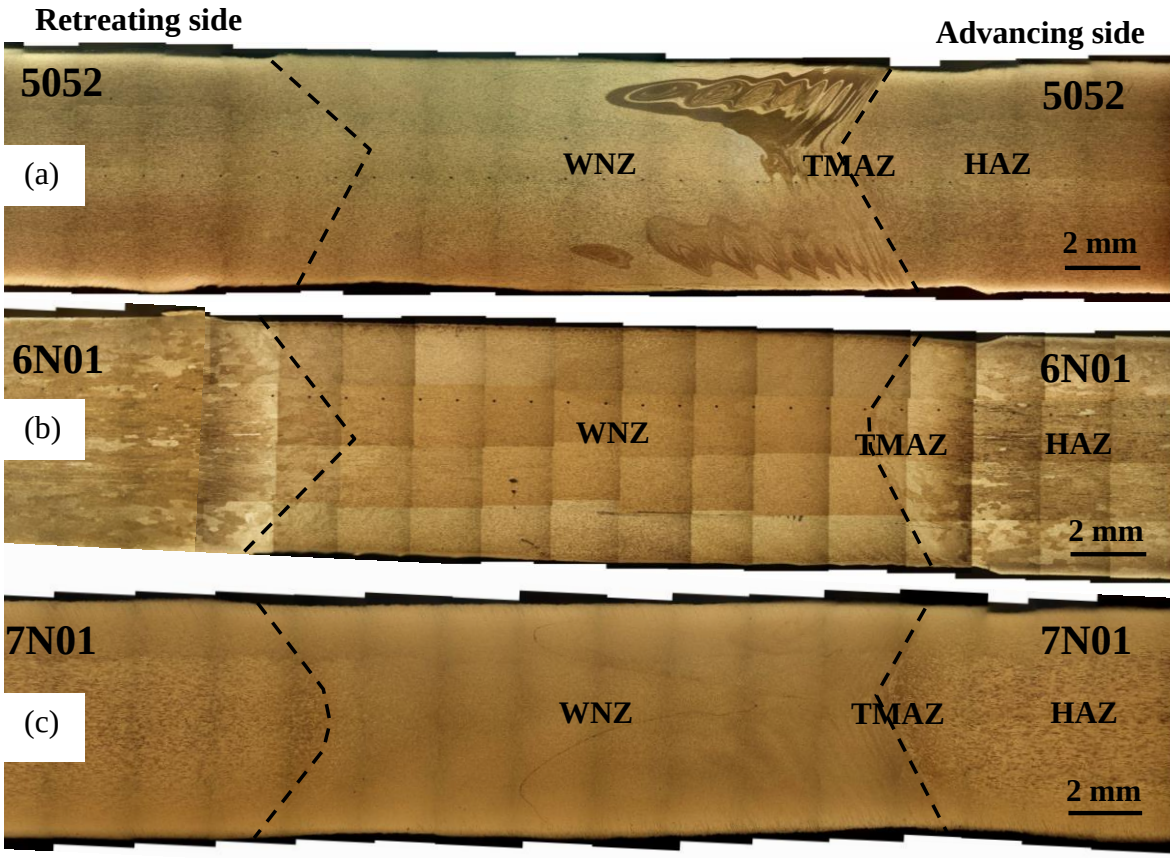


Fig. 3.2 Welded structure in transverse cross-section of FSWed (a) 5052, (b) 6N01 and (c) 7N01 joints.

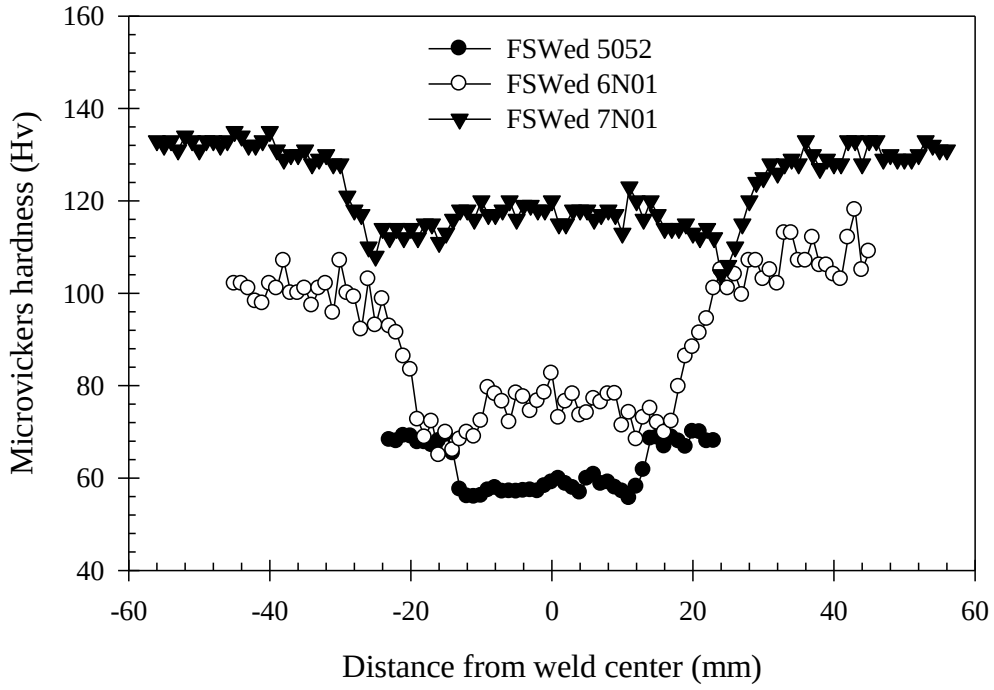


Fig. 3.3 Hardness distribution at mid-thickness position in FSWed 5052, 6N01 and 7N01 joints.

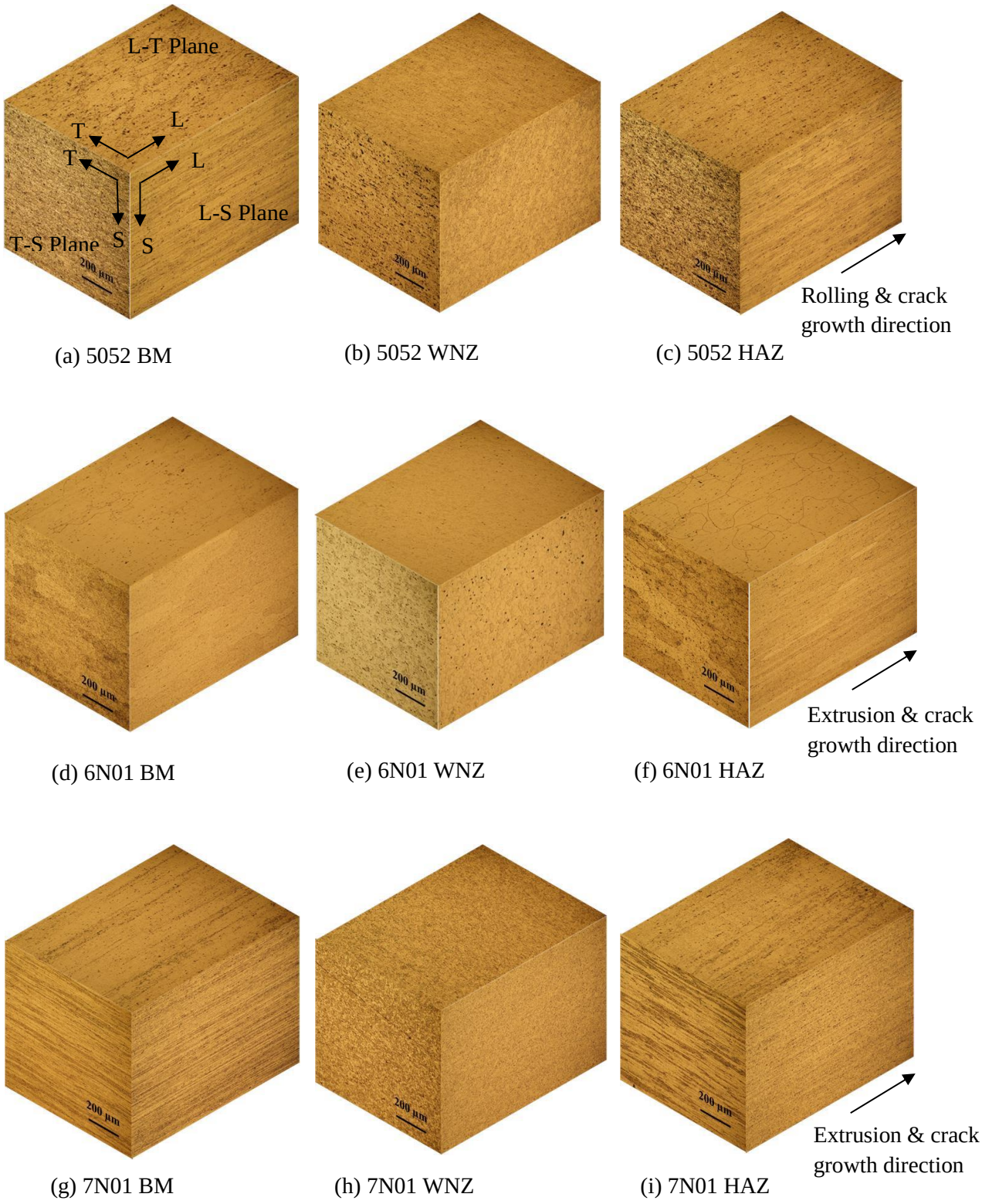


Fig. 3.4 Microstructures of FSWed 5052, 6N01 and 7N01 joints and the base materials.

compared to microstructure in T-S plane. Moreover, extremely elongated band structure was observed in 7N01 base material microstructure in L-T and L-S plane which parallel to

the extrusion direction. In T-S plane of 7N01 BM, it is not significantly observed as L-T and L-S planes, however, elongated band structure is still observed and which is different from 5052 and 6N01 BM T-S plane. Microstructures of the HAZ in all joints are the similar to that of the base materials. Fine equiaxed-recrystallized grains are found in the WNZ in all joints. In the WNZ of FSWed 7N01 joint, much finer equiaxed microstructure is observed which is significantly different from strong elongated band structure observed in both the BM and the HAZ of FSWed 7N01 joint.

### 3.3.2 Fatigue crack growth

Fatigue crack growth curves of FSWed 5052, 6N01 and 7N01 aluminum alloy joints are shown in Fig. 3.5. In case of 5052 alloy, WNZ showed lower FCG resistance near-threshold region compared to the BM and the HAZ. In high ΔK region, FCG resistance of the WNZ is almost the same with that of the BM and the HAZ in 5052 alloy. There was almost no difference in the crack growth behaviors between the BM and the HAZ regardless of ΔK level in 5052 alloy. In case of 6N01 alloy, FCG resistance of the WNZ near threshold region and also higher ΔK region is lower than that of the BM and the HAZ. The lowest FCG resistance was observed in the WNZ in 6N01 alloy. It could be summarized that 5052 and 6N01 WNZ which have the fine-equiaxed dynamic recrystallized grains showed lower FCG resistance near-threshold region compared to FCG resistance of the BM and the HAZ. The similar and contradiction results have also been mentioned in previous studies. T.H. Tra et al. studied FCG behavior in FSWed AA 6063-T5 joint and reported that FCG resistance in the WNZ was lower than that in the BM [6]. S. Kim et al. was studied FCG behavior in FSWed 5083-H32 and 6061-T651 joints. Their result showed FCG resistance in the WNZ was higher than that in the BM. They suggested that compressive residual stress in the WNZ induced higher FCG resistance [7]. On the contrast, in case of 7N01 alloy in the present study, it was different from 5052 and 6N01 joints as mentioned in above, FCG resistance in WNZ was higher than that of the BM and the HAZ at near-threshold region. In higher ΔK region, fatigue crack growth behavior of WNZ is the similar to that of HAZ, however, BM showed slightly higher FCG resistance in 7N01 alloy. K.V. Jata et al. studied FCG behavior in FSWed 7050-T7451 joint and reported that FCG resistance in WNZ was lower than that in the BM and the HAZ in all ΔK regions [5]. In this present study, FCG behavior in 7N01 was strongly affected by the microstructure which will be discussed later.

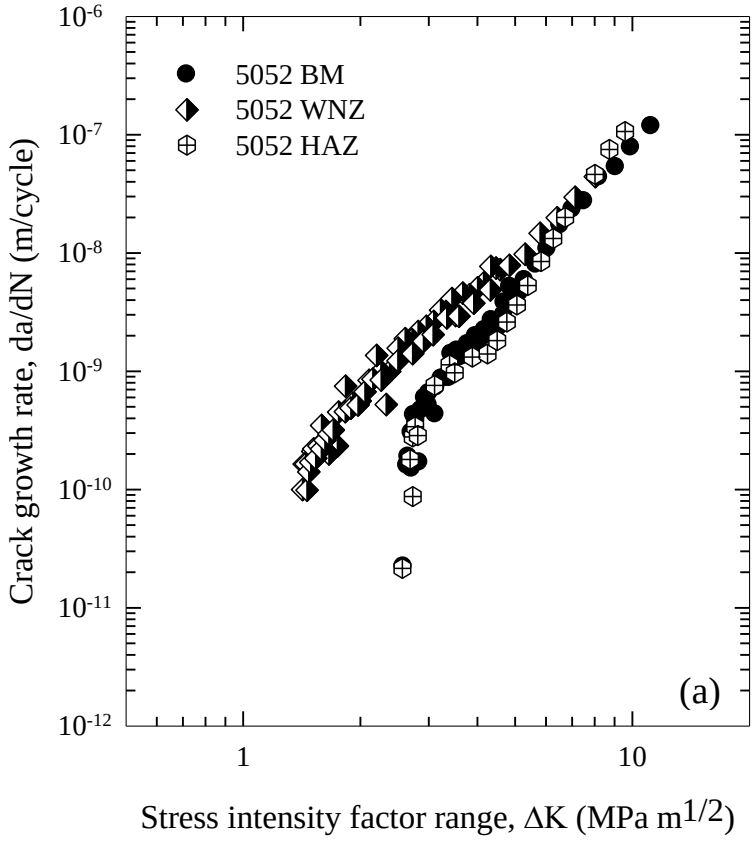
5052 BM
5052 WNZ
5052 HAZ
Crack growth rate, da/dN (m/cycle)
10-6
10-7
10-8
10-9
10-10
10-11
10-12
1
10
(a)
Stress intensity factor range, ΔK (MPa m1/2)

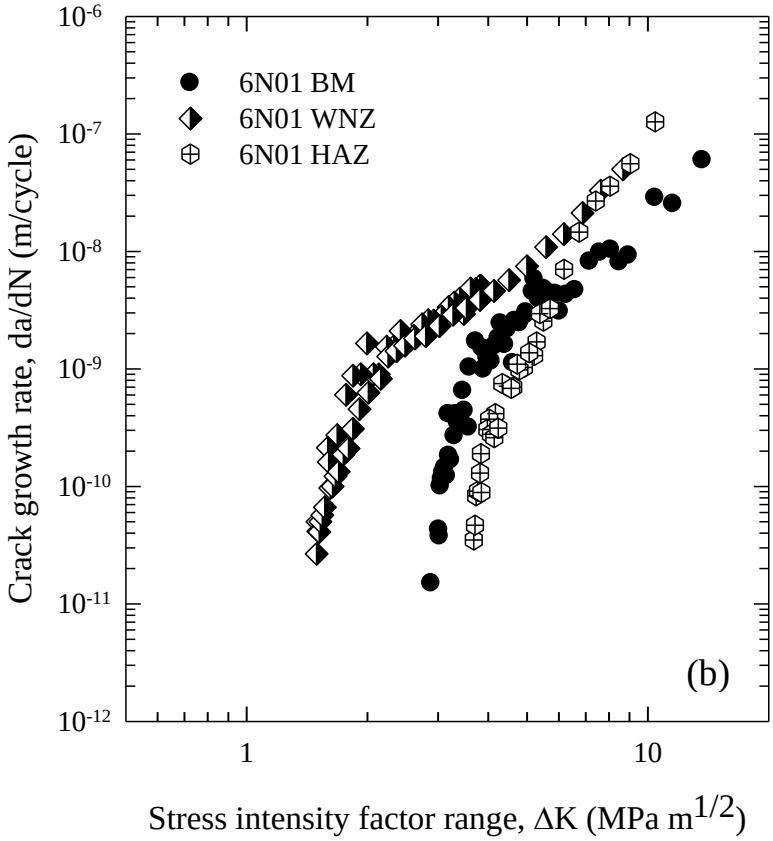
6N01 BM
6N01 WNZ
6N01 HAZ
Crack growth rate, da/dN (m/cycle)
10-6
10-7
10-8
10-9
10-10
10-11
10-12
1
10
(b)
Stress intensity factor range, ΔK (MPa m1/2)

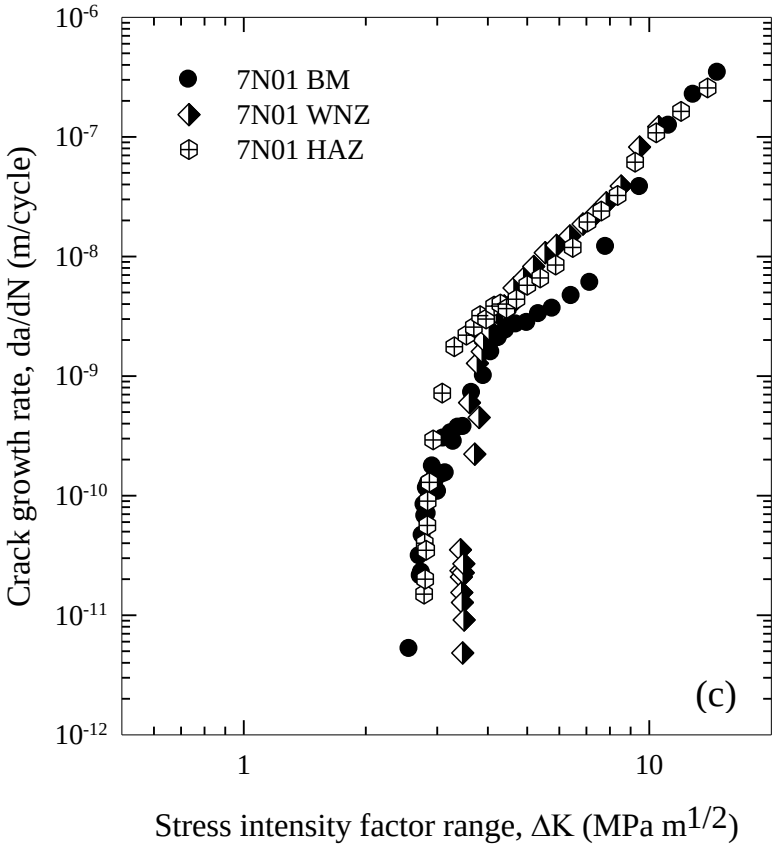


Fig. 3.5 Fatigue crack growth curves of (a) FSWed 5052 joint, (b) FSWed 6N01 joint, (c) FSWed 7N01 joint.

### 3.3.3 Residual stresses investigation

In generally, residual stresses produced in FSW process was very little comparing to conventional fusion welding. However in previous study, many researchers investigated the effect of residual stresses on fatigue crack growth behavior. It is showed that tensile residual stress induced to increase effective stress intensity factor range and increase driving force for crack propagation. In contrast, compressive residual stresses induced to reduce effective stress intensity factor and reduce driving force for crack propagation. They suggested that residual stresses significantly affected on fatigue crack growth behavior of FSWed joints. In this work, residual stresses were measured on CT specimen before fatigue crack growth tests in relation with distance from weld center line for WNZ samples and distance from the notch root in HAZ samples by using X-ray diffractmeter. The results are shown in Fig 3.6, 3.7 and 3.8. In this study, the CT specimens are prepared from the large plate and residual stress might be fewer remains in testing specimens.

Moreover, the residual tresses measurement results in all FSWed joints obtained in this study showed very small value. Therefore, it can be suggested that residual stresses effect in this study is negligible.

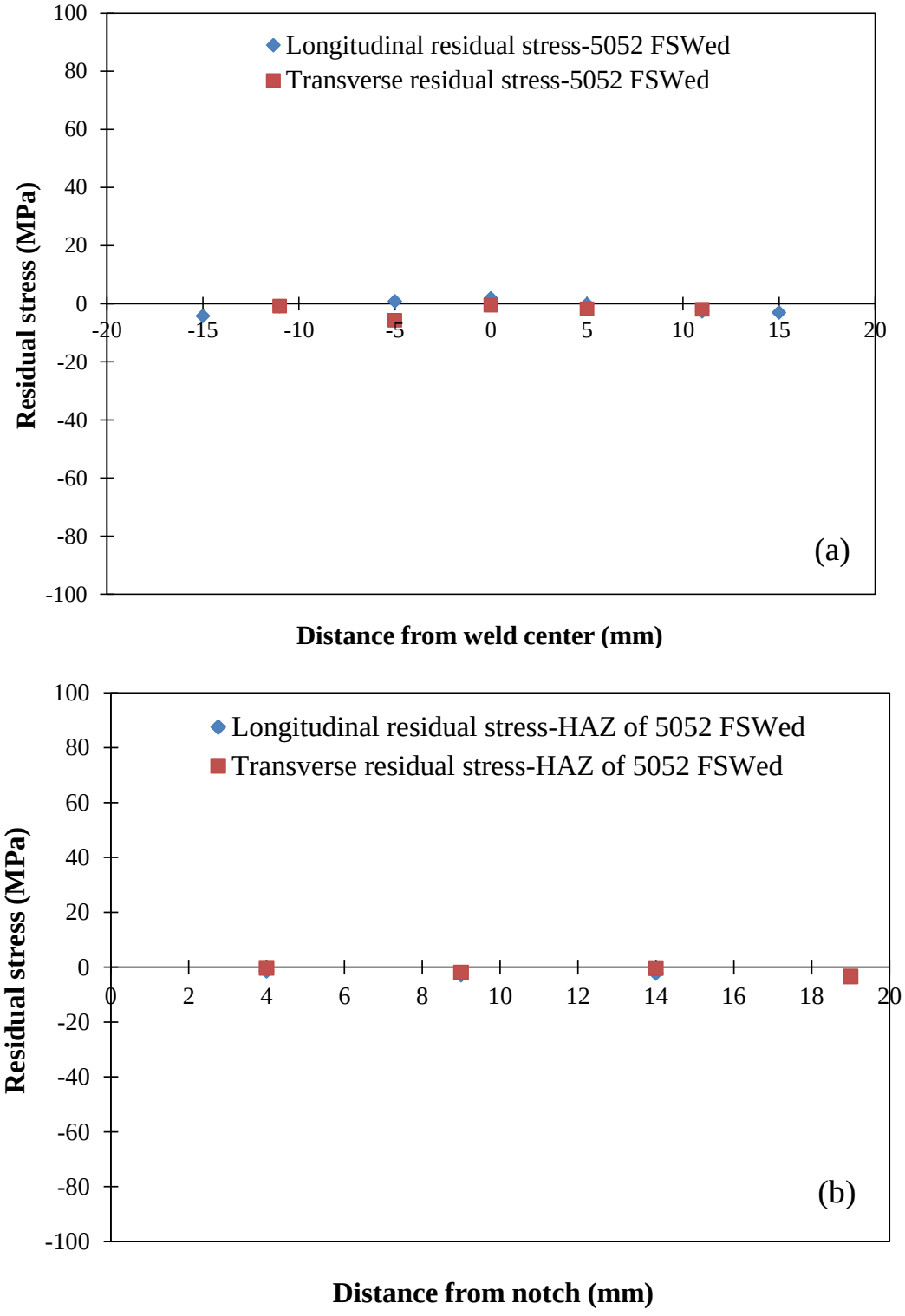


Fig. 3.6 Residual stresses distribution in FSWed 5052 joint (a) relation between residual stresses and distance from weld center line (b) residual stresses along the notch in HAZ sample.

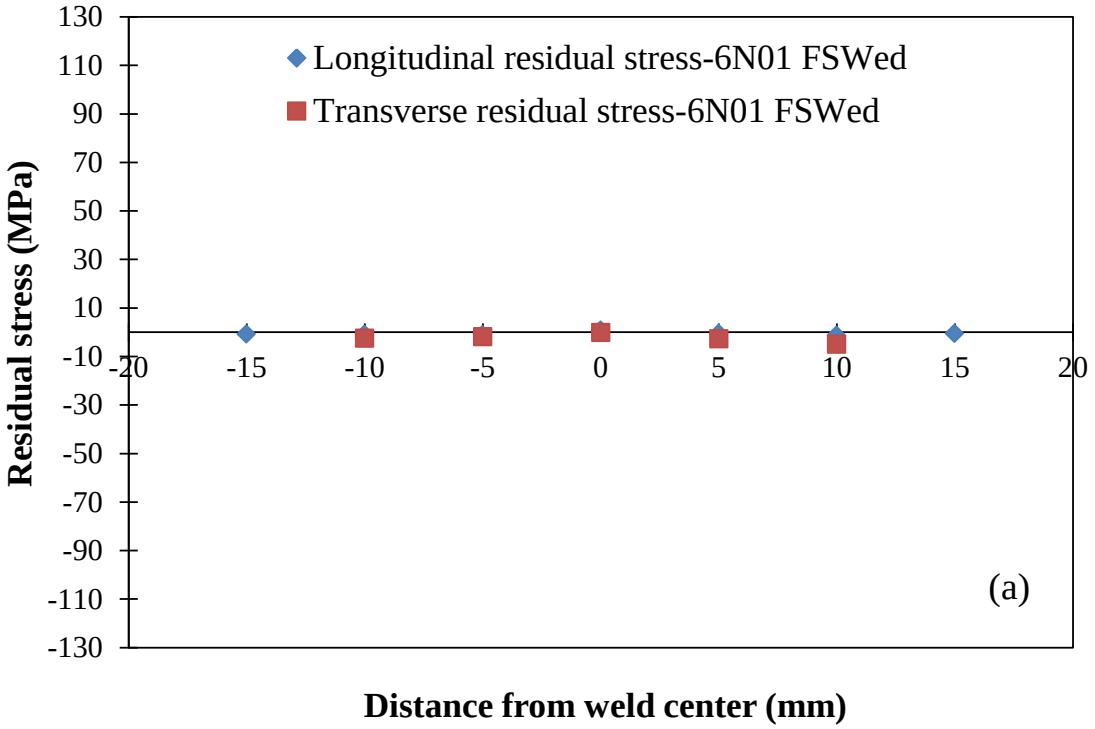


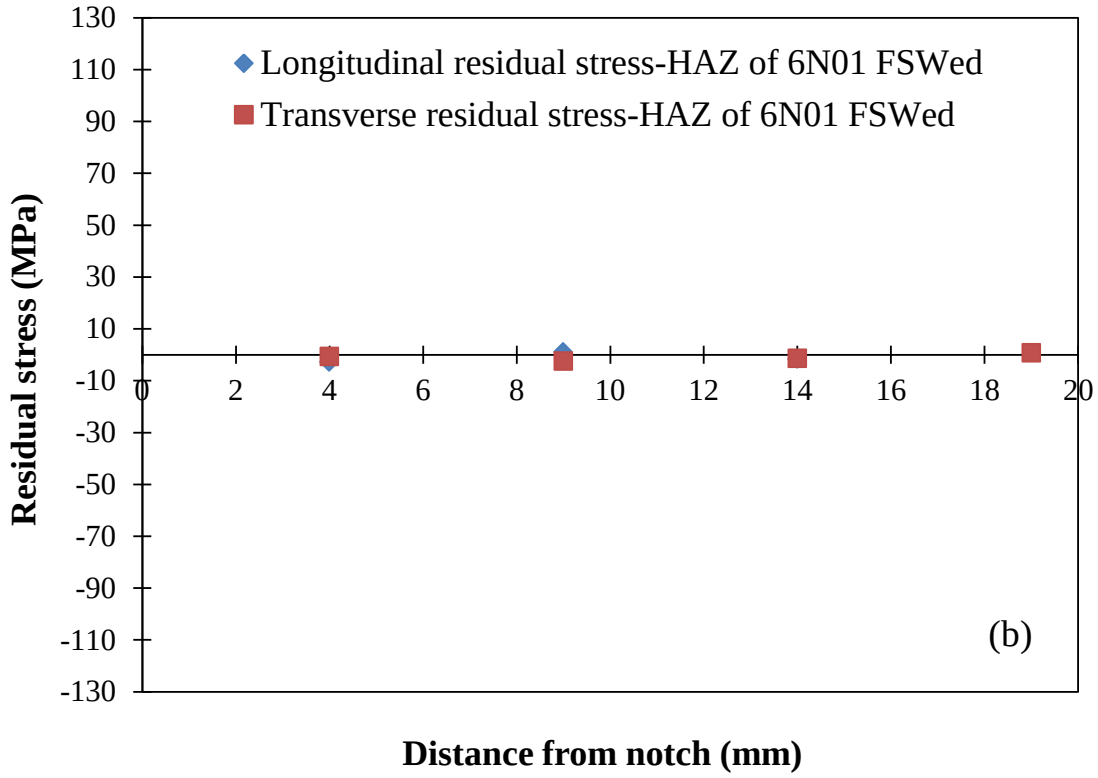


Fig. 3.7 Residual stresses distribution in FSWed 6N01 joint (a) relation between residual stresses and distance from weld center line (b) residual stresses along the notch in HAZ sample.

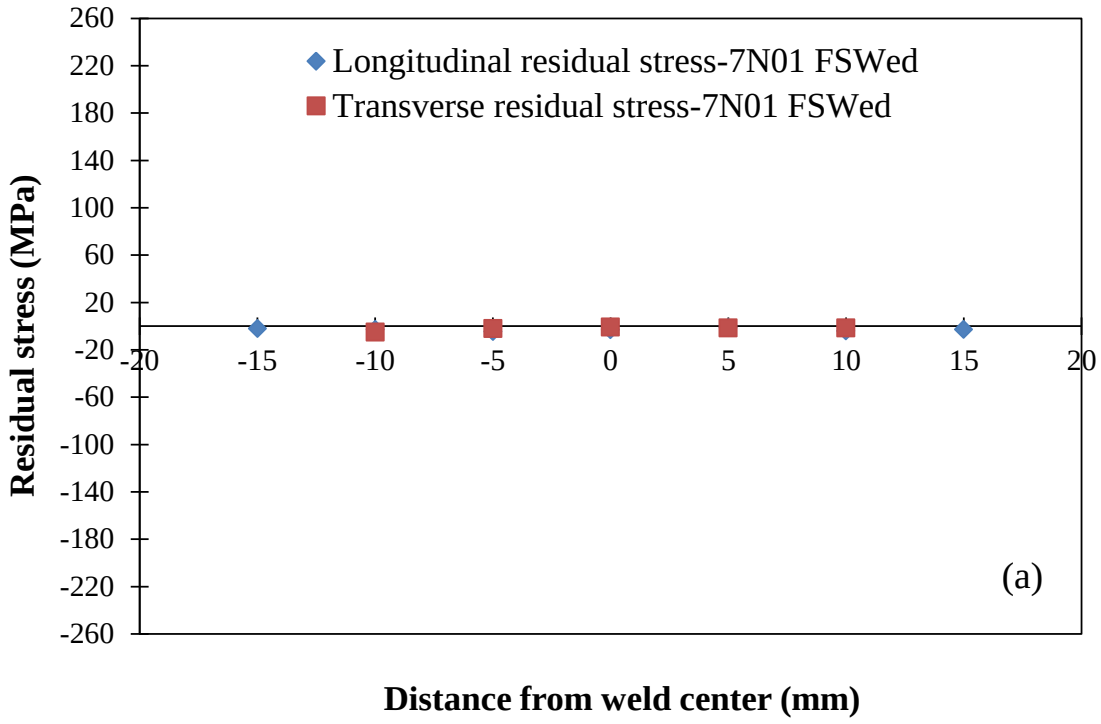


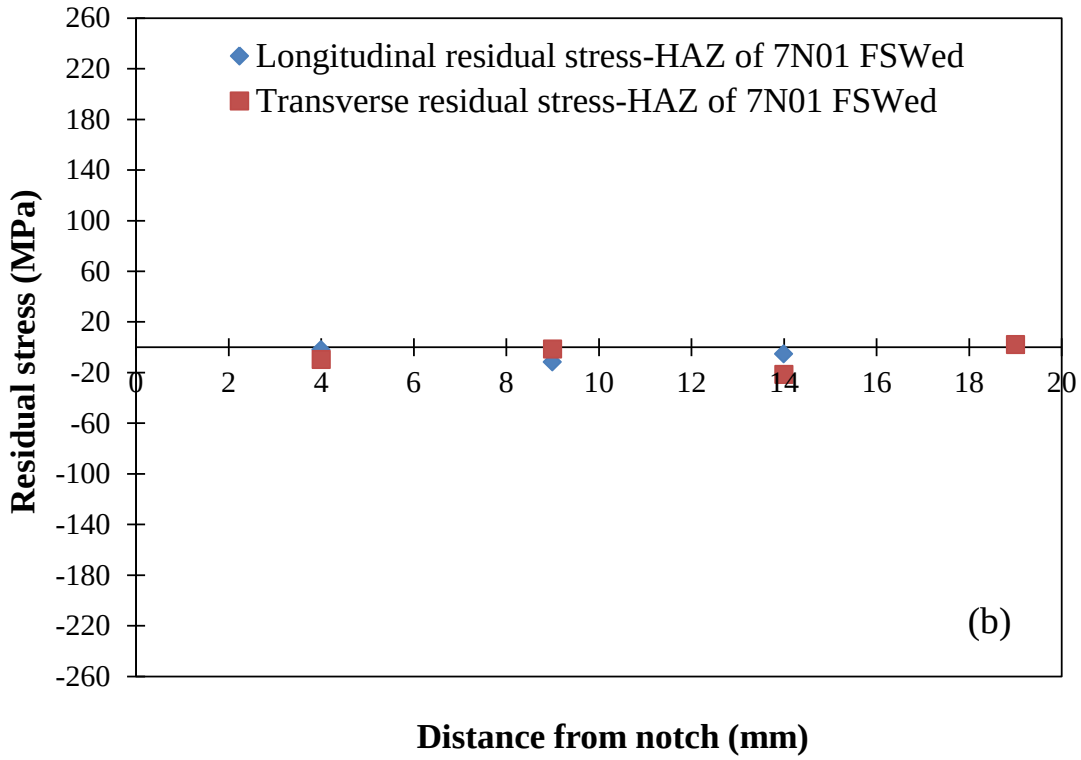


Fig. 3.8 Residual stresses distribution in FSWed 7N01 joint (a) relation between residual stresses and distance from weld center line (b) residual stresses along the notch in HAZ sample.

### 3.3.4 Fracture surfaces

Fracture surface observations are shown in Fig. 3.9. All FSWed aluminum alloys joints tested in the present study showed the similar trend in its fracture morphology. Trans-granular fracture was observed in BM, HAZ and WNZ at near threshold region. Moreover, in higher ΔK region, trans-granular fracture was still observed in BM and HAZ. On the other hand, transition in fracture morphology from trans-granular fracture at low ΔK region to mixed mode (intergranular + transgranular) fracture at high ΔK region was observed in WNZ. Difference in fatigue crack growth behaviors among BM, HAZ and WNZ were not the same and depended on alloys. However, the similar fracture morphology was observed regardless of the alloys.

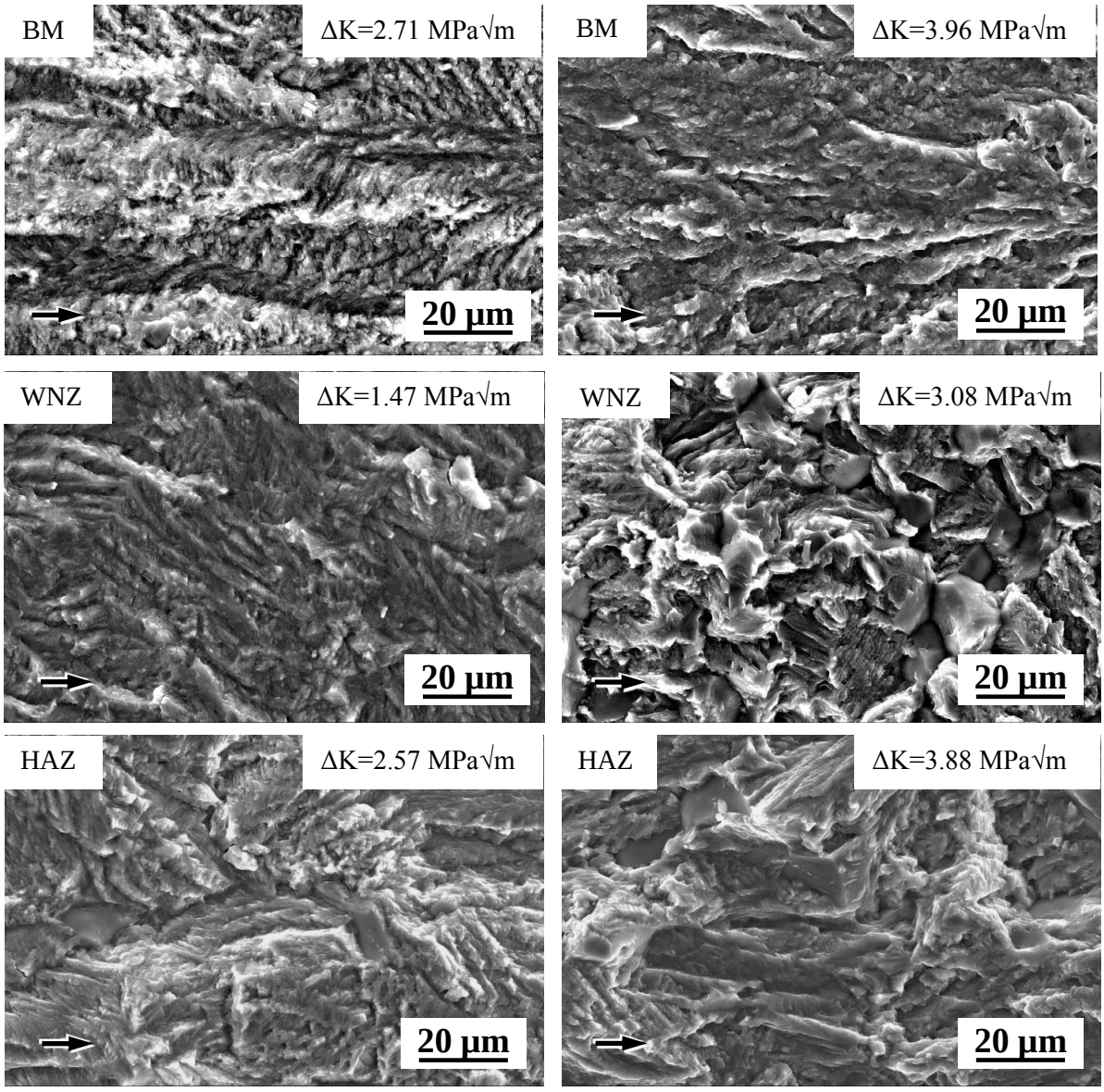


(a) 5052

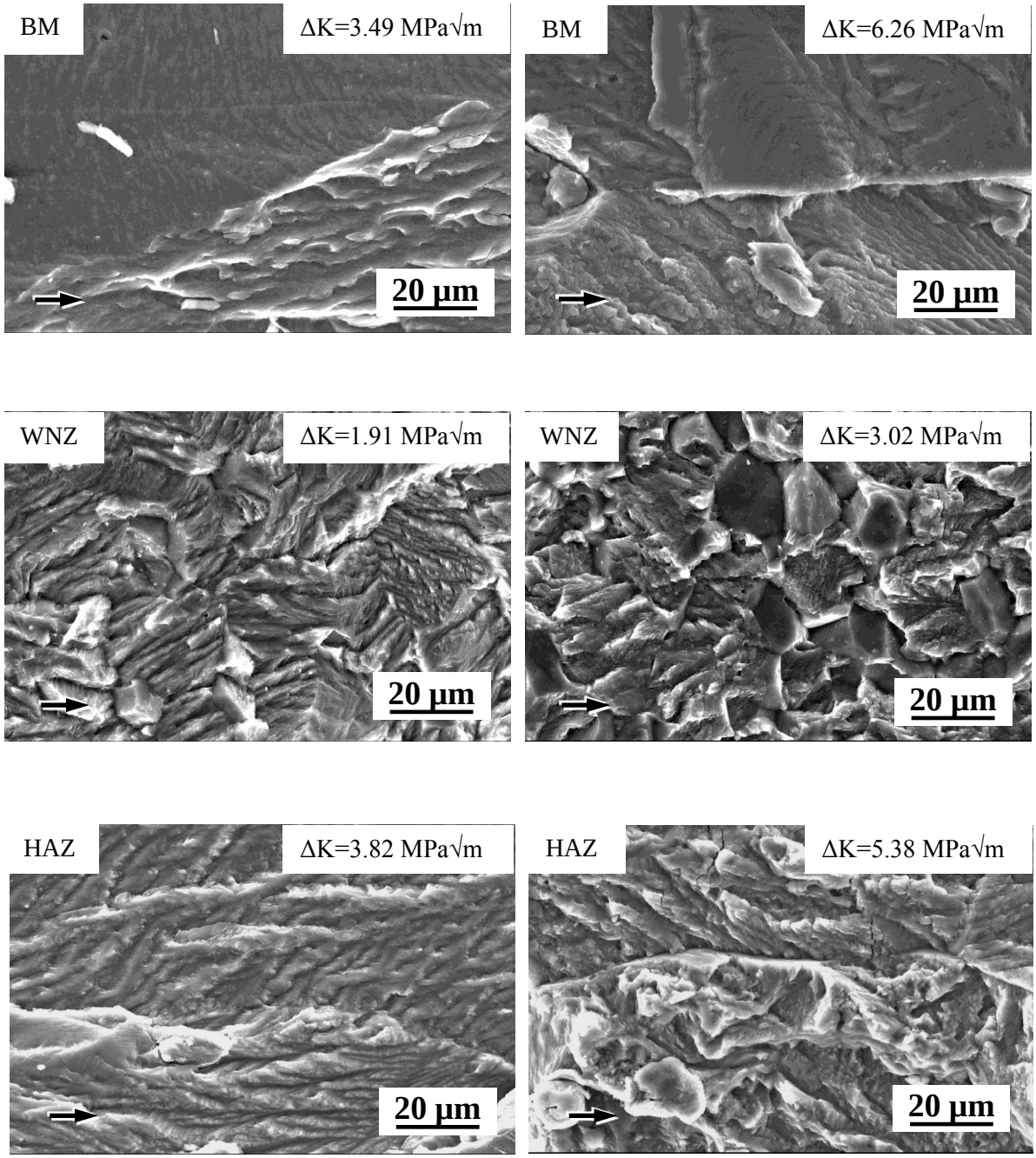
BM
ΔK=3.49 MPa√m
20 μm
BM
ΔK=6.26 MPa√m
20 μm
WNZ
ΔK=1.91 MPa√m
20 μm
WNZ
ΔK=3.02 MPa√m
20 μm
HAZ
ΔK=3.82 MPa√m
20 μm
HAZ
ΔK=5.38 MPa√m
20 μm

(b) 6N01

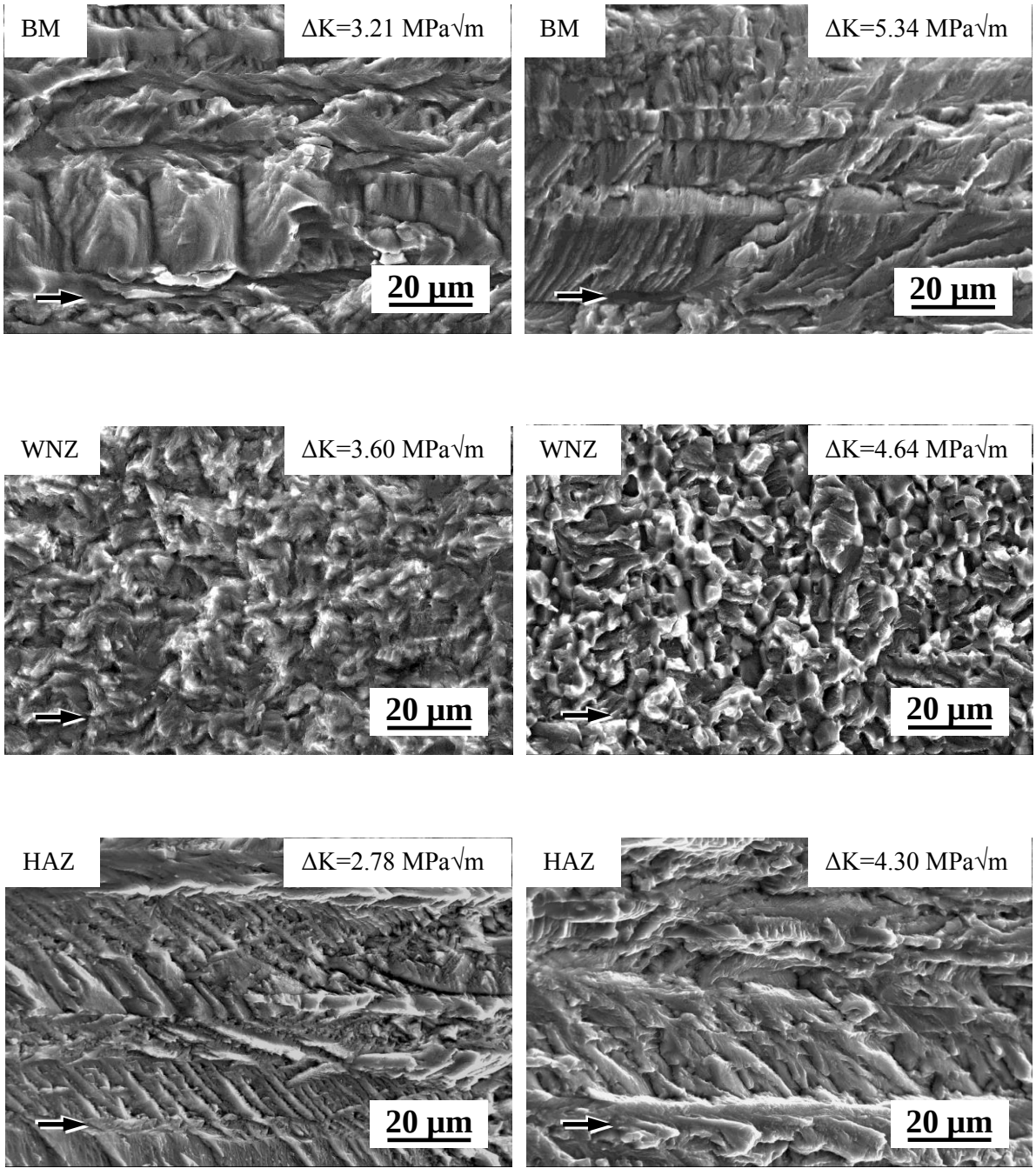


(c) 7N01

Fig. 3.9 Fracture surfaces of FSWed (a) 5052, (b) 6N01 and (c) 7N01 joints at low ΔK and high ΔK region. Black arrows show the crack growth direction.

### 3.3.5 Effect of grain size and hardness on threshold stress intensity factor

In generally, relationship between yield stress or hardness and grain size is well agreement in accordance to Hall-Petch relation as below equations;

$$\sigma_{ys} = \sigma_{y0} + \frac{k_y}{\sqrt{d}}$$

$$H_v = H_{v0} + \frac{K_H}{\sqrt{d}}$$

Where $\sigma_{ys}$ is yield stress, $H_v$ is Vickers hardness, $d$ is grain size and $\sigma_{y0}$, $H_{v0}$, $k_y$ and $k_H$ are material constants given in Hall-Petch relation.

According to Hall-Petch relation, smaller grain size materials should show higher in hardness and yield strength compared to larger grain size materials for grain boundary strengthening. In contrast, the bobbin type FSW microstructure obtained in this study, smaller grain size of fine-equiaxed dynamic recrystallized grains in WNZ showed lower hardness and yield strength compared to the larger elongated grains base material. Moreover, HAZ of FSWed joint joined by using a bobbin type tool which has similar grain size with the BM showed lower hardness and yield strength compared to the base materials.

The effect of grain size and yield stress on threshold stress intensity factor has been reported in previous study [13]. Materials used in the previous study showed the trend between grain size and yield stress in accordance to Hall-Petch relation. In this study, the bobbin type FSW materials which shown contradiction trend with Hall-Petch relation will be discussed on the effect of grain size and hardness on threshold stress intensity factor.

Fig. 3.10 shows the relationship between hardness and grain size. The results of bobbin type FSWed material showed clearly contradiction trend with Hall-Petch relation which smaller grain size was lower in hardness. As a consequence, the relationship between grain size, hardness and threshold stress intensity factor was shown in Fig. 3.11, 3.12 and Table 3.3 respectively.

In case of FSWed 5052 and 6N01 similar aluminum alloys joints and their base materials, larger grain size showed significantly higher threshold stress intensity factor

which was the similar to general trend with other materials studied as shown in Fig. 3.11. However, the relation between hardness and threshold stress intensity factor for FSWed 5052 and 6N01 joints as shown in Fig. 3.12, the result in this study did not show significant relation between hardness and threshold stress intensity factor. In previous study showed that the lower yield stress or lower hardness materials had higher threshold stress intensity factor range.

On the other hand, in case of FSWed 7N01 similar aluminum alloy joint and its base material, when the grain size parameter is considered, extreamly elongated grains of the BM and the HAZ showed lower threshold stress intensity factor compared to fine-equiaxed DRX grains in the WNZ. However, the BM and the HAZ of 7N01 alloy was contained the fine sub-grains or sub-structures inside the highly elongated grains as observed in their microstructures as shown in Fig 3.13. In Fig. 3.11, by using sub-grains size parameter instead of grain size, the result showed the similar to general trend with other materials studied. In this study, smaller sub-grain was contained in highly elongated grains of the BM and the HAZ of 7N01 alloy which showed lower threshold stress intensity factor range compared to larger equiaxed DRX grain in the WNZ. When considering the relation between hardness and threshold stress intensity factor for FSWed 7N01 joints as shown in Fig. 3.12, the result in this study did not show significant trend between hardness and threshold stress intensity factor range.

Different FSWed similar aluminum alloys joints joined by using a bobbin type tool showed similar trend with previous study in the effect of microstructural dimensions on threshold stress intensity factor range. In case of FSWed 5052 and 6N01 aluminum alloys joints, larger grain size showed higher threshold stress intensity factor range. In contrast, in case of FSWed 7N01 aluminum alloy joint, the threshold stress intensity factor was dominated by sub-grain size. It can be mentioned that the grain size was a factor to control the threshold stress intensity factor in case of FSWed 5052 and 6N01 aluminum alloy joints. However, in case of FSWed 7N01 aluminum alloy joints, sub-grain size was a factor to control the threshold stress intensity factor. The relation between hardness and threshold stress intensity factor for the all FSWed 5052, 6N01 and 7N01 aluminum alloys joints did not show significant trend.

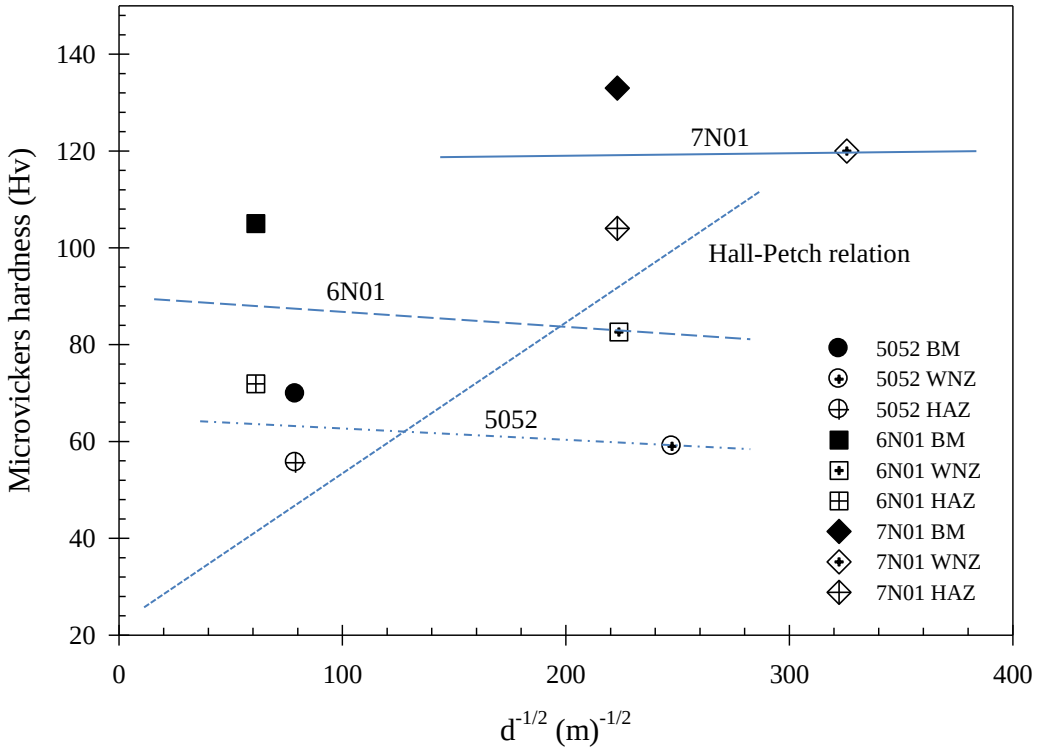


Fig. 3.10 Relation between microvickers hardness and grain size.

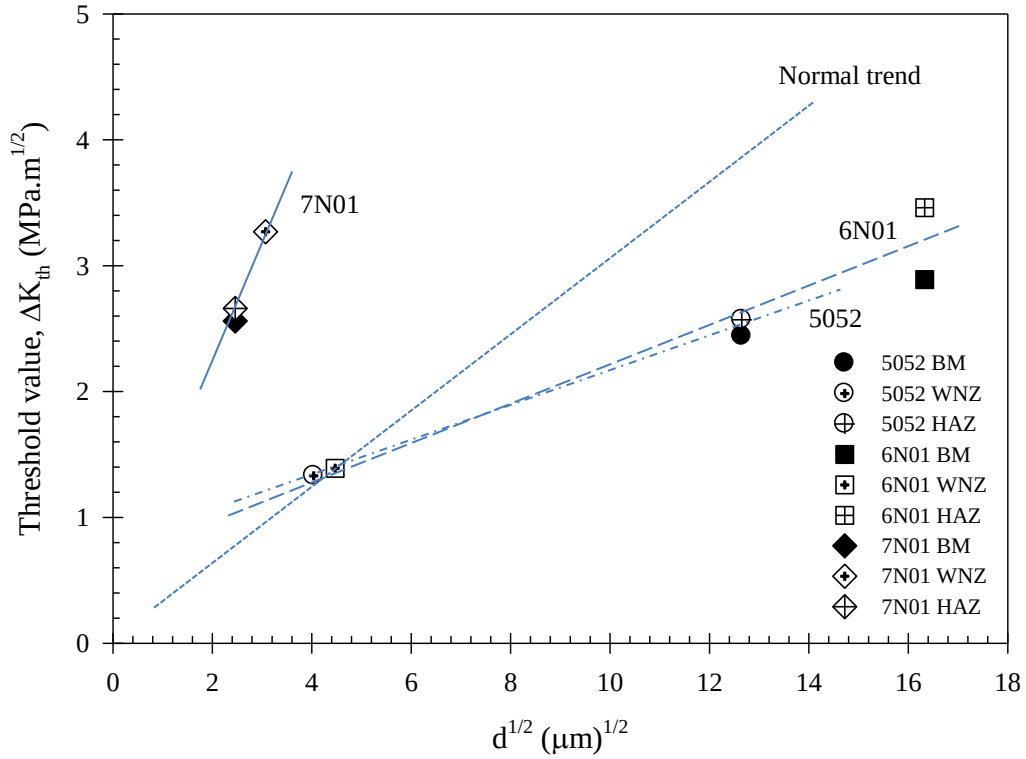


Fig. 3.11 Relation between threshold stress intensity factor range and grain size.

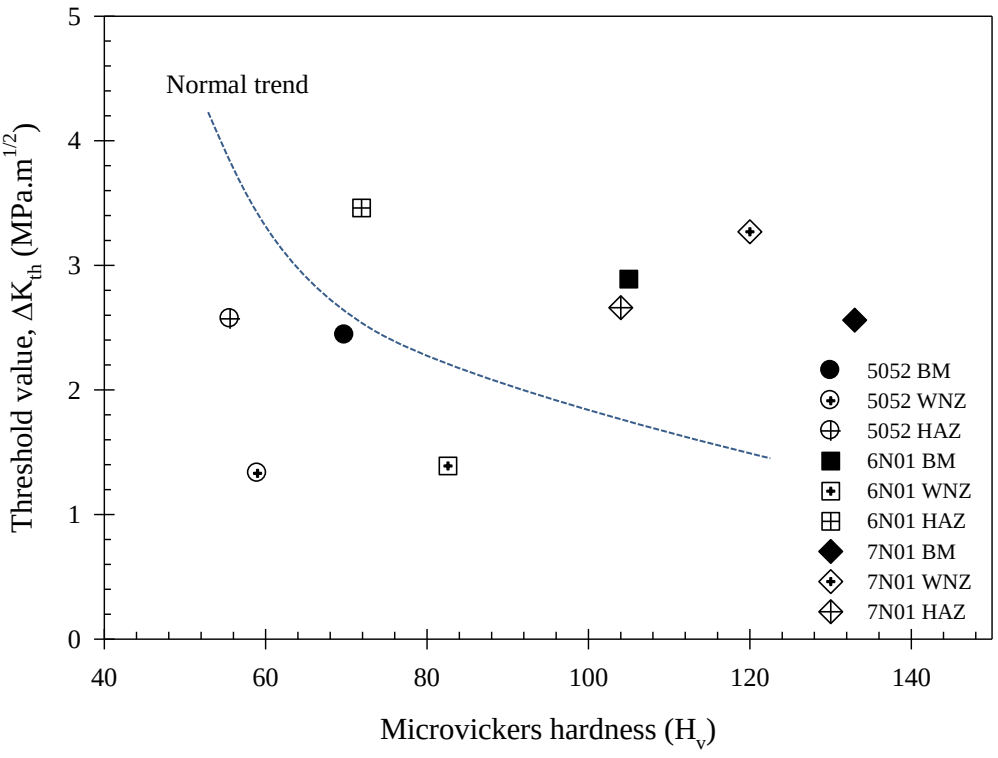


Fig. 3.12 Relation between threshold stress intensity factor range and microvickers hardness.

Table 3.3 Relationship between $\Delta K_{th}$, hardness and grain sizes.

| Materials | $\Delta K_{th}$ (MPa√m) | Hardness (Hv) | Observed Grain Size (μm) | $\Delta K_T$ (MPa√m) | Estimated Cyclic PZS at $\Delta K_T$ (μm) |
|---|---|---|---|---|---|
| 5052 BM | 2.44 | 69.8 | 160.00 | 2.78 | 11.50 |
| 5052 WNZ | 1.33 | 59.0 | 16.32 | 1.62 | 9.25 |
| 5052 HAZ | 2.57 | 55.6 | 160.00 | 2.77 | 26.91 |
| 6N01 BM | 2.89 | 105 | 266.67 | 3.98 | 8.85 |
| 6N01 WNZ | 1.39 | 82.6 | 20.00 | 2.13 | 10.20 |
| 6N01 HAZ | 3.46 | 71.9 | 266.67 | 4.02 | 36.11 |
| 7N01 BM | 2.56 | 133.0 | 6.06 (sub-grain diameter) | 4.09 | 4.17 |
| 7N01 WNZ | 3.27 | 120.0 | 9.41 | 3.91 | 7.72 |
| 7N01 HAZ | 2.66 | 104.4 | 6.06 (sub-grain diameter) | 3.31 | 5.53 |

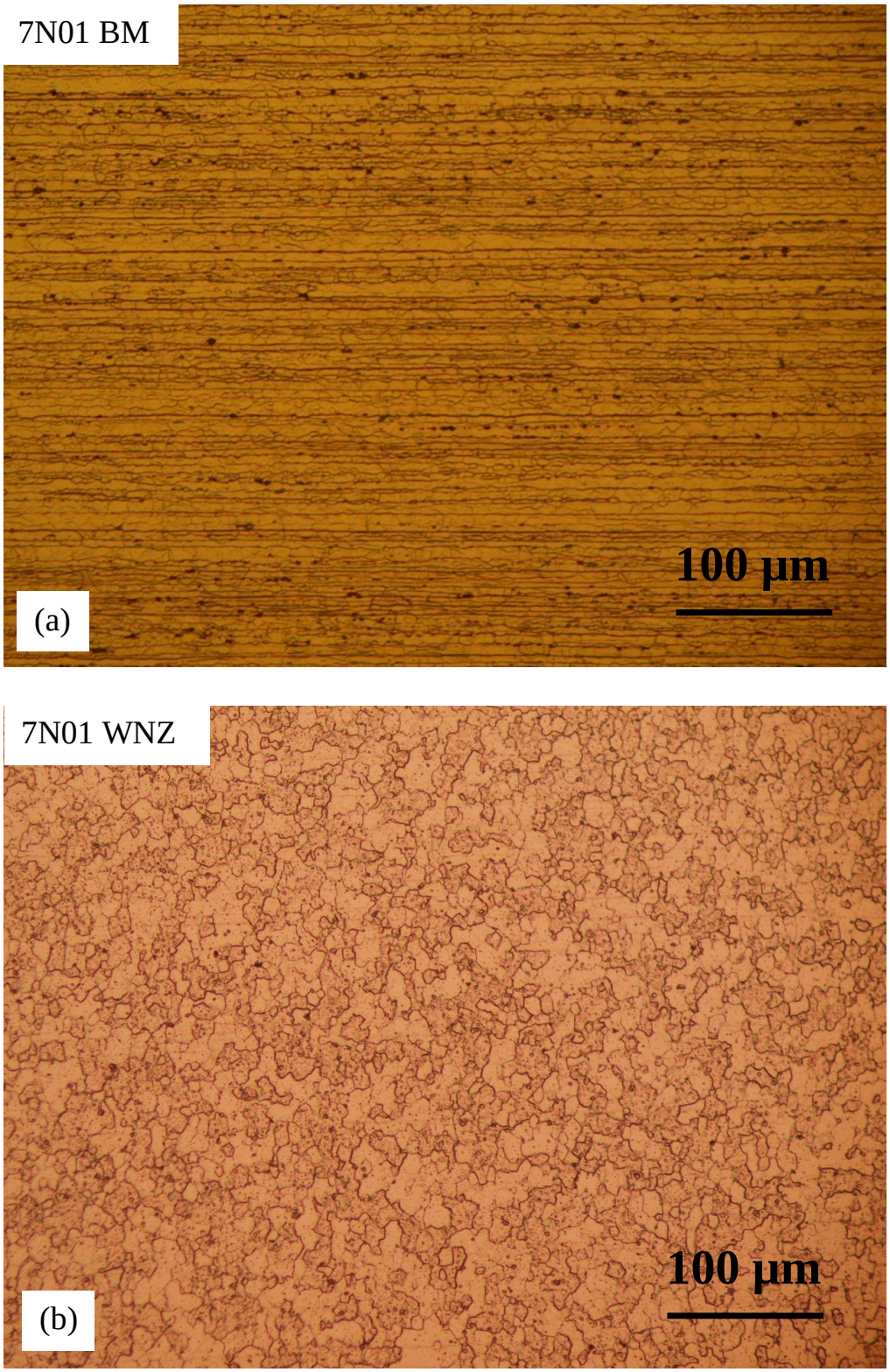


Fig. 3.13 Microstructure of (a) highly elongated grains in 7N01 base material and (b) DRX grains in WNZ of 7N01 similar aluminum alloy joint.

### 3.3.6 Effect of microstructural dimension on fatigue crack growth characteristic

As considered on microstructural dimension, fatigue crack growth behavior in near-threshold region and Paris region can be described in different mechanisms. The transition behavior between near-threshold and Paris region was explained by the correlation of microstructural dimension and plastic zone size ahead the crack tip during crack propagation.

At near-threshold region, the region that cyclic plastic zone size (CPZS) during crack propagation was less than microstructural dimensions or grain size which so called microstructural sensitive due to limited number of slip systems only one or few slip planes are operative at crack tip at low level of stress intensity factor range. Microstructural boundaries act as barrier to restrict or retard the slip spreading across to the adjacent grains. Crack path was deflected at grain boundaries and degree of deflection or roughness is comparable to grain size. Larger grain sizes tend to higher FCG resistance due to large deflection and increase in surface roughness which causes to increase in crack closure due to crack faces contact. In according to mismatching of rough crack faces, the Mode I (opening mode) and Mode II (sliding mode) crack growth are in cooperated in this region [29]. Previous studies [29-32] suggested that fine or small grain size is less FCG resistance compared to large grain size at near-threshold region.

In Paris region, the region that CPZS during crack propagation larger than grain size, the high local stress concentrations induced slip on several sets of crystal planes in each grain and also slip spreads across the barriers like grain boundaries. The plastic deformation is therefore homogeneous and the fatigue crack propagates by a continuum mechanism.

In near-threshold region, increase in grain size of materials or decrease in yield strength generally results in a marked reduction in near-threshold FCG rate and increase in threshold value, $\Delta K_{th}$. In case of HAZ, similar grain size with the base material but lower in yield strength showed lower near-threshold FCG rate and higher and comparable threshold value, $\Delta K_{th}$ comparing with the base materials for 6N01 and 5052, 7N01 respectively. In case of WNZ of FSWed similar aluminum alloys joints, smaller microstructural dimension showed higher near-threshold FCG rate and lower $\Delta K_{th}$ compared to the base materials and the HAZs. In case of FSWed 5052 and 6N01 aluminum alloys joints, larger grain size showed higher threshold stress intensity factor. In

contrast, in case of FSWed 7N01 aluminum alloy joint, the threshold stress intensity factor was dominated by sub-grain size. It can be mentioned that the grain size was a factor to control the threshold stress intensity factor in case of FSWed 5052 and 6N01 aluminum alloy joints. However, in case of FSWed 7N01 aluminum alloy joints, sub-grain size was a factor to control the threshold stress intensity factor.

At near-threshold region, transgranular fracture mechanism was observed in all cases of BM, WNZ and HAZ in all FSWed similar aluminum joints. It might be explained that due to the PZS ahead the crack tip during crack propagate in this region was less than grain size and slip cannot spread encompassed the adjacent grains and then resulted in transgranular fracture occurred.

In Paris region, the fracture surfaces of the BM and the HAZ showed transgranular fracture mechanism. In contrast, when PZS during FCG in this region larger than the grain size, the fine-equiaxed DRX grains in the WNZ of all FSWed similar joints changed in fracture mechanism from transgranular as observed at near-threshold region to mixed mode (intergranular + transgranular) at Paris region. FCG resistance was converged to the similar with the HAZ and the BM in Paris region for FSWed 5052 and 6N01 joints. However, different in FCG resistance was still observed in Paris region for FSWed 7N01 joint. Moreover, intergranular crack growth observed only in WNZ at higher $\Delta K$ levels when PZS ahead the crack tip is expected in order of or larger than the grain size. However, when PZS is smaller than the grain size at near threshold region, slip cannot encompass or across the grain boundaries and then result in transgranular fracture.

In this study, the transition behavior did not well match when correlated between grain size and plastic zone size at transition stress intensity factor range, $\Delta K_T$ as shown in Table 3.3. It might be suggested that not only grain size influenced the correlation in transition behavior in this study but also other microstructural dimensions would be a factor to correlate transition behavior such as dispersoid spacing, sub-grain size and etc. Especially in case of 7N01 alloy, a good agreement in transition behavior was shown when using a smaller microstructural size as sub-grain size instead of grain size in correlation with plastic zone size at transition stress intensity factor range, $\Delta K_T$.

### 3.3.7 Crack closure

Crack closure behaviors of the specimens with a crack in different regions of the FSWed joint were evaluated in this study. Figure 3.14 shows FCG curves arranged by effective stress intensity factor range, $\Delta K_{eff}$. The BM and the HAZ in all materials tested showed crack closure behavior. Closure behavior was not observed in the WNZ of FSWed 5052 and 6N01 joints, but that was observed in the WNZ of FSWed 7N01 joint. As shown in Fig. 3.14 (a) and (b), crack growth curves of the BM, the HAZ and the WNZ almost coincide and showed a one curve when the curves were arranged by $\Delta K_{eff}$ in 5052 and 6N01 alloys. It is considered that the difference in FCG behavior observed in the different regions of the FSWed 5052 and 6N01 joints as shown in Fig. 3.5 is mainly due to the difference in crack closure behavior. However, at near-threshold region, the 5052 and 6N01 BM showed sligthly lower FCG resistance and lower $\Delta K_{th}$ than that of thier WNZ and HAZ. Higher hardness and yield strength in the BM comparing with the WNZs and the HAZs was observed in this study. Hardness reduction in the WNZ and the HAZ was reported due to dissolution and coarsening of precipitates occurred during FSW processing [1, 5]. Previous study [13] reported that the materials which higher hardness and yield strength showed lower threshold stress intensity factor range. However, the result in this study did not show significant relation between hardness and threshold stress intensity factor. Moreover, FSWed materials was changed in microstructure characteristics from the BM that might be resulted in slightly different in threshold stress intensity factor range even when arranged by $\Delta K_{eff}$. In case of 7N01 alloy, crack growth curves obtained from the different regions fell into one curve at near threshold region. However, the curves did not coincide in higher $\Delta K$ region and the WNZ showed lower FCG resistance compared to the BM and the HAZ.

Fig. 3.15 shows comparison of the alloys in FCG curves arranged by $\Delta K_{eff}$ in the BM, the HAZ and the WNZ. According to the figures, it is not observed significantly difference in the FCG curves between 5052 and 6N01 alloys, the both alloys show the similar curves regardless of $\Delta K$ level. At near threshold region of FCG behavior in the WNZ and the HAZ, crack growth curve of 7N01 alloy arranged by $\Delta K_{eff}$ is almost the same with that of the other two alloys. However, in high $\Delta K$ region, FCG resistance of 7N01 alloy is higher in the HAZ and that is lower in the WNZ, as shown in Fig. 3.15 (b) and (c). It is also observed in FCG behavior of the BM as shown in Fig. 3.15 (a), FCG resistance of 7N01 alloy is higher than those of 5052 and 6N01 alloys in all regions regardless of $\Delta K$ level.

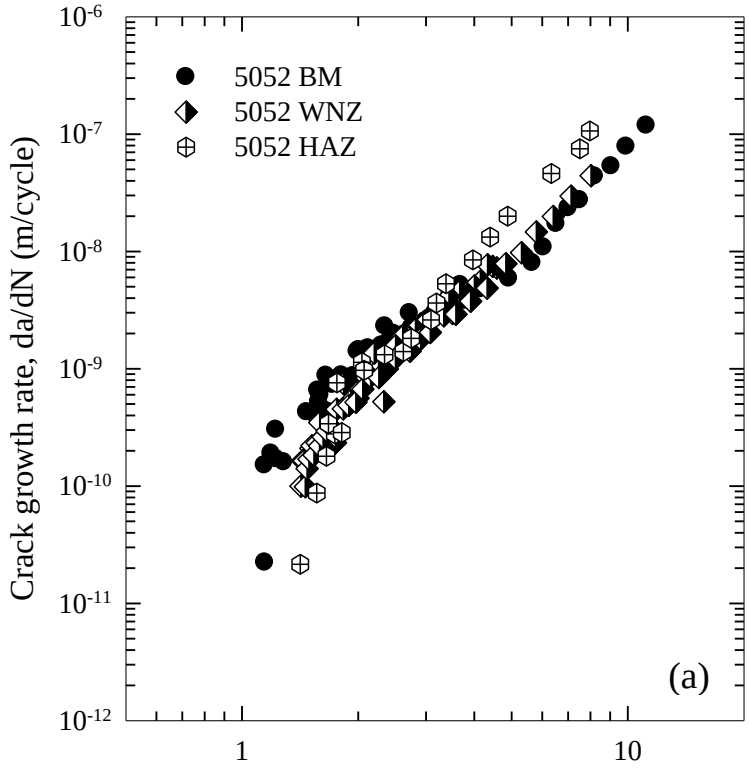


Effective stress intensity factor range, $\Delta K_{eff}$ (MPa $m^{1/2}$)

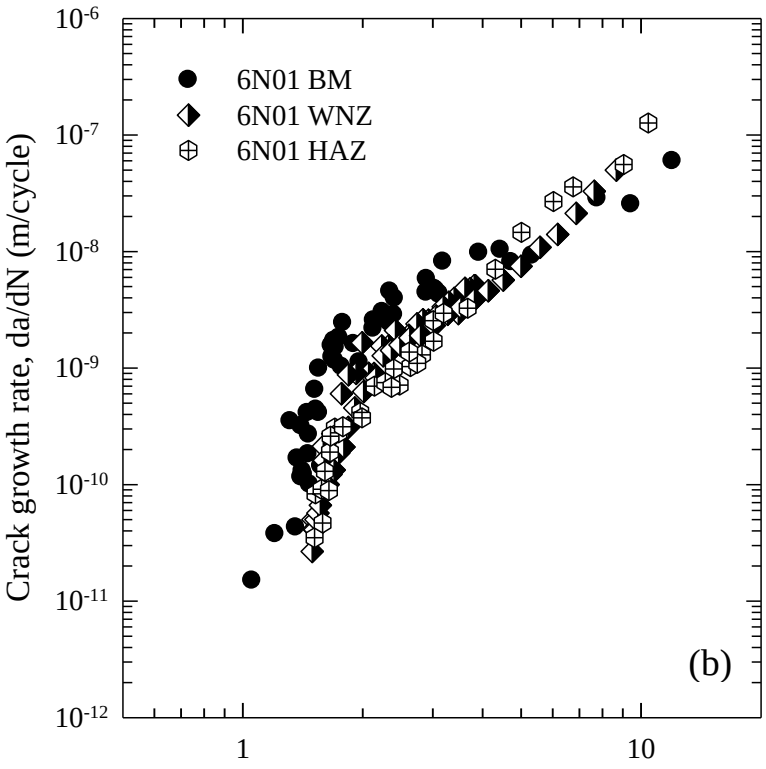


Effective stress intensity factor range, $\Delta K_{eff}$ (MPa $m^{1/2}$)

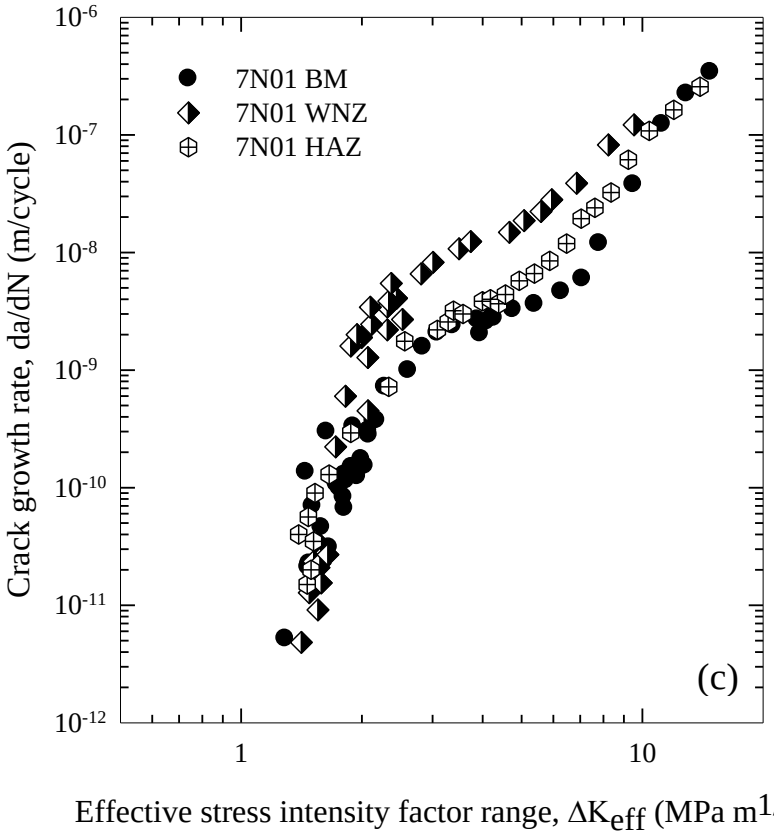


Fig. 3.14 Crack growth rate versus effective stress intensity factor range of (a) FSWed 5052 joint, (b) FSWed 6N01 joint, (c) FSWed 7N01 joint.

According to the discussion in the above, in basically, the BM of 7N01 alloy has higher FCG resistance compared to the BM of 5052 and 6N01 alloys as shown in Fig. 3.15 (a). This is understandable according to its higher mechanical properties. In the HAZ, microstructure morphology is the similar with the BM in 7N01 and the FCG resistance is still higher than that of 5052 and 6N01 in high ΔK region. However, microstructure of the WNZ significantly changed from that of the BM in 7N01 alloy and lower FCG resistance in 7N01 compared to 5052 and 6N01 was observed. Plates tested in the present study were produced by rolling or extrusion and then resulted in formation of elongated microstructure in the specific direction, as shown in Fig. 3.4. Microstructure effect on FCG behavior is significantly observed near threshold region in generally. However, some materials show microstructure dependence in FCG behavior even in Paris region [18]. It is speculated that the microstructure would affect significantly on FCG behavior in 7N01 alloy and that might be caused by severe deformation in the production process of the material.

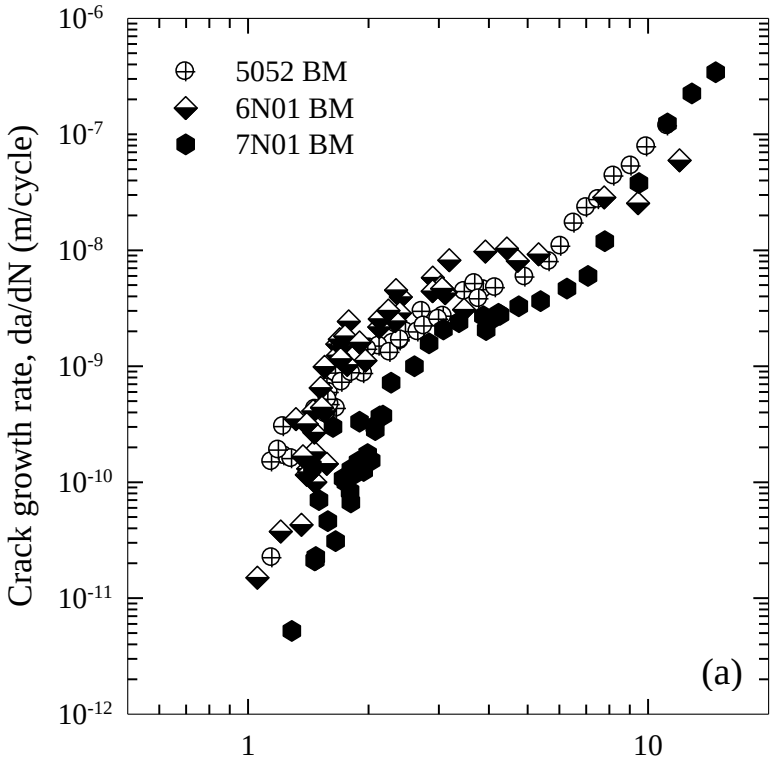


Effective stress intensity factor range, $\Delta K_{eff}$ (MPa $m^{1/2}$)

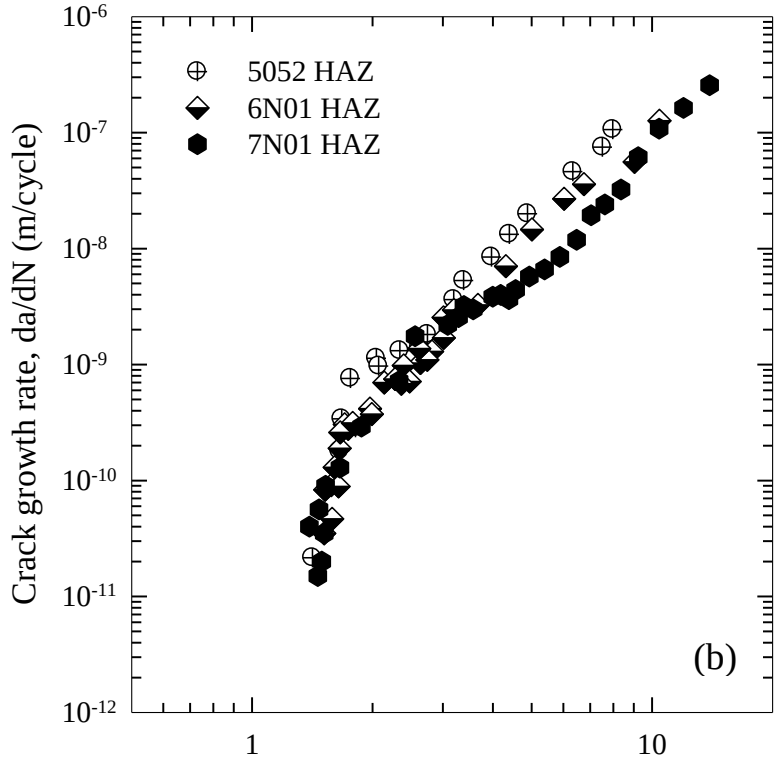


Effective stress intensity factor range, $\Delta K_{eff}$ (MPa $m^{1/2}$)

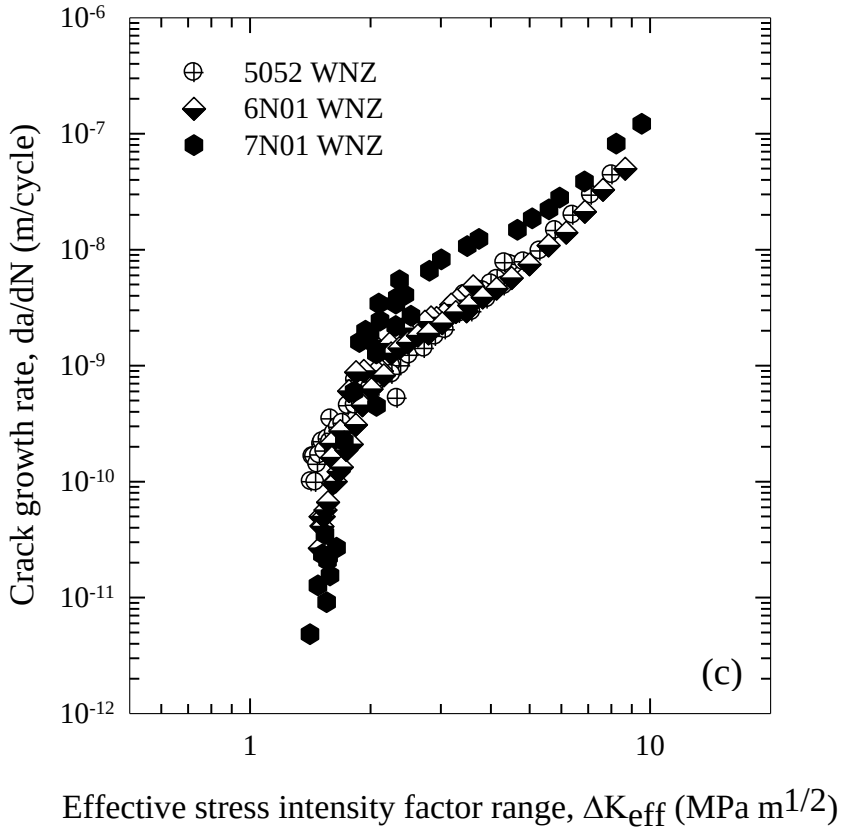


Fig. 3.15 Comparision of alloys on fatigue crack growth curves arranged by $\Delta K_{eff}$ for (a) BM, (b) HAZ and (c) WNZ.

In order to clarify the discussion in the above, that the microstructure would significantly affected on FCG behavior in 7N01 aluminum alloy compared to 5052 and 6N01 aluminum alloys. Effect of microstructure on FCG resistance has been studied in 5052 and 7N01 base materials by fatigue crack was propagated in parallel and perpendicular to the rolling/extrusion direction. In Fig. 3.16 (a), FCG resistance of 5052 BM in parallel and perpendicular to the rolling direction was almost the similar in all $\Delta K$ regions and can be arranged into a single curve by $\Delta K_{eff}$. In contrast, 7N01 BM showed different in FCG resistance when crack propagated in parallel and perpendicular to the extrusion direction and cannot be arranged into a single curve by $\Delta K_{eff}$ as shown in Fig. 3.16 (b). When the crack propagated in parallel to the extrusion direction which more significantly strong banded structure, higher FCG resistance is obtained compared to the crack propagated in perpendicular to the extrusion direction especially in near-threshold region which is microstructural affected region. In Paris region and high $\Delta K$ region, crack

propagation in parallel and perpendicular to the extrusion direction in 7N01 BM was shown the similar FCG resistance.

Fracture surfaces of 5052 BM that crack propagated in parallel and perpendicular to the rolling direction showed the similar fracture morphology in transgranular fracture mode and have no significant different fracture mechanism in all ΔK regions as shown in Fig. 3.17. In case of 7N01 BM, at near-threshold region which have significantly different in FCG resistance, different in fracture morphology was observed as shown in Fig. 3.18 (a). Fracture surfaces of specimen that crack propagated perpendicular to the extrusion direction which lower FCG resistance showed cleavage and more flat fracture morphology compared to fracture morphology observed in crack propagated parallel to the extrusion direction which shown more rough fracture morphology. In addition, roughness induced crack closure (RICC) has been reported that affected to FCG behavior in low ΔK region. In Paris region and high ΔK region, the FCG resistance when crack propagated in parallel and perpendicular to the extrusion direction showed the similar and have no significant difference in fracture mechanism as shown in Fig. 3.18 (b) and (c).

It can be mentioned that 7N01 aluminum alloy was more significantly microstructural affected on FCG resistance compared to 5052 and 6N01 aluminum alloys. In Paris region, 7N01 BM which has more strong banded structure showed higher FCG resistance compared to 5052 BM and 6N01 BM as confirmed by FCG behavior in that both of crack propagated in parallel and perpendicular to the extrusion direction. There is reported [19] that 7xxx series aluminum alloys or aluminum-zinc alloys which contained high dispersoid concentration and pronounced banding inherited from cast structure then resulted in extremely elongated recrystallized grains or strong banded structure after hot working process. In case of the WNZ of 7N01, microstructure vastly changed due to FSW process from strong banded structure in the BM to fine-equiaxed recrystallized grains. Therefore, the WNZ of 7N01 showed different FCG behavior from the both of BM and HAZ which have similar microstructure. Moreover, the microstructural effect and intergranular fracture mechanism in Paris region and high ΔK region would be expected reason to reduce the FCG resistance in WNZ of FSWed 7N01 aluminum alloy joint.

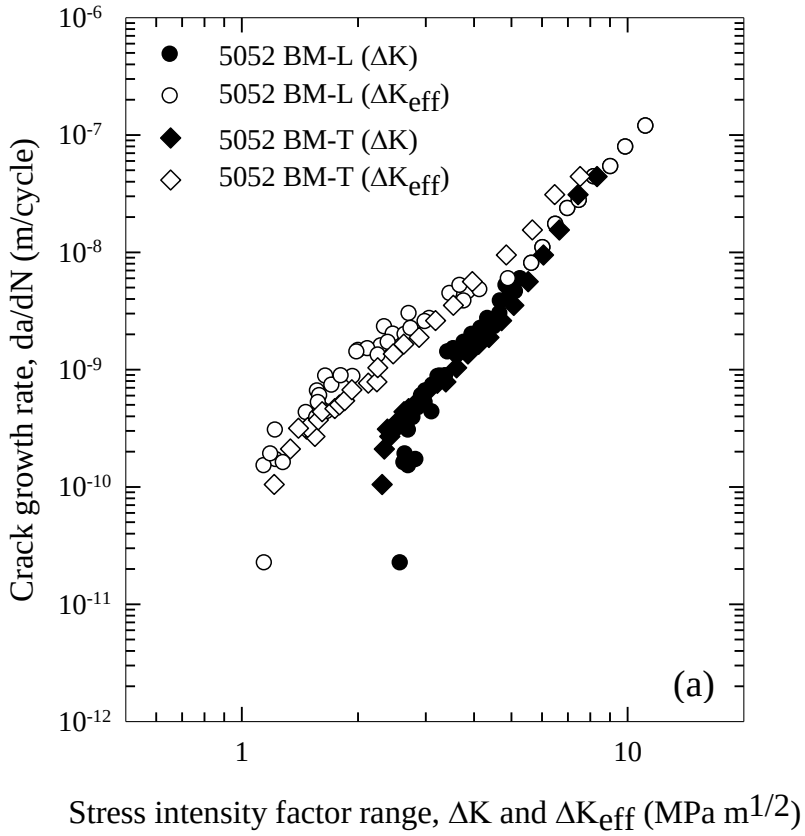


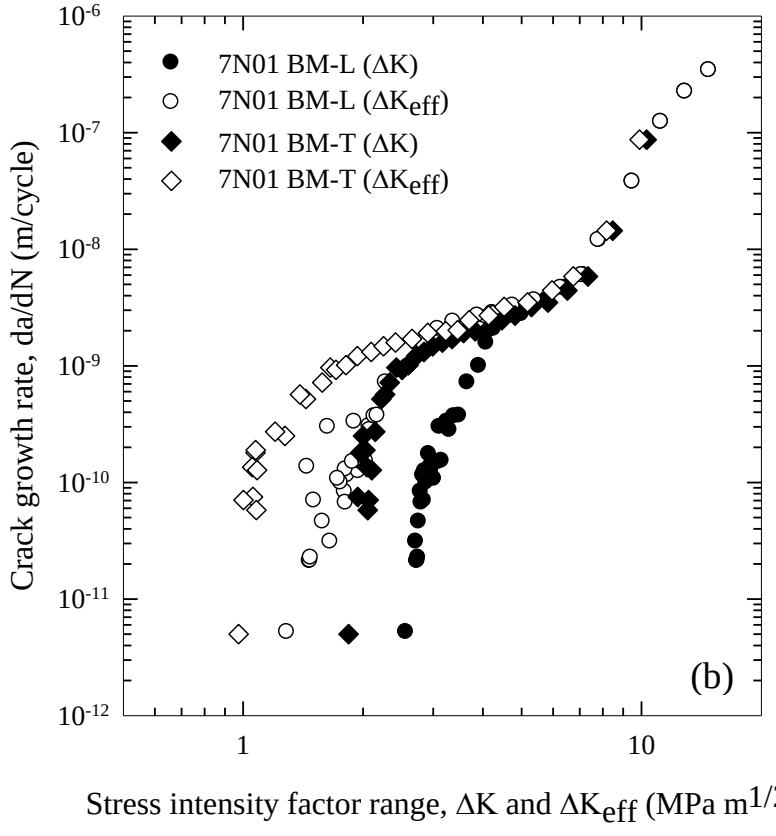


Fig. 3.16 Fatigue crack growth curves of base materials in parallel and perpendicular to rolling/extrusion direction (a) 5052 and (b) 7N01.

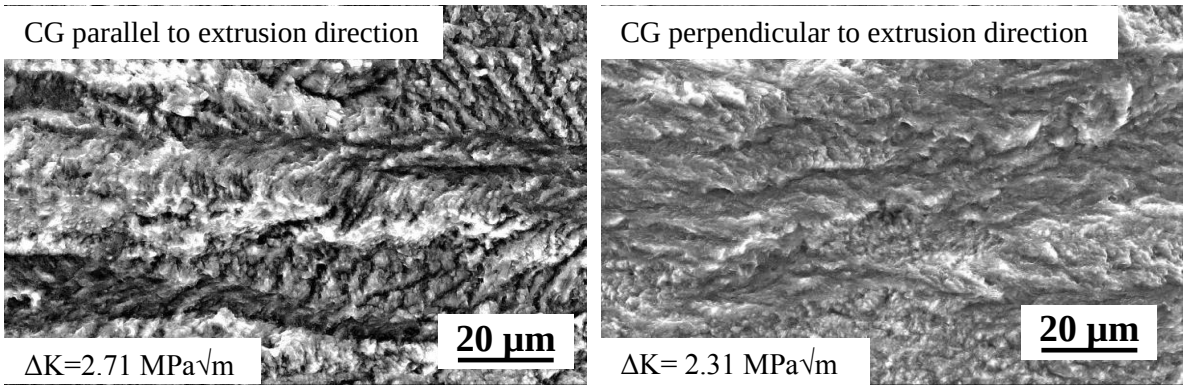


(a) Near-threshold

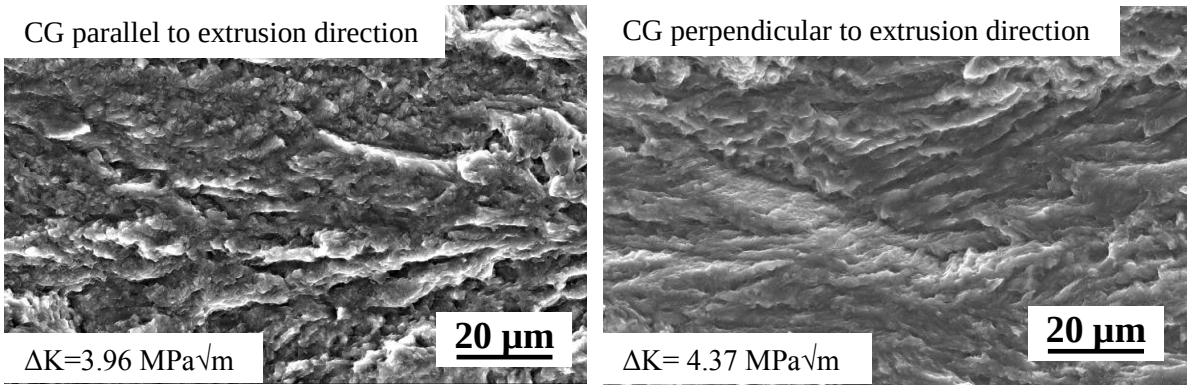


(b) Paris region

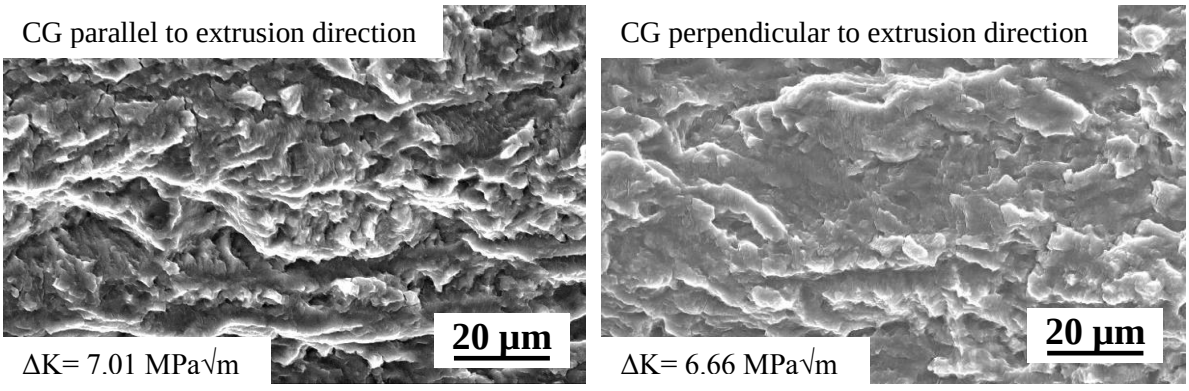


(c) High ΔK

Fig. 3.17 Fracture surfaces of 5052 base material which crack propagate in parallel and perpendicular to rolling direction (a) low ΔK, (b) Paris region and (c) high ΔK region.

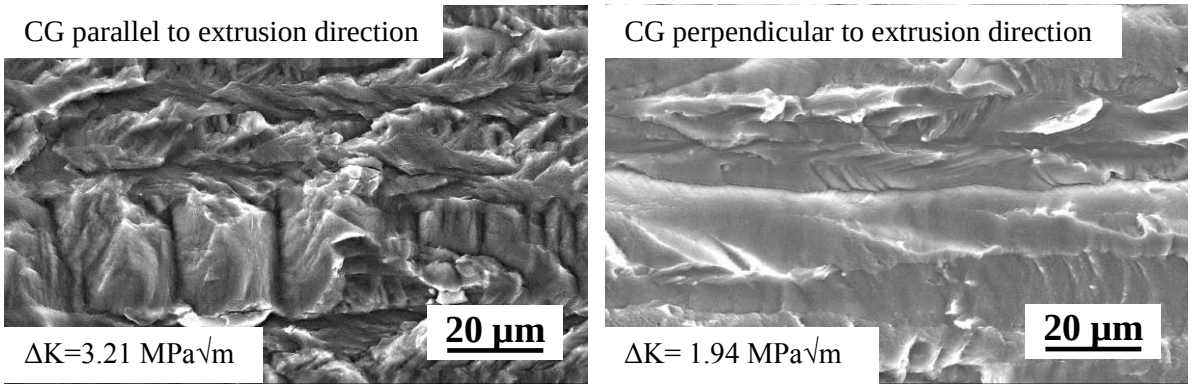


(a) Near-threshold

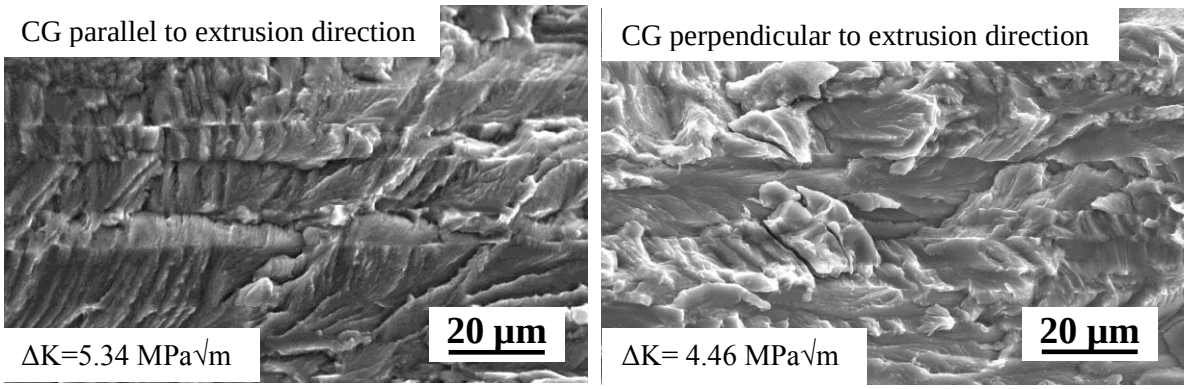


(b) Paris region

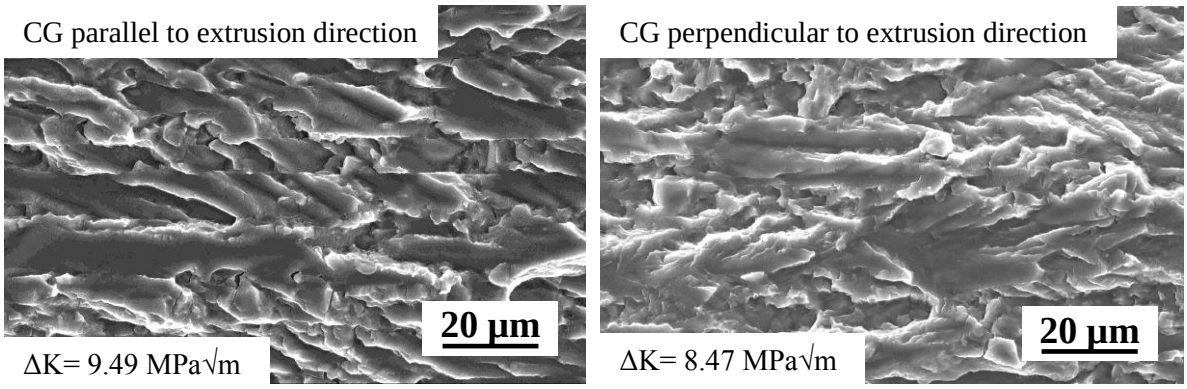


(c) High ΔK

Fig. 3.18 Fracture surfaces of 7N01 base material which crack propagate in parallel and perpendicular to extrusion direction (a) low ΔK, (b) Paris region and (c) high ΔK region.

## 3.4 Conclusions

(1) Weld microstructure in FSWed joints joined by using a bobbin type tool was produced as symmetry between upper and lower sides in thickness direction of the joints.

(2) Fatigue crack growht resistance of the WNZ was lower than that of the BM and the HAZ at near-threshold region in FSWed 5052 and 6N01 joints. At high ΔK region, the WNZ of FSWed 5052 joint has the similar FCG resistance to the both of BM and HAZ. The WNZ of FSWed 6N01 joint showed the lowest FCG resistnace compared to the BM and the HAZ. In FSWed 7N01 joint, FCG resistance of the WNZ was higher than that of the BM and the HAZ at near-threshold region. In high ΔK region, FCG resistance of the WNZ in FSWed 7N01 joint was the similar with that of the HAZ, but the BM showed slightly higher FCG resistance compared to the WNZ and the HAZ.

(3) Microstructural dimension was dominant on threshold stress intensity factor range in this study. In case of FSWed 5052 and 6N01 aluminum alloy joints, grain size was a factor to control the threshold stress intensity factor range. However, in case of FSWed 7N01 aluminum alloy joints, sub-grain size was a factor to control the threshold stress intensity factor range.

(4) Fatigue crack growth curves obtained in different regions coincided into a single curve when the curves were arranged by $\Delta K_{eff}$ in FSWed 5052 and 6N01 joints. Difference in FCG behavior in different regions of the FSWed joints is mainly due to difference in crack closure behavior in 5052 and 6N01 alloys.

(5) In case of FSWed 7N01 joint, FCG curves obtained in different region can be arranged by $\Delta K_{eff}$ at near threshold region. However, at high ΔK region, the curves were not well arranged by $\Delta K_{eff}$. It is speculated that microstructural effect may significantly influence on FCG behavior of FSWed 7N01 joint.

(6) The results of crack propagation in parallel and perpendicular to the rolling/extrusion direction in the base materials showed that the microstructure significantly affected to FCG behavior in 7N01 aluminum alloys. In contrast of 5052 aluminum alloy, microstructure in different oreintation of rolled specimen did not affect on FCG behavior.

## 3.5 References

[1] R.S. Mishra and Z.Y. Ma, Mat. Sci. Eng. R. 50 (2005) 1-78.

[2] L.E. Murr, J. Mat. Eng. Perform. 19 (2010) 1071-1089.

[3] A.L. Biro, B.F. Chenelle and D.A. Lados, Met. Mat. Tran. B. 43B (2012) 1622-1636.

[4] G. Bussu and P.E. Irving, Int. J. Fat. 25 (2003) 77-88.

[5] K.V. Jata, K.K. Sankaran and J.J. Ruschau, Met. Mat. Trans. A. 31A (2000) 2181-2192.

[6] T.H. Tra, M. Okazaki and K. Suzuki, Int. J. Fat. 43 (2012) 23-29.

[7] S. Kim, C.G. Lee and S.J. Kim, Mat. Sci. Eng. A. 478 (2008) 56-64.

[8] ASTM E 647-08, Annual Book of ASTM standards, 2008.

[9] G. Pouget and A.P. Reynolds, Int. J. Fat. 30 (2008) 463-472.

[10] L. Fratini, S. Pasta and A.P. Reynolds, Int. J. Fat. 31 (2009) 495-500.

[11] Y.E. Ma, P. Staron, T. Fischer and P.E. Irving, Int. J. Fat. 33 (2011) 1417-1425.

[12] Y.E. Ma, Z.Q. Zhao, B.Q. Liu and W.Y. Li, Mat. Sci. Eng. A. 569 (2013) 41-47.

[13] Y. Mutoh and V.M. Radhakrishnan, J. Eng. Mat. Tech., 108 (1986) 174-178.

[14] S. Suresh, Fatigue of Materials, 2nd edition, Cambridge University Press, 1998.

[15] K. Minakawa, G. Levan and A.J. McEvily, Met. Mat. Trans. A, 17 (1986) 1787-1795.

[16] R.D. Carter, E.W. Lee, E.A. Starke, Jr. and C.J. Beevers, Met. Trans. A, 15 (1984) 555-563.

[17] M. Janssen, J. Zuidema and R. Wanhill, Fracture Mechanics, 2nd edition, Spon Press, 2002.

[18] A.A. Korda, Y. Miyashita, Y. Mutoh and T. Sadasue, Int. J. Fat. 29 (2007) 1140-1148.

[19] John E. Hatch, Aluminum: Properties and Physical Metallurgy, ASM, 1984.

# Chapter 4

# Fatigue crack growth behavior of FSWed 6N01-5052 dissimilar aluminum alloys joints joined with a bobbin type tool

In this chapter, 5052 and 6N01 aluminum alloys which showed the similar FCG behaviors as shown in Chapter 3 were joined to FSWed 6N01-5052 dissimilar materials joint for investigating the effect of materials combination on fatigue crack growth behavior in the WNZ of the joint. FCG resistance in the WNZ of FSWed 6N01-5052 dissimilar materials joint was lower than that of the BMs and almost the same as that in WNZ of the FSWed 5052 and 6N01 similar material joints. In case of materials combination between two alloys which showed the similar FCG behavior in the joints, FCG behavior of the FSWed dissimilar materials joint was the similar with that of the similar materials joints in those alloys.

## 4.1 Introduction

Currently, high strength aluminum alloys and dissimilar materials can be joined by friction stir welding (FSW) process even these materials are difficult to join by conventional fusion welding. In previous study, FSWed dissimilar materials joint was mainly focused on material flow and the microstructure observation [1, 2, 3]. Un-welded seam, large open (void) zones, and oxide inclusions have been reported to observe in FSWed dissimilar materials joints. Complex material flow was also observed in WNZ of FSWed dissimilar materials joint [2, 3]. Difference in materials combination would show difference in materials mixing and flowing in WNZ of FSWed joint and results in different fatigue crack growth behavior. Moreover, previous studies reported mainly fatigue crack growth behavior in FSWed similar aluminum alloys joints and the joint was welded by using a conventional FSW tool [4, 5, 6, 7]. On the other hand, FSW by using a bobbin type tool will be able to suppress formation of root flaws, obtain symmetry in welded structures, make low distortion of welded plate and join a thick plate.

In this chapter, The effect of materials combination on FCG resistance was investigated in FSWed 6N01-5052 dissimilar aluminum alloys joint which represented the combination of alloys which were similar FCG behavior in WNZ of FSWed similar aluminum alloys joints as the result obtained in Chapter 3. In this study, 6N01-5052 dissimilar aluminum alloys and 5052, 6N01 similar aluminum alloys were joined by FSW using a bobbin type tool. Fatigue crack growth behavior and crack closure at WNZ of FSWed 6N01-5052 dissimilar aluminum alloys joint was investigated with comparing to these at WNZ of FSWed 5052, 6N01 similar aluminum alloy joints and of the BM.

## 4.2 Experimental Procedure

Rolled 5052 and extruded 6N01 aluminum alloys plates with thickness of 6 mm were used to joining in this study. Similar and dissimilar aluminum alloys joints were welded parallel to the rolling/extrusion direction by using a bobbin type tool. The tool with shoulder diameter of 20 mm has a pin with diameter of 12 mm and distance between shoulders is 5.8 mm. In case of similar material joining, 5052 and 6N01 aluminum alloy were joined with rotating speed/traverse speed of 300 rpm/200 mm/min and 500 rpm/400 mm/min respectively. In dissimilar materials joining, 6N01-5052 aluminum alloys joint was joined with rotating speed/traverse speed of 300 rpm/200 mm/min. Chemical compositions of 5052 and 6N01 base materials aluminum alloys used in this study was

shown in Table 4.1. Table 4.2 shows tensile properties of the base materials in direction perpendicular to the rolling/extrusion direction and of the FSWed joints in direction perpendicular to the welding direction. Gage length of the tensile test specimen was 50 mm for the base materials and the FSWed joints.

Compact tension (CT) specimens following ASTM E 647-08 were cut from the BM and FSWed plates as shown in Fig 4.1. Fatigue crack growth direction was parallel to the rolling/extrusion direction in the base materials and the welding direction in the FSWed joints. In case of FSWed similar and dissimilar aluminum alloys joint specimen, fatigue pre-crack was introduced at the weld center line (WCL) in WNZ for all welded joints.

Fatigue crack growth test was conducted by using an electro servo-hydraulic fatigue testing machine under constant load amplitude condition according to ASTM E 647-08 [8] in laboratory air. Fatigue loading with stress ratio of 0.1 and frequency of 20 Hz was applied with sinusoidal wave form. Crack length was measured in both sides of a specimen by using travelling microscopes during the test. In order to investigate crack closure behavior, cyclic load-strain curve was measured under frequency of 2 Hz during the test by using strain gage with gage length of 2 mm attached at the back face of the specimen. Crack opening load was determined by unloading elastic compliance method to calculated effective stress intensity factor range, $\Delta K_{eff}$.

Table 4.1 Chemical compositions of base materials aluminum alloys used (Wt%).

| Alloy | Si | Mg | Zn | Fe | Mn | Cu | Ti | Cr | Zr | V |
|---|---|---|---|---|---|---|---|---|---|---|
| 5052 | 0.10 | 2.53 | 0.01 | 0.29 | 0.04 | 0.03 | 0.02 | 0.19 | - | - |
| 6N01 | 0.58 | 0.66 | 0.01 | 0.09 | 0.08 | 0.11 | 0.01 | 0.06 | - | - |

Table 4.2 Tensile properties of base materials and FSWed joints.

| Specimen | 0.2% Proof Strength (MPa) | Tensile Strength (MPa) | Elongation (%) |
|---|---|---|---|
| 5052 BM | 157 | 229 | 16.20 |
| 5052 FSW | 102 | 202 | 13.70 |
| 6N01 BM | 256 | 285 | 9.05 |
| 6N01 FSW | 128 | 185 | 8.65 |
| 6N01-5052 FSW | 106 | 187 | 9.70 |

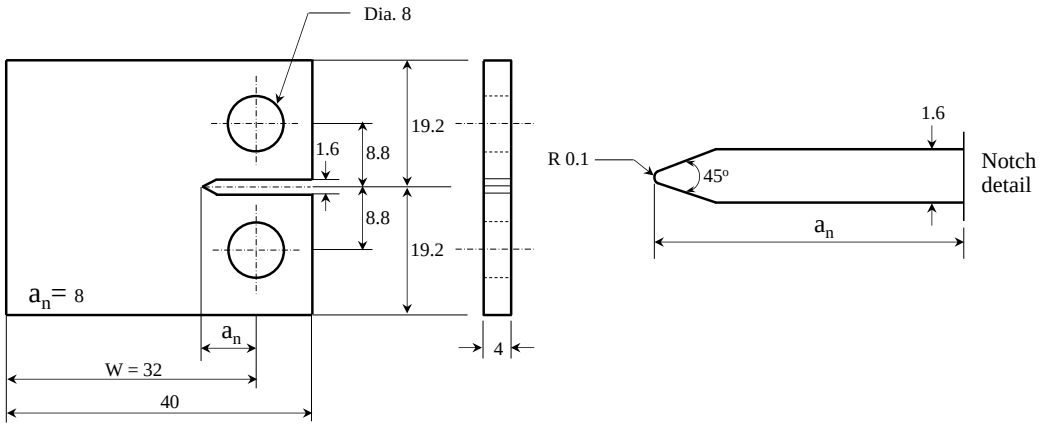


Fig. 4.1 Geometry of CT specimen used (in mm).

## 4.3 Results and Discussions

### 4.3.1 Microstructure observation

Welded structures in cross section perpendicular to the welding direction of FSWed 5052, 6N01 similar and 6N01-5052 dissimilar aluminum alloys joints were shown in Fig 4.2. Welded structures in the welded joints can be divided into three different regions, WNZ, thermo-mechanically affected zone (TMAZ) and heat affected zone (HAZ). In FSWed similar aluminum alloys joints, welded regions were observed as symmetry in upper and lower side of the welded joints which formed by using a bobbin type tool. However, in case of FSWed dissimilar aluminum alloys joint, more complex material flow in welded region was observed compared to that observed in the FSWed similar aluminum alloys joints. Homogeneous microstructure composed of fine equiaxed dynamic-recystallized (DRX) grains at WNZ was observed as shown at area A, B and C in Fig 4.2 for FSWed 5052, 6N01 similar and 6N01-5052 dissimilar aluminum alloys joints, respectively. High magnification of WNZ structure at area A, B and C were shown in Fig 4.3 (b), (d) and (e) respectively. Homogeneous DRX grain structure of FSWed 6N01-5052 dissimilar joint was clearly observed in 3D microstructural planes at WCL as shown in Fig 4.4. Large elongated grain structure was observed in 5052 BM and 6N01 BM as shown in Fig 4.3 (a) and (c). The microstructure of HAZ in all joints are similar to the base materials. The WNZ and HAZ were bounded by TMAZ which observed distorted and elongated grains.

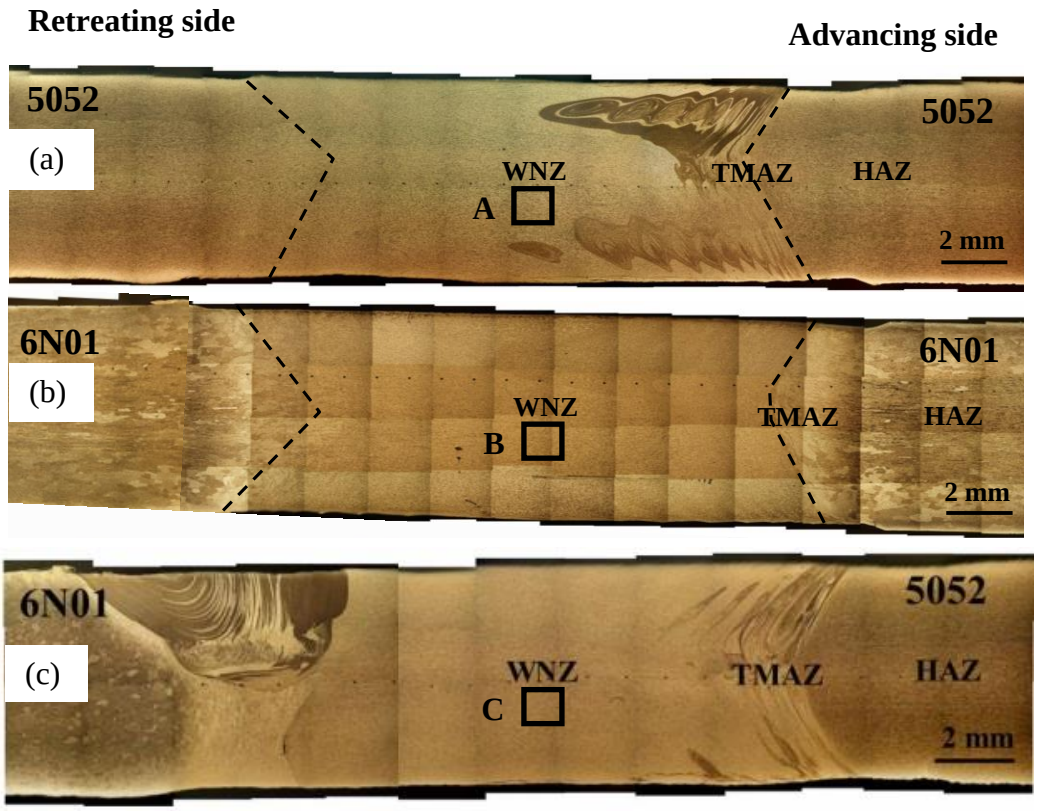


Fig. 4.2 Welded structure in transverse cross-section of (a) 5052, (b) 6N01 and (c) 6N01-5052 FSWed joints.

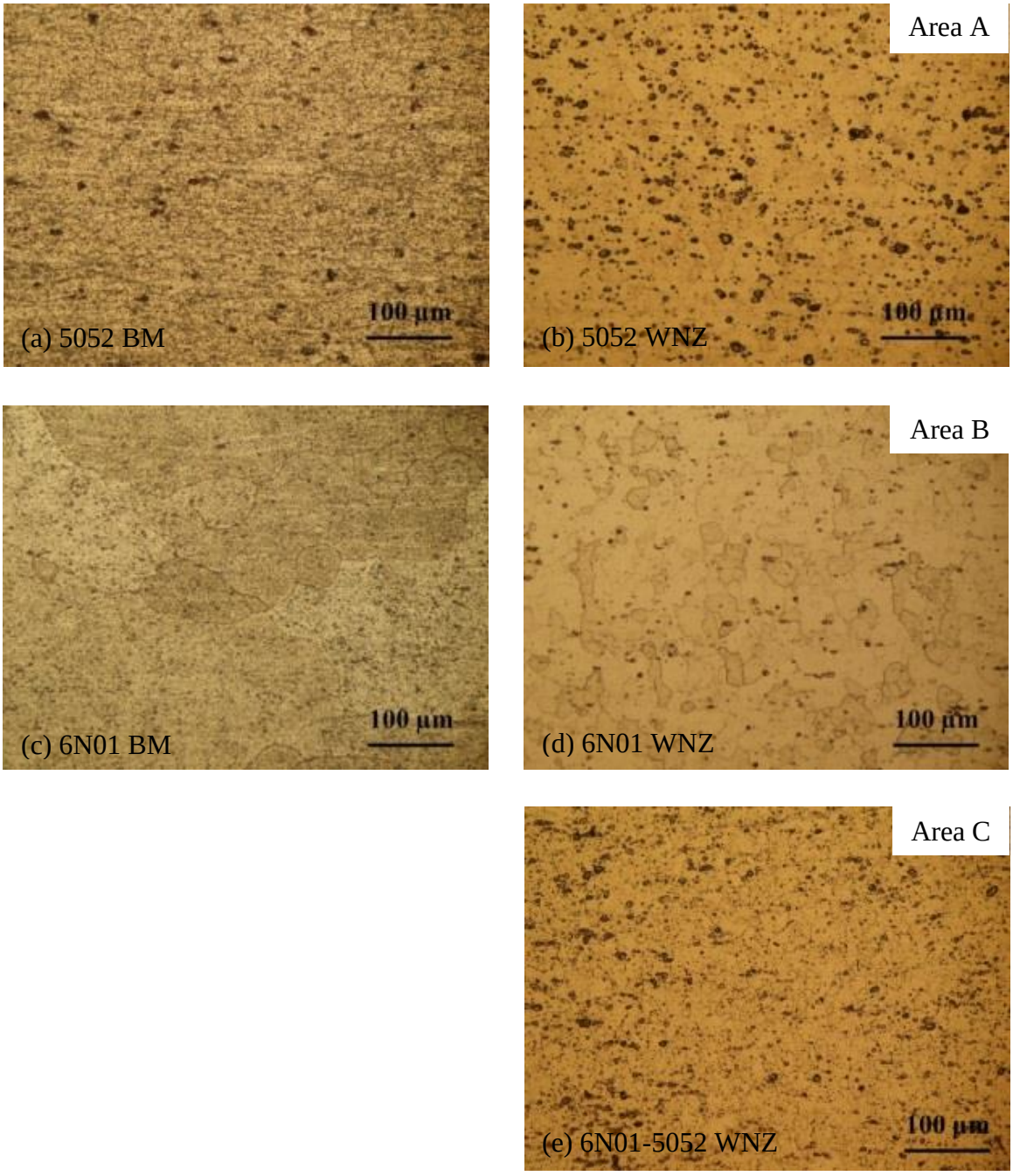


Fig. 4.3 Microstructues in WNZ of FSWed 5052, 6N01 similar and 6N01-5052 dissimilar aluminum alloys joints and the base materials.

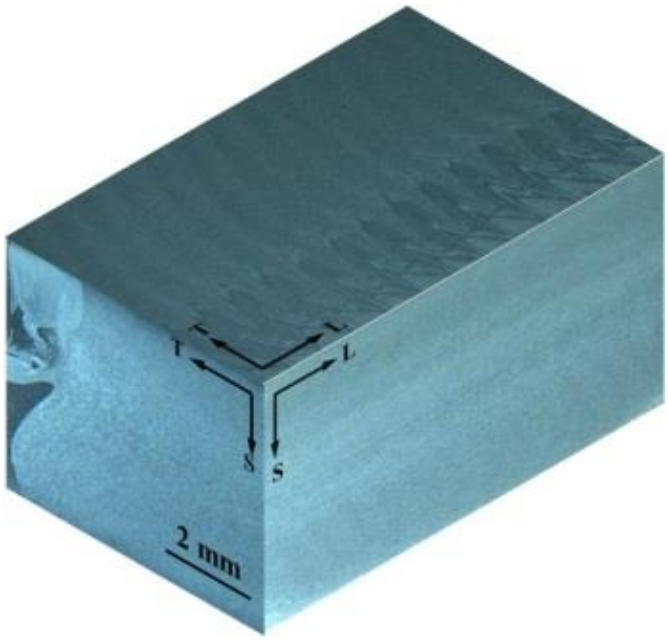


Fig. 4.4 Microstructues shown in three dimensional planes at WCL of FSWed 6N01-5052 dissimilar aluminum alloys joint.

### 4.3.2 Hardness distribution

Hardness distributions at the mid-thickness of the FSWed similar and dissimilar aluminum alloys joints in cross section perpendicular to the welding direction are shown in Fig 4.5. In all of FSWed similar and dissimilar aluminum alloys joints, the welded regions showed lower hardness compared to the BM. FSWed 6N01 similar aluminum alloy joints showed higher hardness and wider welded regions compared to FSWed 5052 similar aluminum alloy joint. In FSWed dissimilar aluminum alloys joint, hardness distribution in welded region was not uniform. Hardness distribution in WNZ of the FSWed dissimilar aluminum alloys joint for each material side was almost comparable and corresponding to hardness distribution in WNZ of the FSWed similar aluminum alloy joints. FSWed 6N01-5052 dissimilar aluminum alloys joint showed slightly lower hardness in WNZ at 6N01 side when compared to hardness in WNZ of FSWed 6N01 similar aluminum alloy joint. However, hardness in the WNZ at 5052 side and at the WCL was the similar with hardness in WNZ of FSWed 5052 similar aluminum alloy joint. Hardness distribution obtained in WNZ in each material side was almost the similar as that observed in the each FSWed similar aluminum alloy joints.

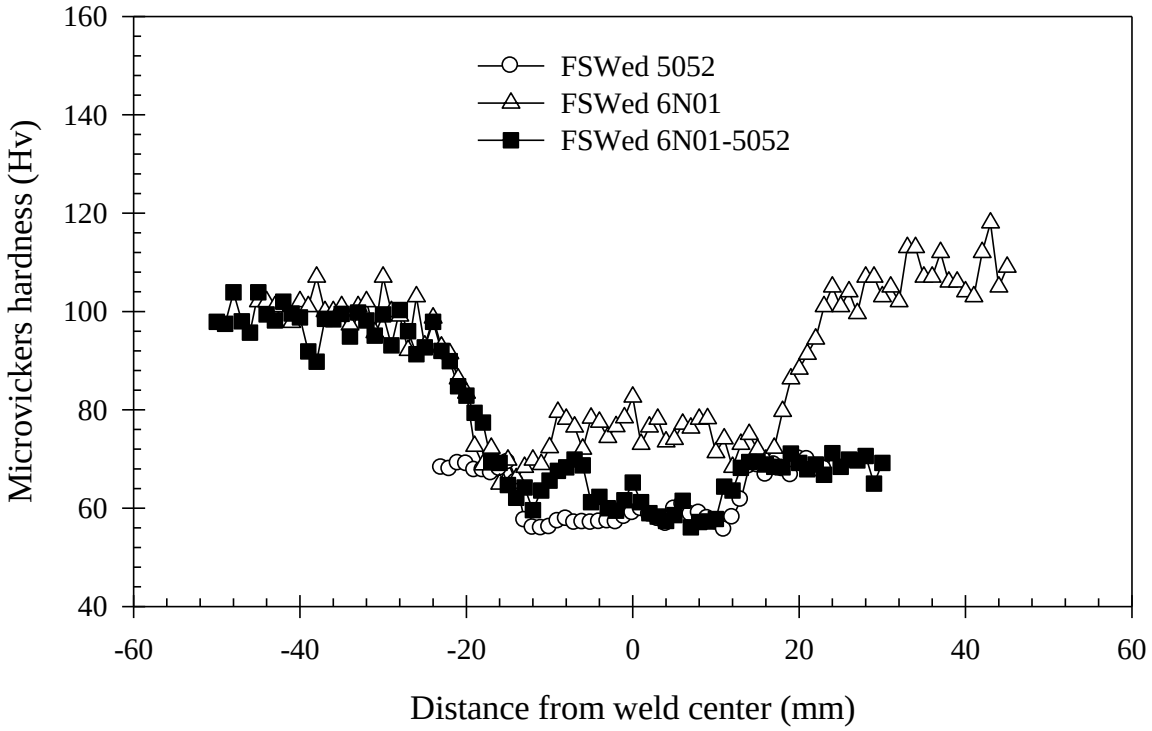


Fig. 4.5 Hardness distribution at mid-thickness position of FSWed similar and dissimilar aluminum alloys joints.

### 4.3.3 Fatigue crack growth behavior

Fig 4.6 shows fatigue crack growth (FCG) curves of BMs, and at WNZs for FSWed similar aluminum alloy joints and FSWed dissimilar aluminum alloys joint. The 6N01 BM showed higher FCG resistance compared to 5052 BM in all ΔK regions. Both 5052 BM and 6N01 BM showed higher FCG resistance compared to WNZ of FSWed 5052, 6N01 similar and FSWed 6N01-5052 dissimilar aluminum alloys joint. However, region of ΔK above 6 $MPam^{1/2}$, 5052 BM shows similar FCG resistance with WNZ of FSWed similar and dissimilar aluminum alloys joints. WNZ of FSWed 5052 and 6N01 similar aluminum alloy joints showed the similar FCG resistance. In case of materials combination between 5052 and 6N01 aluminum alloy, FCG resistance in WNZ of FSWed 6N01-5052 dissimilar aluminum alloy joint was also the similar to that of the WNZ of FSWed 5052 and 6N01 similar aluminum alloy joints as clearly shown in Fig 4.6.

Fracture surfaces of the BMs and at WNZs for FSWed joints were shown in Fig 4.7. Transgranular fracture was observed for 5052 BM and 6N01 BM in both of low and high ΔK regions. In case of the WNZ of FSWed similar and dissimilar aluminum alloy

joints, transgranular fracture was observed at near-threshold region as shown in the left picture of Fig 4.7 (b) and (c). However, at higher ΔK region, fracture morphology in the WNZ in all FSWed joints were changed from transgranular fracture to mixed mode fracture (transgranular + intergranular) as shown in the right picture of Fig 4.7 (b) and (c).

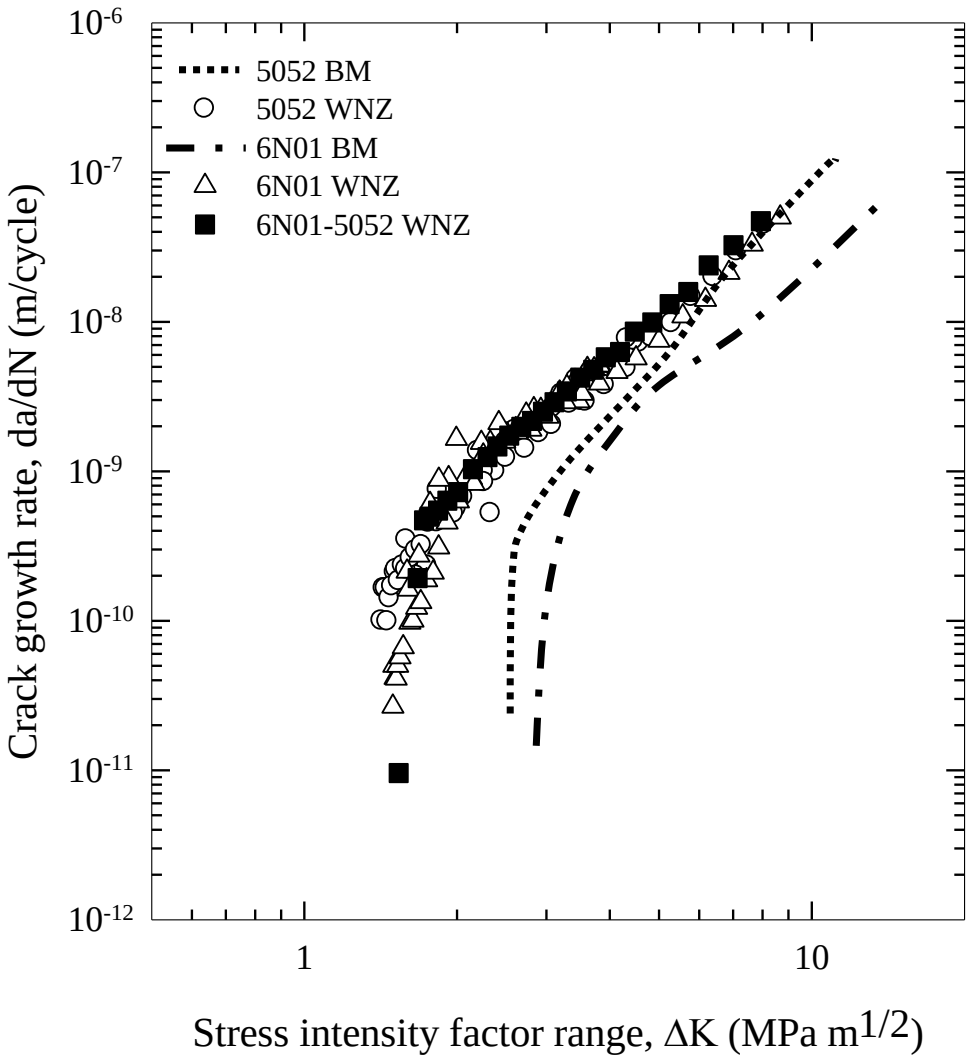


Fig. 4.6 Fatigue crack growth curves of FSWed similar and dissimilar aluminum alloys joints.

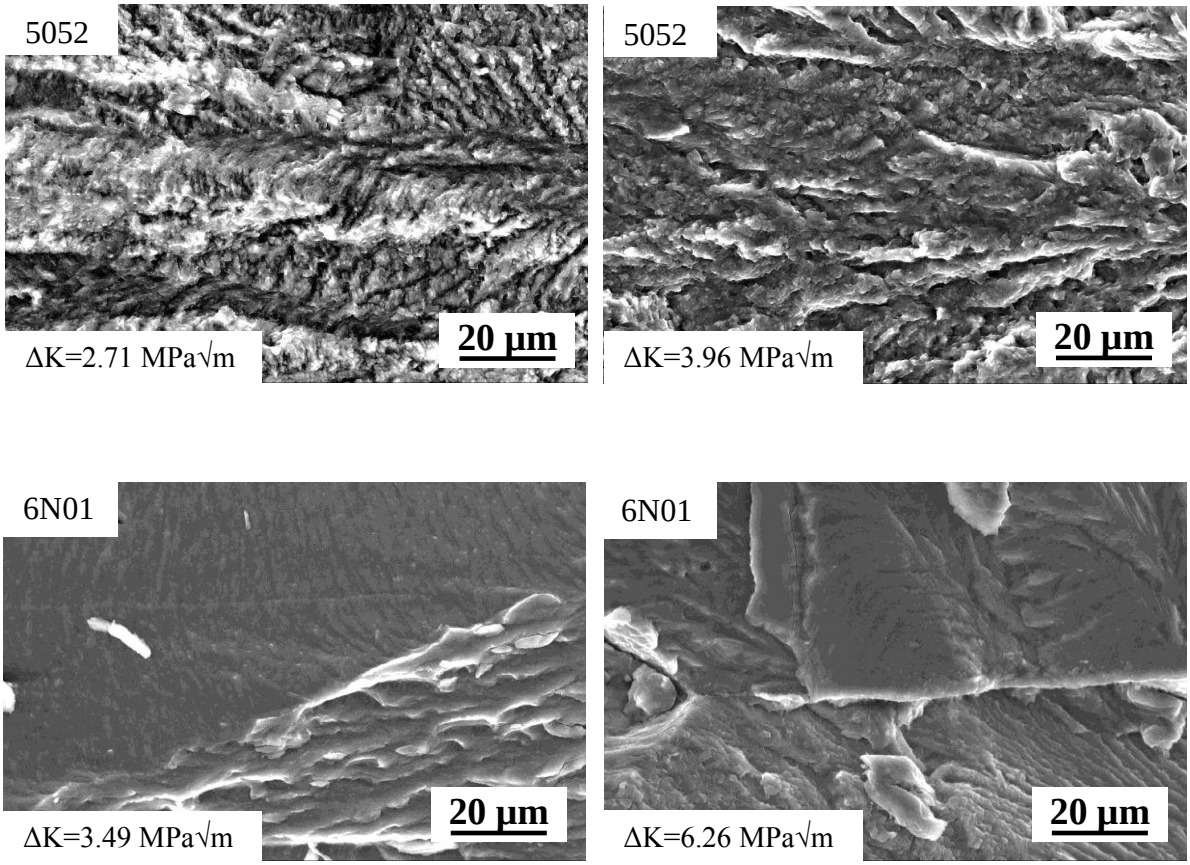


(a) Base materials

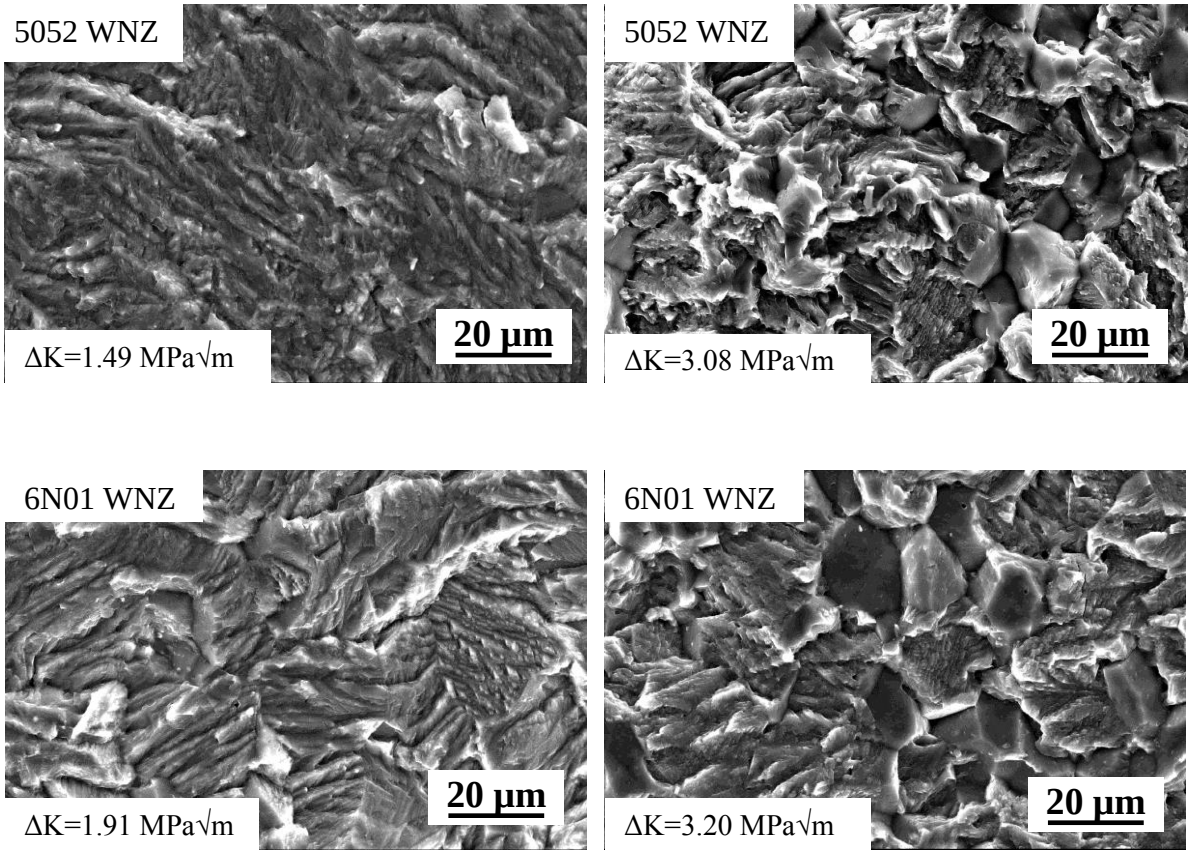


(b) WNZ of FSWed similar aluminum alloy joints

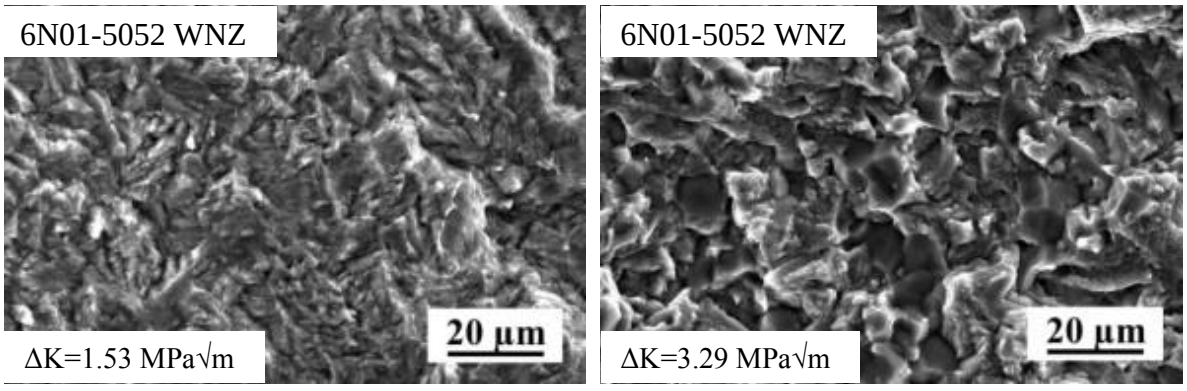


(c) WNZ of FSWed 6N01-5052 dissimilar aluminum alloys joint

Fig. 4.7 Fracture surfaces of FSWed similar and dissimilar aluminum alloys joints at low ΔK and high ΔK region.

Crack closure was observed in both of 5052 BM and 6N01 BM. However, crack closure was not observed in the WNZ of FSWed 5052 similar, 6N01 similar and 6N01-5052 dissimilar aluminum alloys joints. Fig 4.8 shows FCG curves arranged by $\Delta K_{eff}$ for the BM, the WNZ of FSWed similar aluminum alloy joints and the WNZ of FSWed dissimilar aluminum alloys joint. According to Fig 4.8, FCG curves were almost coincided into a single curve when the curves arranged by $\Delta K_{eff}$. WNZ of FSWed 5052 similar and 6N01 similar and 6N01-5052 dissimilar aluminum alloys joints showed the similar FCG resistance when the FCG behaviors were arranged by $\Delta K_{eff}$. It is important to note that, the WNZ of dissimilar materials joint joined by combination of two materials which showed the similar FCG behavior in the WNZ of similar material joints will be resulting in the same FCG resistance and crack closure behavior as both of combining materials.

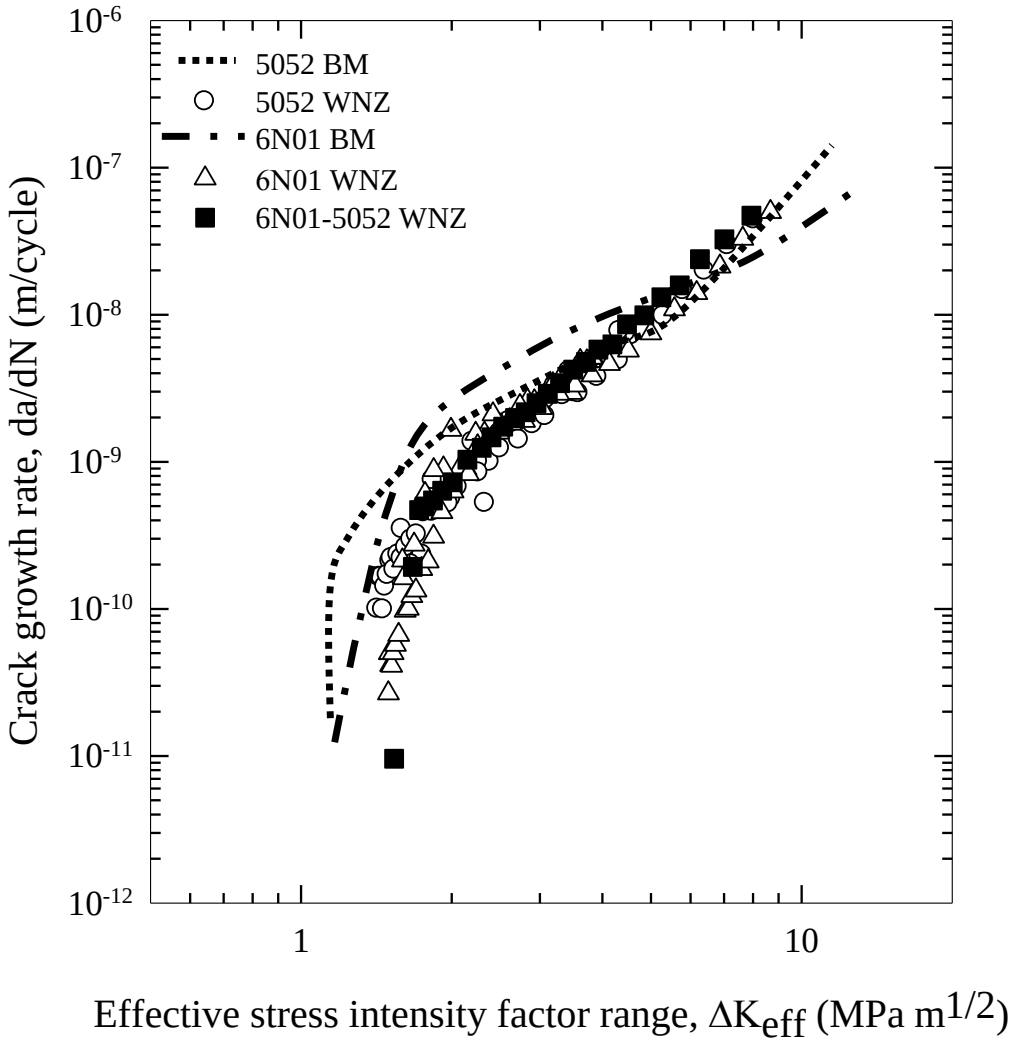


Fig. 4.8 Crack growth rate versus effective stress intensity factor range for FSWed similar and dissimilar aluminum alloys joints.

## 4.4 Conclusions

(1) Weld structure in FSWed similar aluminum alloys joints joined by using a bobbin type tool was produced as the symmetry between upper and lower sides of the joints. In case of FSWed dissimilar aluminum alloys joint, more complex materials flow was observed.

(2) Similar FCG resistance was observed in the WNZ of FSWed 5052, 6N01 similar and 6N01-5052 dissimilar aluminum alloys joints. All those FSWed joints have lower FCG resistance compared to 5052 BM and 6N01 BM.

(3) Fatigue crack growth curves were almost coincided into a single curve when the curves were arranged by $\Delta K_{eff}$ for WNZ of FSWed 5052, 6N01 similar and 6N01-5052 dissimilar aluminum alloys joints. It can be suggested that the difference in FCG behavior was mainly due to difference in the crack closure behavior. Materials combination between 5052 and 6N01 aluminum alloys in WNZ of FSWed dissimilar aluminum alloy joint induced the similar FCG and crack closure behaviors as WNZ of both FSWed 5052 and 6N01 similar aluminum alloys joints.

(4) Fatigue crack growth behavior in WNZ of FSWed dissimilar aluminum alloys joints was influenced by FCG behavior of the WNZ of FSWed similar aluminum alloy joints of the both materials combination.

## 4.5 References

[1] R.S. Mishra and Z.Y. Ma, Friction stir welding and processing, Materials Science and Engineering R, Vol. 50 (2005), p. 1-78.

[2] Y. Li, L.E. Murr and J.C. McClure, Flow visualization and residual microstructures associated with the friction-stir weldingof 2024 aluminum to 6061 aluminum, Materials Science and Engineering A, Vol. 271 (1999), p. 213-223.

[3] L.E. Murr, A review of FSW research on dissimilar metal and alloy systems, Journal of Materials Engineering and Performance, Vol. 19 (2010), p. 1071-1089.

[4] K.V. Jata, K.K. Sankaran and J.J. Ruschau, Friction-stir welding effects on microstructure and fatigue of aluminum alloy 7050-T7451, Metallurgical and Materials Transaction A, Vol. 31A (2000), p. 2181-2192.

[5] T.H. Tra, M. Okazaki and K. Suzuki, Fatigue crack propagation behavior in friction stir welding of AA6063-T5: Role of residual stress and microstructure, International Journal of Fatigue, Vol. 43 (2012), p. 23-29.

[6] S. Kim, C.G. Lee and S-J. Kim, Fatigue crack propagation behavior of friction stir welded 5083-H32 and 6N01-T651 aluminum alloys, Materials Science and Engineering A, Vol. 478 (2008), p. 56-64.

[7] Y.E. Ma, Z.Q. Zhao, B.Q. Liu and W.Y. Li, Mechanical properties and fatigue crack growth rates in friction stir welded nugget of 2198-T8 Al–Li alloy joints, Materials Science and Engineering A, Vol. 569 (2013), p. 41-47.

[8] Annual Book of ASTM standards 2008: ASTM E 647-08, p. 1-45.

# Chapter 5

# Fatigue crack growth behavior of FSWed 6N01-7N01 dissimilar aluminum alloys joints joined with a bobbin type tool

In this chapter, 6N01 and 7N01 aluminum alloys which showed different FCG behavior as observed in Chapter 3 were joined to FSWed 6N01-7N01 dissimilar materials joint for investigating the effect of materials combination on fatigue crack growth behavior in the WNZ of the joint. Fatigue crack growth behavior in WNZ of the FSWed dissimilar aluminum alloys joints were investigated comparing to that of the FSWed similar aluminum alloy joints and the BMs. The result showed that the FCG resistance in WNZ of FSWed 6N01-7N01 dissimilar materials joint was higher than that observed in WNZ of FSWed 6N01 similar material joint, however, lower than that observed in WNZ of FSWed 7N01 similar material joint. Fatigue crack growth behavior of FSWed 6N01-7N01 dissimilar materials joint was influenced by combined effect of FCG behaviors of the both alloys joint. Difference in fatigue crack growth curves observed in WNZ of the dissimilar materials joints was smaller than difference in fatigue crack growth curves observed in different BMs when the curves were arranged by effective stress intensity factor range. Fatigue crack growth resistance in WNZ was the similar or higher than that of BMs for the similar and the dissimilar materials FSWed joints when crack closure effect was taken into account.

## 5.1 Introduction

Currently, high strength aluminum alloys and dissimilar materials can be joined by friction stir welding (FSW) process even these materials are difficult to join by conventional fusion welding. In previous study, FSWed dissimilar materials joint was mainly focused on material flow and the microstructure observation [1, 2, 3]. Un-welded seam, large open (void) zones, and oxide inclusions have been reported to observe in FSWed dissimilar materials joints. Complex material flow was also observed in WNZ of FSWed dissimilar materials joint [2, 3]. Difference in materials combination would show the difference in materials mixing and flowing in WNZ of FSWed joint and results in different fatigue crack growth behavior. Moreover, previous studies reported mainly fatigue crack growth behavior in FSWed similar aluminum alloys joints and the joint was welded by using a conventional FSW tool [4, 5, 6, 7]. On the other hand, using bobbin type tool will be able to suppress formation of root flaws, obtain symmetry in welded structures, make low distortion of welded plate and join a thick plate.

In this chapter, the effect of materials combination on FCG resistance was investigated in FSWed 6N01-7N01 dissimilar aluminum alloy joint which represented the combination of alloys which were different FCG behavior in WNZ of FSWed similar aluminum alloys joints as the result obtained in Chapter 3. In this study, 6N01-7N01 dissimilar aluminum alloys and 6N01, 7N01 similar aluminum alloys were joined by FSW using a bobbin type tool. Fatigue crack growth behavior and crack closure at WNZ of FSWed 6N01-7N01 dissimilar aluminum alloys joint were investigated with comparing to these at WNZ of FSWed 6N01, 7N01 similar aluminum alloy joints and of the BM.

## 5.2 Experimental Procedure

Extruded 6N01 and 7N01 aluminum alloys plates with thickness of 6 mm were used to joining in this study. Similar and dissimilar aluminum alloys joints were welded parallel to the extrusion direction by using a bobbin type tool. The tool with shoulder diameter of 20 mm has a pin with diameter of 12 mm and distance between shoulders is 5.8 mm. In case of similar material joining 6N01 and 7N01 aluminum alloy were joined with rotating speed/traverse speed of 500 rpm/400 mm/min and 300 rpm/200 mm/min respectively. In dissimilar materials joining, 6N01-7N01 aluminum alloys joints were joined with rotating speed/traverse speed of 400 rpm/300 mm/min. Chemical compositions

of base material aluminum alloys used in this study were shown in Table 5.1. Table 5.2 shows tensile properties of the base materials in direction perpendicular to the extrusion direction and of the FSWed joints in direction perpendicular to the welding direction. Gage length of the tensile test specimen was 50 mm for the base materials and the FSWed joints.

Compact tension (CT) specimens following ASTM E 647-08 were cut from the BM and FSWed plates as shown in Fig 5.1. Fatigue crack growth direction was parallel to the extrusion direction in the base materials and the welding direction in the FSWed joints. In case of FSWed similar and dissimilar aluminum alloys joint specimen, fatigue pre-crack was introduced at the weld center line (WCL) in WNZ for all welded joints.

Fatigue crack growth test was conducted by using an electro servo-hydraulic fatigue testing machine under constant load amplitude condition according to ASTM E 647-08 [8] in laboratory air. Fatigue loading with stress ratio of 0.1 and frequency of 20 Hz was applied with sinusoidal wave form. Crack length was measured in both sides of a specimen by using travelling microscopes during the test. In order to investigate crack closure behavior, cyclic load-strain curve was measured under frequency of 2 Hz during the test by using strain gage with gage length of 2 mm attached at the back face of the specimen. Crack opening load was determined by unloading elastic compliance method to calculated effective stress intensity factor range, $\Delta K_{eff}$.

Table 5.1 Chemical compositions of base materials aluminum alloys used (Wt%).

| Alloy | Si | Mg | Zn | Fe | Mn | Cu | Ti | Cr | Zr | V |
|---|---|---|---|---|---|---|---|---|---|---|
| 6N01 | 0.58 | 0.66 | 0.01 | 0.09 | 0.08 | 0.11 | 0.01 | 0.06 | - | - |
| 7N01 | 0.08 | 1.38 | 4.49 | 0.21 | 0.37 | 0.18 | 0.02 | 0.10 | 0.14 | 0.01 |

Table 5.2 Tensile properties of base materials and FSWed joints.

| Specimen | 0.2% Proof Strength (MPa) | Tensile Strength (MPa) | Elongation (%) |
|---|---|---|---|
| 6N01 BM | 256 | 285 | 9.05 |
| 6N01 FSW | 128 | 185 | 8.65 |
| 7N01 BM | 383 | 431 | 14.20 |
| 7N01 FSW | 269 | 308 | 3.45 |
| 6N01-7N01FSW | 158 | 197 | 6.5 |

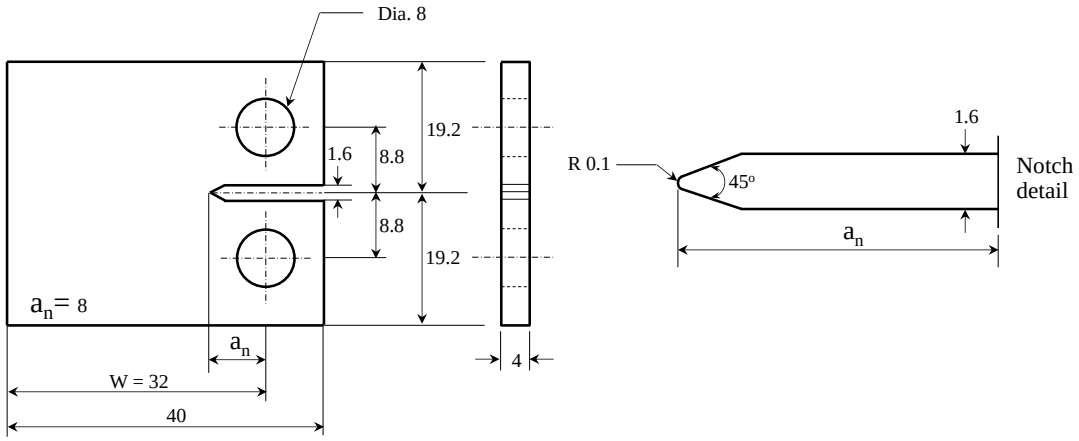


Fig. 5.1 Geometry of CT specimen used (in mm).

## 5.3 Results and Discussions

### 5.3.1 Microstructure observation

Welded structures in cross section perpendicular to the welding direction of FSWed 6N01, 7N01 similar and 6N01-7N01 dissimilar aluminum alloys joints were shown in Fig 5.2. Welded structures in the welded joints can be divided into three different regions, WNZ, thermo-mechanically affected zone (TMAZ) and heat affected zone (HAZ). In FSWed similar aluminum alloys joints, welded regions were observed as symmetry in upper and lower side of the welded joints which formed by using a bobbin type tool. However, in case of FSWed dissimilar aluminum alloys joint, more complex material flow in welded region was observed compared to that observed in the FSWed similar aluminum alloys joints. Homogeneous microstructure composed of fine equiaxed dynamic-recystallized (DRX) grains at WNZ was observed as shown at area A and B in Fig 5.2 for FSWed 6N01 and 7N01 similar aluminum alloys joints, respectively. High magnification of WNZ structure at area A and B were shown in Fig 5.3 (b) and (d) respectively. In contrast, inhomogeneous microstructure was observed in WNZ of FSWed 6N01-7N01 dissimilar aluminum alloys joint as shown in Fig 5.2 (c) and Fig 5.3 (e). Difference of DRX regions between 6N01 and 7N01 in WNZ of FSWed 6N01-7N01 dissimilar aluminum alloys joint was also clearly seen in L-S plane as shown in Fig 5.4. Large elongated grain structure was observed in 6N01 BM as shown in Fig 5.3 (a). In contrast, a strong elongated band structure was observed in 7N01 BM as shown in Fig 5.3 (c) which is significantly different from very fine equiaxed DRX grains structure observed in WNZ of FSWed 7N01 similar aluminum alloy joint in Fig 5.3 (d). The microstructures of HAZ

in all joints are similar to the base materials. The WNZ and HAZ were bounded by TMAZ which observed distorted and elongated grains.

### 5.3.2 Hardness distribution

Hardness distributions at the mid-thickness of the FSWed similar and dissimilar aluminum alloys joints in cross section perpendicular to the welding direction are shown in Fig 5.5. In all of FSWed similar and dissimilar aluminum alloys joints, welded regions showed lower hardness compared to the BM. FSWed 7N01 similar aluminum alloy joints showed higher hardness and wider welded regions compared to FSWed 6N01 similar aluminum alloy joint. In FSWed dissimilar aluminum alloys joint, hardness distribution in welded region was not uniform. Hardness distribution in WNZ of the FSWed dissimilar aluminum alloys joint for each material side was almost comparable and corresponding to hardness distribution in WNZ of the FSWed similar aluminum alloy joints. In FSWed 6N01-7N01 dissimilar aluminum alloys joint, the hardness in WNZ near the WCL changed significantly from lower hardness in 6N01 DRX grains region to higher hardness in 7N01 DRX grains region. Hardness distribution obtained in WNZ in each material side was almost the similar as that observed in the each FSWed similar aluminum alloy joints.

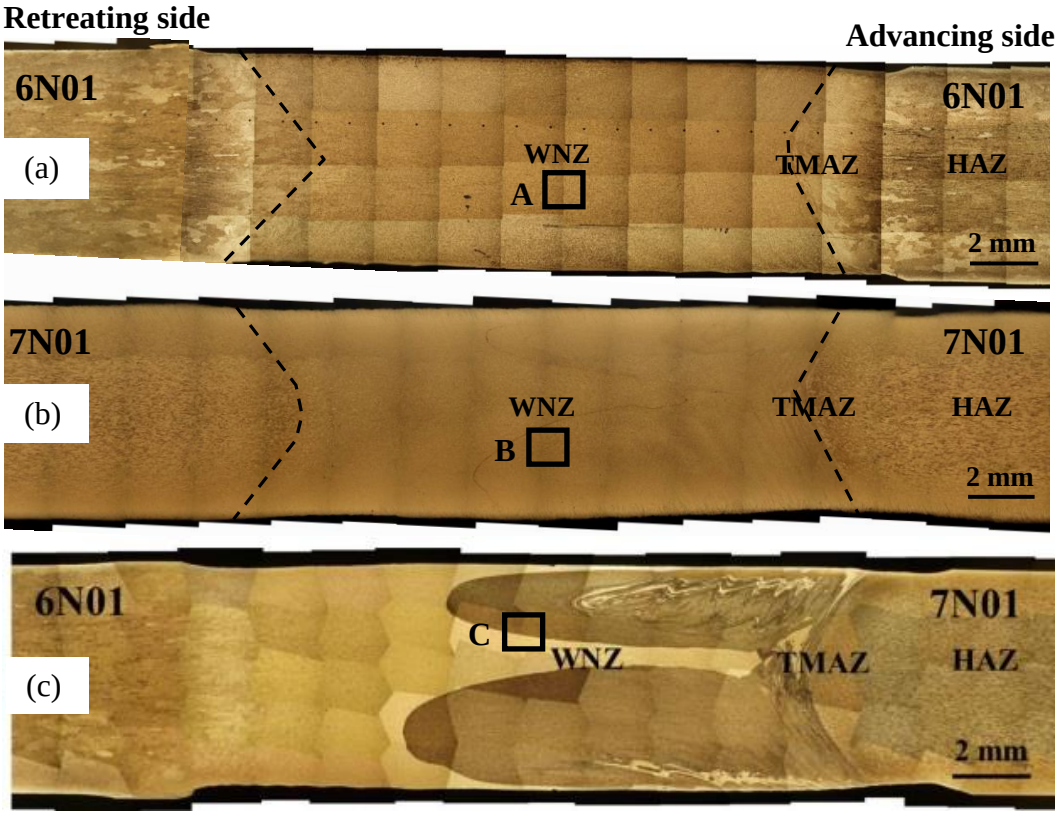


Fig. 5.2 Welded structure in transverse cross-section of (a) 6N01, (b) 7N01 and (c) 6N01-7N01 FSWed joints.

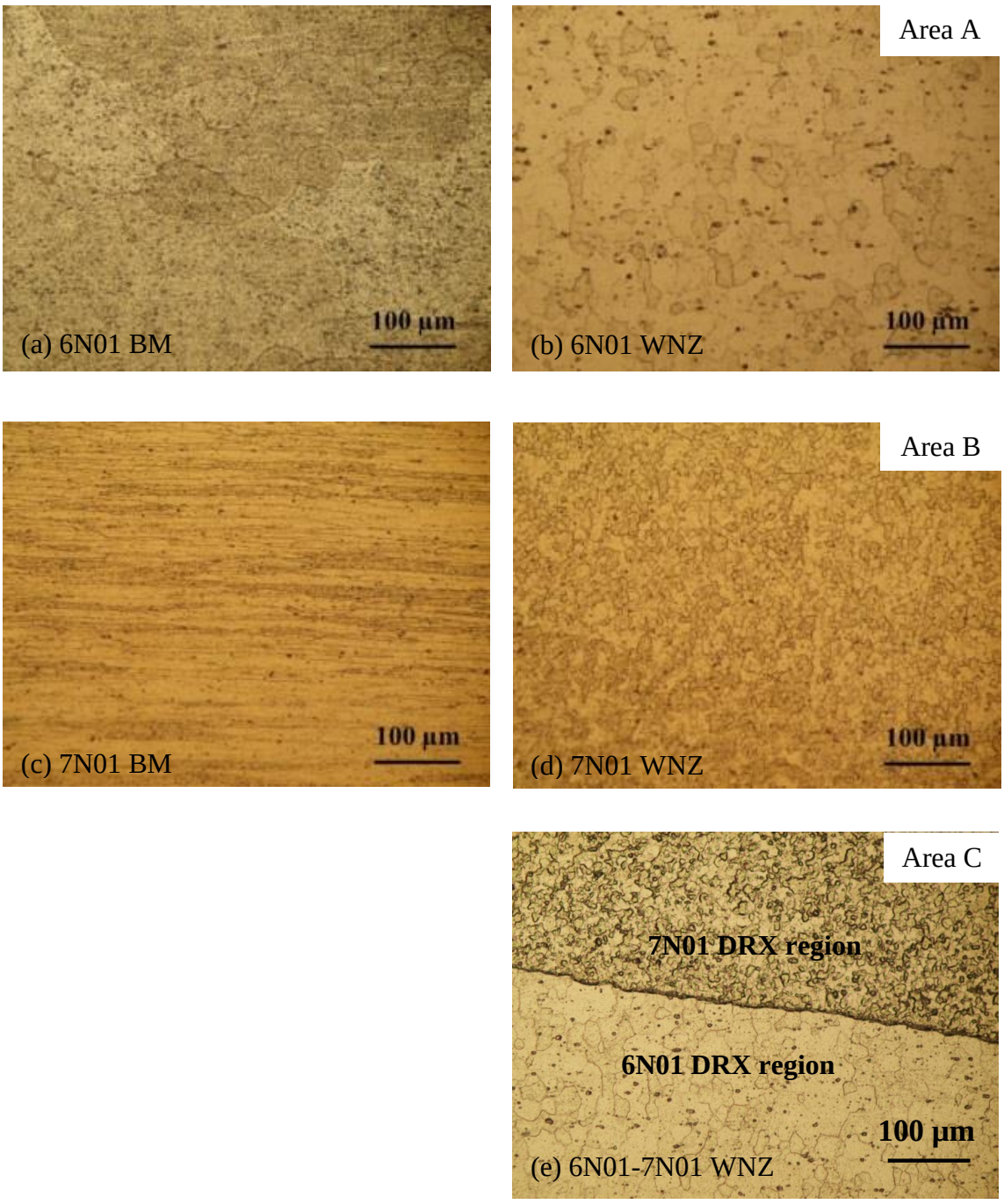


Fig. 5.3 Microstructues in WNZ of FSWed 6N01, 7N01 similar and 6N01-7N01 dissimilar aluminum alloys joints and the base materials.

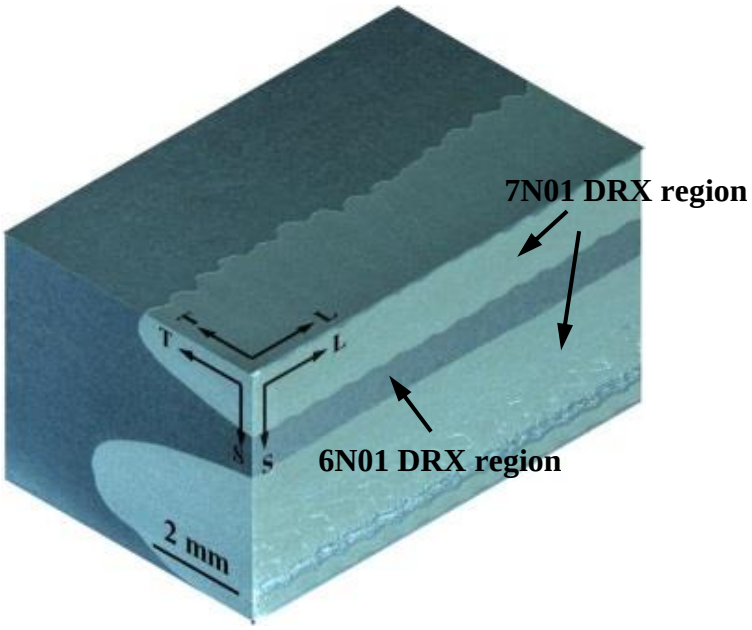


Fig. 5.4 Microstructues showed in three dimensional planes at WCL of FSWed 6N01-7N01 dissimilar aluminum alloys joint.

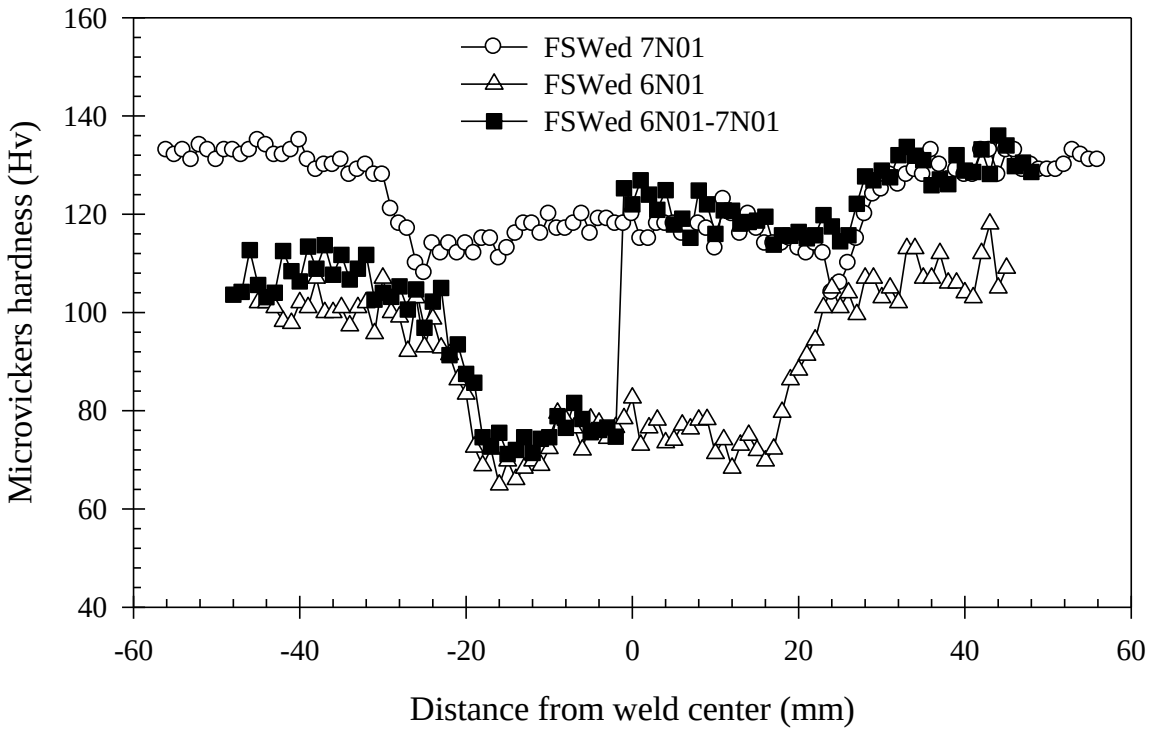


Fig. 5.5 Hardness distribution at mid-thickness position of FSWed similar and dissimilar aluminum alloys joints.

### 5.3.3 Fatigue crack growth behavior

Figure 5.6 shows fatigue crack growth (FCG) curves of BMs, and at WNZs for FSWed similar aluminum alloy joints and FSWed dissimilar aluminum alloys joint. The 6N01 BM showed comparable FCG resistance compared to 7N01 BM. However, region of ΔK above 8 $MPam^{1/2}$, 6N01 BM shows higher FCG resistance than 7N01 BM. WNZ of FSWed 6N01 similar aluminum alloys joint was lower FCG resistance compared to 6N01 BM in all ΔK regions. In contrast, at near-threshold region, WNZ of FSWed 7N01 similar aluminum alloy joint showed higher FCG resistance compared to 7N01 BM. However, in higher ΔK region, FCG resistance of WNZ in FSWed 7N01 similar aluminum alloy joint was lower than that of the 7N01 BM. WNZ of FSWed 6N01 and 7N01 similar aluminum alloy joints showed the difference in FCG behavior compared to the BMs. FCG resistance in WNZ of FSWed 6N01-7N01 dissimilar aluminum alloy joint was higher than that in WNZ of FSWed 6N01 similar aluminum alloy joint and slightly lower than that in WNZ of FSWed 7N01 similar aluminum alloy joint at low ΔK region. Large difference in FCG resistance was observed in the WNZ of FSWed 6N01, 7N01 similar and 6N01-7N01 dissimilar aluminum alloys joints at low ΔK region. However, at high ΔK region, FCG resistances in WNZ of those joints were the similar. FCG resistance in WNZ of FSWed 6N01-7N01 dissimilar aluminum alloys joint closes to that of 6N01 BM and 7N01 BM at low ΔK region. However, at higher ΔK region WNZ of FSWed 6N01-7N01 dissimilar aluminum alloys joint showed lower FCG resistance compared to 6N01 BM and 7N01 BM.

Fracture surfaces of the BMs and at WNZs for FSWed joints were shown in Fig 5.7. Transgranular fracture was observed for 6N01 BM and 7N01 BM in both of low and high ΔK regions. In case of the WNZ of FSWed similar and dissimilar aluminum alloy joints, transgranular fracture was observed at near-threshold region as shown in the left picture of Fig 5.7 (b) and (c). However, at higher ΔK region, fracture morphology in the WNZ in all FSWed joints were changed from transgranular fracture to mixed mode fracture (transgranular + intergranular) as shown in the right picture of Fig 5.7 (b) and (c). Different weld nugget grains structures was observed in the fracture surface of the WNZ of FSWed 6N01-7N01 dissimilar aluminum alloys joint which showed the mixing between 7N01 DRX grains and 6N01 DRX grains as shown in Fig 5.7 (c) corresponding to welded structure observed in Fig 5.3 (e) and Fig 5.4. Combination of different FCG behavior of 7N01 DRX grains and 6N01 DRX grains in the WNZ of FSWed 6N01-7N01 dissimilar

aluminum alloy joint might induce different in FCG resistance compared to FCG resistance in WNZ of FSWed 6N01 and 7N01 similar aluminum alloy joints. Moreover, larger portion of 7N01 DRX grains compared to 6N01 DRX grains in crack propagation plane as clearly revealed in Fig 5.4 and Fig 5.7 (c) might influence to improve FCG resistance in WNZ of FSWed 6N01-7N01 dissimilar aluminum alloys joint shift to more closer to FCG curve of WNZ of FSWed 7N01 similar aluminum alloy joint as compared to FCG curve of WNZ of FSWed 6N01 similar aluminum alloy joint as shown in Fig 5.6.

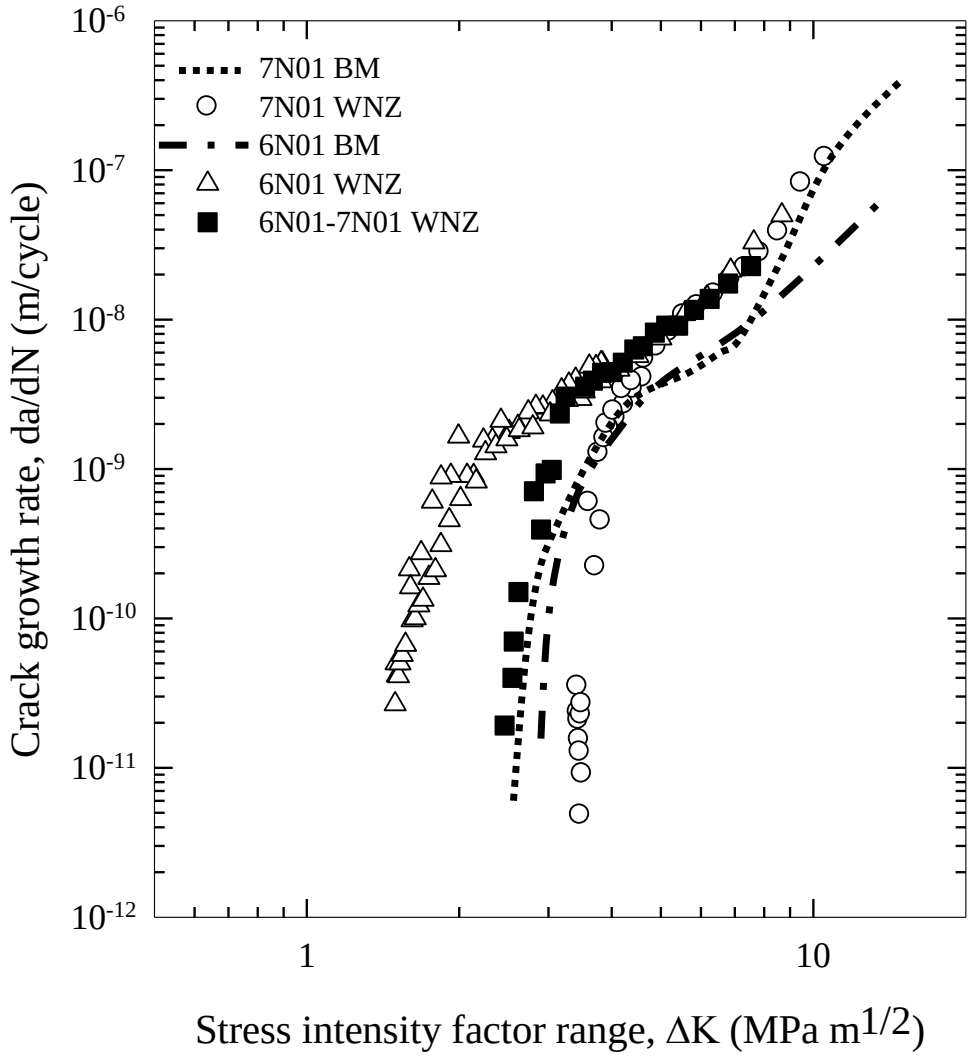


Fig. 5.6 Fatigue crack growth curves of FSWed similar and dissimilar aluminum alloys joints.

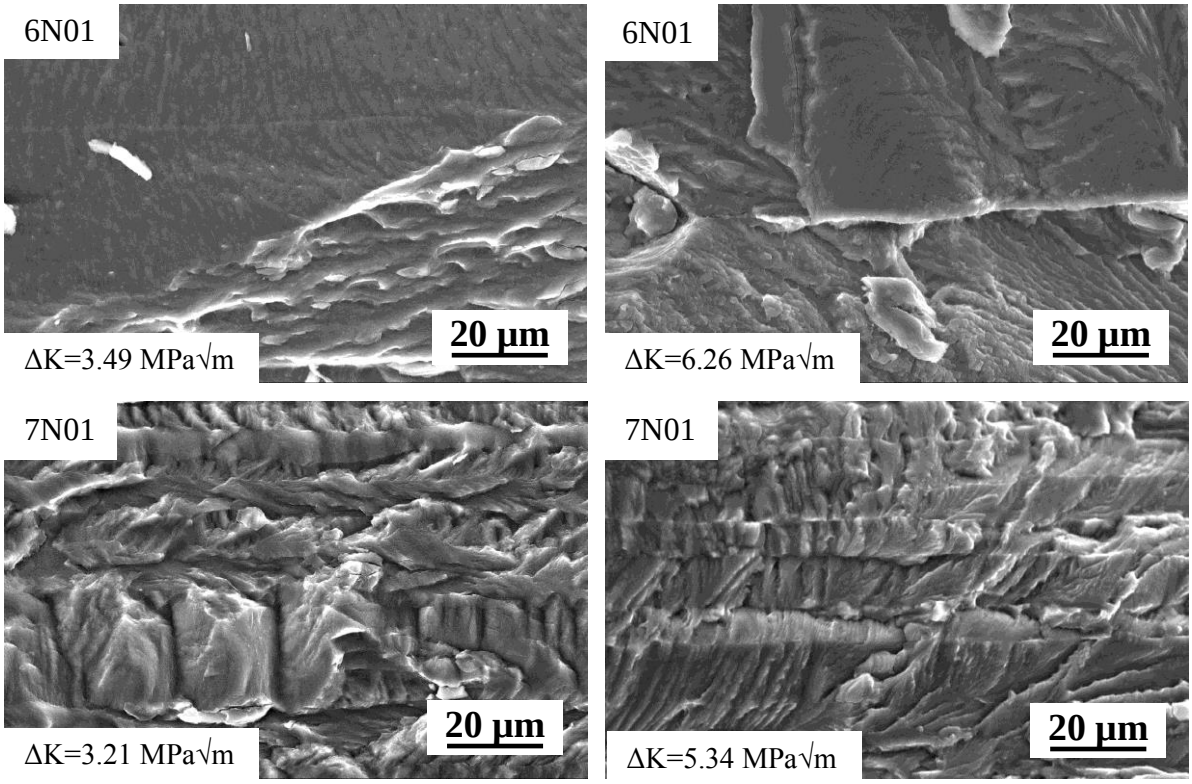


(a) Base materials

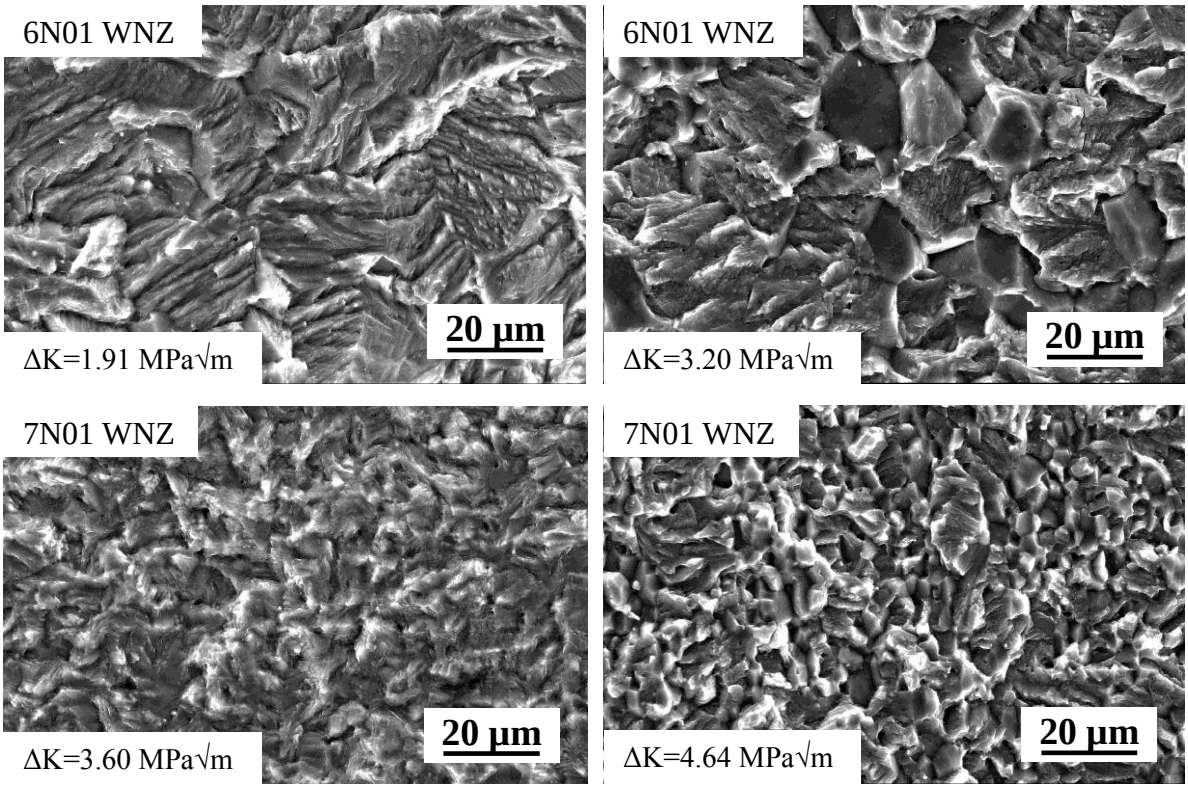


(b) WNZ of FSWed similar aluminum alloy joints

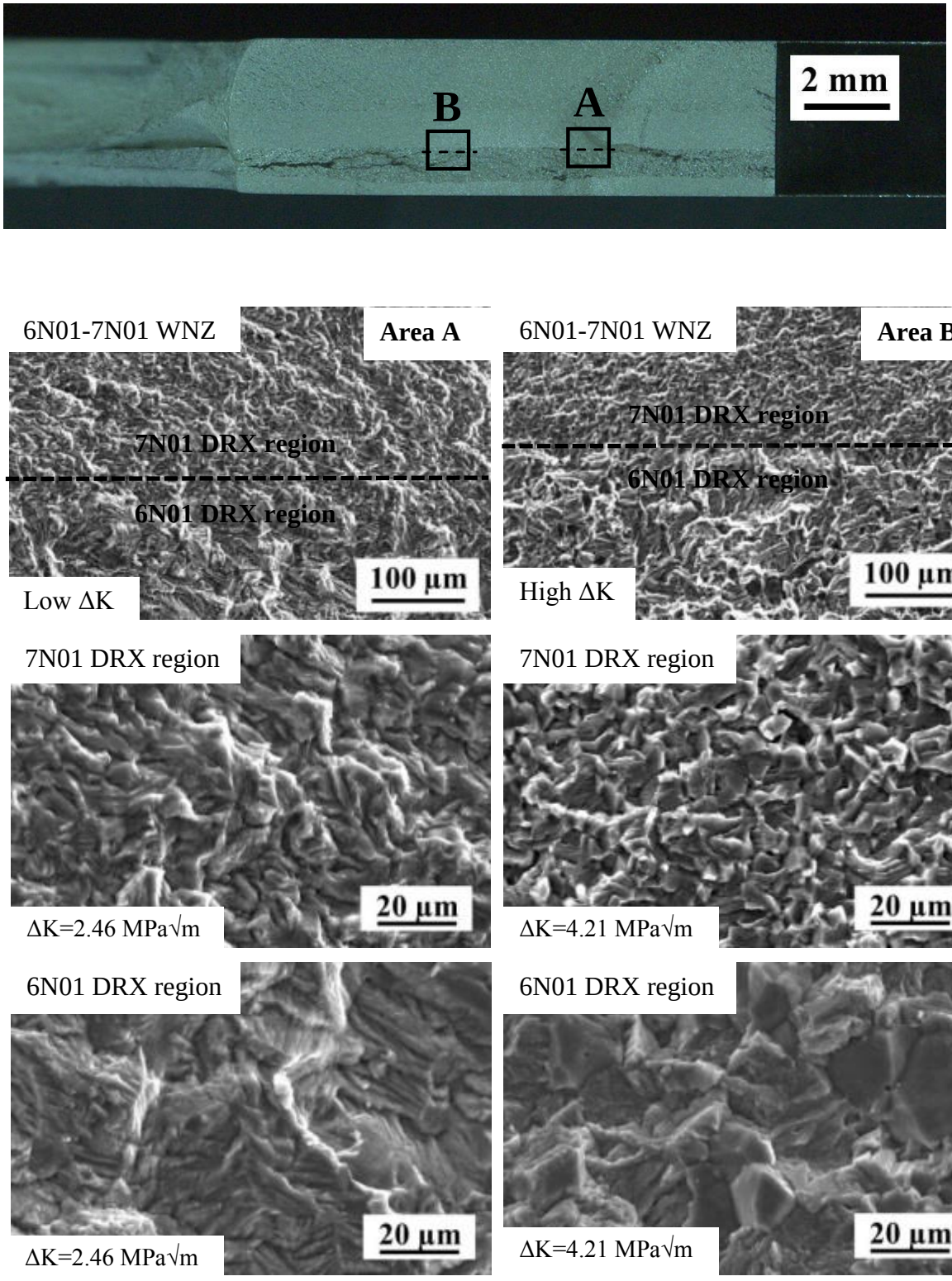


(c) WNZ of FSWed 6N01-7N01 dissimilar aluminum alloys joint

Fig. 5.7 Fracture surfaces of FSWed similar and dissimilar aluminum alloys joints at low ΔK and high ΔK region.

Figure 5.8 shows FCG curves arranged by $\Delta K_{eff}$ for the BM, the WNZ of FSWed similar aluminum alloy joints and the WNZ of FSWed dissimilar aluminum alloys joint. 6N01 BM and 7N01 BM showed the difference in FCG resistance in all $\Delta K$ regions even when the FCG curves arranged by $\Delta K_{eff}$. 7N01 BM showed significant higher FCG resistance. Crack closure was observed in both of 6N01 BM and 7N01 BM. FCG curves of WNZ in FSWed 6N01 similar, 7N01 similar and 6N01-7N01 dissimilar aluminum alloys joints almost coincide into a single curve when the curves are arranged by $\Delta K_{eff}$ at near-threshold region. At high $\Delta K$ region, FCG curves for the WNZ of FSWed 6N01 similar and 6N01-7N01 dissimilar aluminum alloys joints almost coincide in the same curve, however, WNZ of FSWed 7N01 similar aluminum alloy joint showed lower in FCG resistance which the 7N01 alloy has significant microstructural effect on FCG behavior. The result in chapter 3 showed that the 7N01 aluminum alloy shows significant microstructural effect on FCG resistance than that of 5052 and 6N01 aluminum alloys. In Paris region, 7N01 BM which more strong banded structure showed higher FCG resistance compared to 5052 BM and 6N01 BM as confirmed by FCG behavior in both of crack propagated in parallel and perpendicular to the extrusion direction was shown in similar trend. In case of WNZ of 7N01 alloy, microstructure was vastly changed due to FSW process from strong banded structure in the BM to fine-equiaxed recrystallized grains. Therefore, the WNZ of 7N01 alloy showed different FCG behavior from the both of the BM and the HAZ which have the similar microstructure. Moreover, the microstructural effect and intergranular fracture mechanism in Paris region and high $\Delta K$ region would be expected reason to reduce the FCG resistance in WNZ of 7N01 FSWed aluminum alloy joint. Crack closure was observed in WNZ of FSWed 7N01 similar and 6N01-7N01 dissimilar aluminum alloys joints, but was not found in WNZ of FSWed 6N01 similar aluminum alloy joint. It was clearly seen that at near threshold region, the difference in FCG resistance of the WNZ in FSWed 6N01 similar, 7N01 similar and 6N01-7N01 dissimilar aluminum alloys joints was mainly due to the difference in crack closure behavior. It can be mentioned that FCG and crack closure behavior of the WNZ in FSWed 6N01-7N01 dissimilar aluminum alloys joint was affected by combination FCG behaviors of both DRX grains of 6N01 and 7N01 which mixed by the material flow due to stirring action in the WNZ.

It is important to note that the effect of materials on FCG behavior was reduced in the WNZ of FSWed dissimilar materials joints even if the BM had a significant effect of microstructure produced by the wrought process on FCG curves as shown in Fig 5.9.

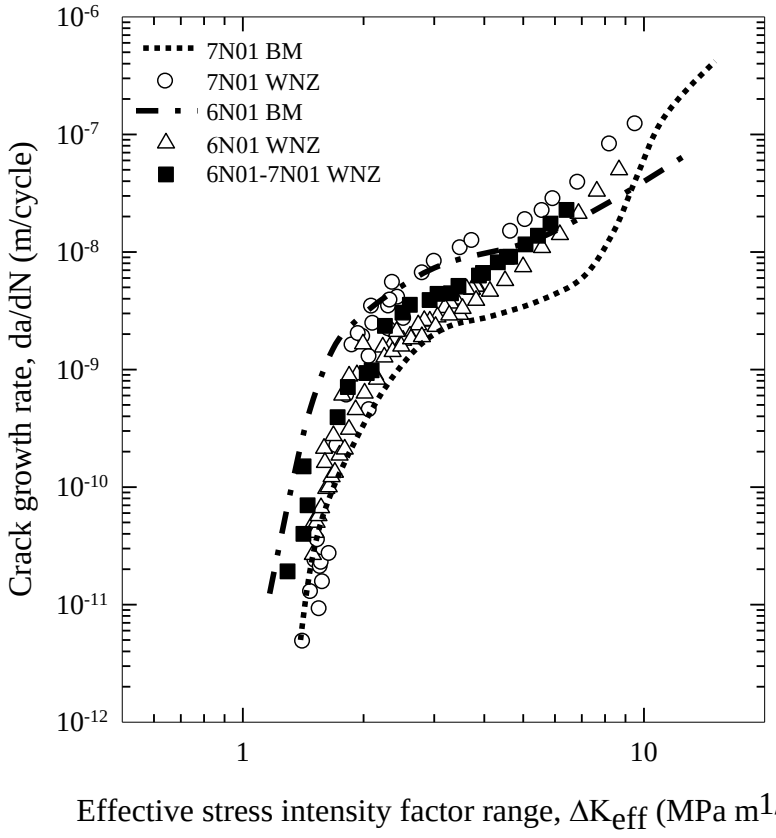


Fig. 5.8 Crack growth rate versus effective stress intensity factor range for FSWed similar and dissimilar aluminum alloys joints.

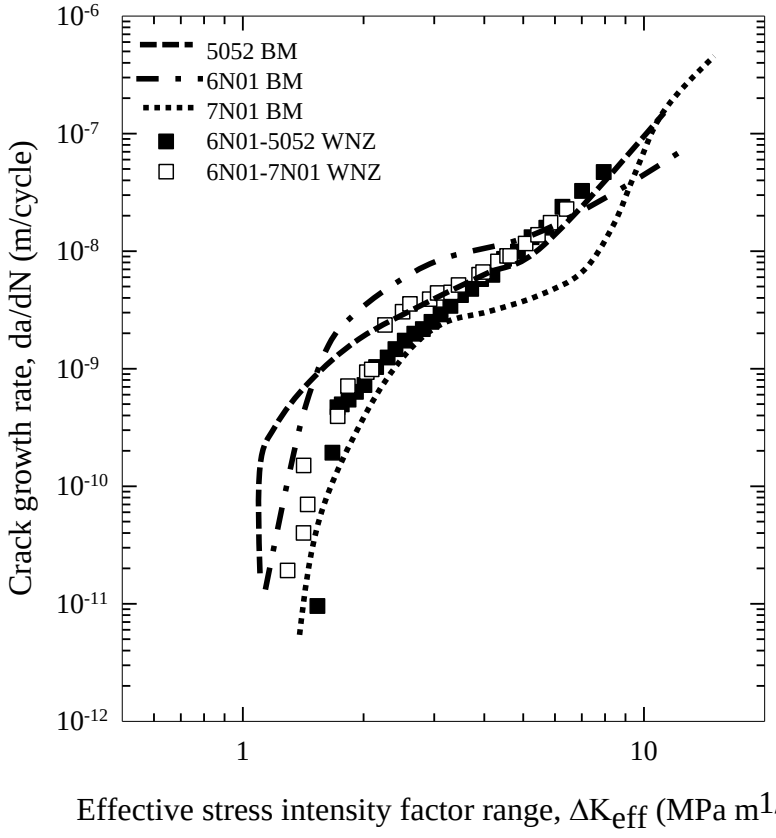


Fig. 5.9 Crack growth rate versus effective stress intensity factor range for WNZ of FSWed dissimilar aluminum alloys joints and base materials.

## 5.4 Conclusions

(1) Weld structure in FSWed similar aluminum alloys joints joined by using a bobbin type tool was produced as the symmetry between upper and lower sides of the joints. In case of FSWed dissimilar aluminum alloys joints, more complex materials flow was observed.

(2) The WNZ of FSWed 6N01 similar aluminum alloy joint showed the difference in FCG behavior compared to the WNZ of FSWed 7N01 similar aluminum alloy joint. FCG resistance in the WNZ of FSWed 6N01 similar aluminum alloy joint was lower than that of 6N01 BM in all $\Delta K$ regions. In contrast, the WNZ of FSWed 7N01 similar aluminum alloy joint showed higher FCG resistance compared to 7N01 BM at near-threshold region, but in higher $\Delta K$ region, 7N01 BM showed higher FCG resistance. The WNZ of FSWed 6N01-7N01 dissimilar aluminum alloys joint showed higher FCG resistance compared to the WNZ of FSWed 6N01 similar aluminum alloy joint but showed lower FCG resistance compared to the WNZ of FSWed 7N01 similar aluminum alloy joint.

(3) In the WNZ of FSWed 6N01, 7N01 similar and 6N01-7N01 dissimilar aluminum alloys joints, FCG curves obtained can be arranged by $\Delta K_{eff}$ only at near-threshold region. However, in higher $\Delta K$ region, the curves were not arranged well by $\Delta K_{eff}$.

(4) Fatigue crack growth behavior in the WNZ of FSWed 6N01-7N01 dissimilar aluminum alloys joint was combined the effect of FCG behaviors of the both combination materials used.

(5) Effect of materials on FCG behavior in the WNZ of FSWed dissimilar materials joints was reduced when evaluated by effective stress intensity factor range even if the BM had a significant effect of microstructure produced by the wrought process on FCG curves.

(6) Fatigue crack growth resistance in the WNZ was the similar or higher than that of the BMs for the FSWed similar and dissimilar materials joints when crack closure effect was taken into account.

## 5.5 References

[1] R.S. Mishra and Z.Y. Ma, Friction stir welding and processing, Materials Science and Engineering R, Vol. 50 (2005), p. 1-78.

[2] Y. Li, L.E. Murr and J.C. McClure, Flow visualization and residual microstructures associated with the friction-stir weldingof 2024 aluminum to 6061 aluminum, Materials Science and Engineering A, Vol. 271 (1999), p. 213-223.

[3] L.E. Murr, A review of FSW research on dissimilar metal and alloy systems, Journal of Materials Engineering and Performance, Vol. 19 (2010), p. 1071-1089.

[4] K.V. Jata, K.K. Sankaran and J.J. Ruschau, Friction-stir welding effects on microstructure and fatigue of aluminum alloy 7050-T7451, Metallurgical and Materials Transaction A, Vol. 31A (2000), p. 2181-2192.

[5] T.H. Tra, M. Okazaki and K. Suzuki, Fatigue crack propagation behavior in friction stir welding of AA6063-T5: Role of residual stress and microstructure, International Journal of Fatigue, Vol. 43 (2012), p. 23-29.

[6] S. Kim, C.G. Lee and S-J. Kim, Fatigue crack propagation behavior of friction stir welded 5083-H32 and 6N01-T651 aluminum alloys, Materials Science and Engineering A, Vol. 478 (2008), p. 56-64.

[7] Y.E. Ma, Z.Q. Zhao, B.Q. Liu and W.Y. Li, Mechanical properties and fatigue crack growth rates in friction stir welded nugget of 2198-T8 Al–Li alloy joints, Materials Science and Engineering A, Vol. 569 (2013), p. 41-47.

[8] Annual Book of ASTM standards 2008: ASTM E 647-08, p. 1-45.

# Chapter 6

# Conclusion

General conclusions and recommendations for further work have been discussed and summarized.

## 6.1 Effect of welding process on fatigue crack growth behavior

Differences in welding process induced different heat input generated into the joining materials during friction stir welding process. Single-passed conventional FSW introduced lower heat input into the joining material compared to double-passed conventional FSW and FSW by using a bobbin type tool. Difference in material flow pattern in weld regions due to stirring process have been observed among three different kinds of FSW processes. Tensile strength and hardness in welded region showed lower compared to the base material. Heat input during FSW process affected both tensile properties and hardness distribution. Lower heat input induced by conventional FSW showed higher tensile strength compared to FSW by using a bobbin type tool. Hardness in welded regions in single-passed conventional FSWed was higher than that in double-passed FSWed and FSWed joint joined by using a bobbin type tool. The lowest hardness was located in HAZ in all FSWed joints. Dynamic recrystallized grain size in WNZ of conventional FSWed which showed lower heat input during FSW process was smaller than that observed in FSWed joint joined by using a bobbin type tool.

Joints joined by different FSW processes showed different FCG behavior. In case of FSWed joint joined by using a bobbin type tool, FCG resistance of WNZ was lower than that of the BM and the HAZ at near-threshold region. At high ΔK region, WNZ had almost the similar FCG resistance to the both of BM and HAZ. In case of single-passed conventional FSWed, FCG resistance of WNZ was higher than that of the BM but lower FCG resistance than that of the HAZ at near-threshold region. At high ΔK region, WNZ of single-passed conventional FSWed showed the similar FCG resistance to that of the BM and the HAZ. In case of double-passed conventional FSWed, FCG resistance of WNZ was the similar to that of the BM and lower than that of the HAZ at near-threshold region. In high ΔK region, FCG resistance of the BM and the HAZ in double-passed conventional FSWed was almost the similar, but in the WNZ showed slightly lower FCG resistance compared to both the BM and the HAZ. Lower heat input in single-passed conventional FSWed induced higher FCG resistance compared to double-passed conventional FSWed and FSWed joint joined by using a bobbin type tool in the both of WNZ and HAZ. Significant difference in FCG resistance of different FSW processes in the both of WNZ and HAZ was observed at low ΔK rgion. In contrast, at high ΔK region the difference of FCG resistance among three different FSW processes was reduced.

Difference in FCG curves obtained in different welded regions and FSW processes were coincided into a single curve when the curves were arranged by $\Delta K_{eff}$. It can be mentioned that the difference in FCG behavior in different welded regions and different in FSW processes is mainly due to difference in crack closure behavior even if there are different in heat input generated during the FSW processes. It is also found that the grain size was a main factor to control the threshold stress intensity factor range.

## 6.2 Effect of materials on fatigue crack growth behavior in different FSWed similar aluminum alloys joints

Different in base material 5052, 6N01 and 7N01 aluminum alloys used showed different fatigue crack growth behaviors of the FSWed similar aluminum alloy joints. Fatigue crack growth resistance in the WNZ of FSWed 5052 and 6N01 aluminum alloys joints was lower than that of the BM and the HAZ at near-threshold region. At high $\Delta K$ region, the WNZ of FSWed 5052 aluminum alloy joint has the similar FCG resistance to the both BM and HAZ. The WNZ of FSWed 6N01 aluminum alloy joint showed the lowest FCG resistance compared to the BM and the HAZ. In contrast, in the WNZ of FSWed 7N01 aluminum alloy joint, FCG resistance was higher than that of the BM and the HAZ at near-threshold region. In high $\Delta K$ region, FCG resistance in the WNZ of FSWed 7N01 aluminum alloy joint was the similar with that of the HAZ, but the BM showed slightly higher FCG resistance compared to the WNZ and the HAZ.

Fatigue crack growth curves obtained in different welded regions coincided into a single curve when the curves were arranged by $\Delta K_{eff}$ in FSWed 5052 and 6N01 aluminum alloys joints. Meanwhile, the difference in FCG behavior in different welded regions of the FSWed similar aluminum alloys joints is mainly due to the difference in crack closure behavior in 5052 and 6N01 alloys. In case of FSWed 7N01 aluminum alloy joint, FCG curves obtained in different welded regions were arranged by $\Delta K_{eff}$ at near threshold region. However, at high $\Delta K$ region, the curves were not well arranged by $\Delta K_{eff}$. It is speculated that microstructural effect may significantly influence on FCG behavior of FSWed 7N01 aluminum alloy joint in high $\Delta K$ region. However, basically, it can be concluded that the difference in FCG behavior observed in different positions was mainly due to the difference in crack closure behavior. It also found that the grain size and sub-grain size was a main factor to control the threshold stress intensity factor range.

## 6.3 Effect of materials combination on fatigue crack growth behavior in FSWed dissimilar aluminum alloys joints

In order to evaluate the effect of materials combination in FSWed of dissimilar materials joint, in this study, aluminum alloys which showed similar and different FCG behavior in the WNZ of FSWed similar materials joints have been selected to combine for dissimilar materials joining. The FSWed 6N01-5052 dissimilar aluminum alloys joint was represented as the combination of alloy which was the similar in FCG behavior in the WNZ of the FSWed similar aluminum alloys joints. The FSWed 6N01-7N01 dissimilar aluminum alloy joint was represented as the combination of alloy which was different in FCG behavior in the WNZ of FSWed similar aluminum alloys joints.

The results showed that the similar FCG resistance was observed in the WNZ of FSWed 5052, 6N01 similar and 6N01-5052 dissimilar aluminum alloys joints. The WNZ in all those FSWed joints showed lower FCG resistance comparing with 5052 BM and 6N01 BM. FCG resistance in the WNZ of FSWed 6N01 similar aluminum alloy joint was lower than that of 6N01 BM in all $\Delta K$ regions. In contrast, the WNZ of FSWed 7N01 similar aluminum alloy joint showed higher FCG resistance compared to 7N01 BM at near-threshold region, but in higher $\Delta K$ region, 7N01 BM showed higher FCG resistance. However, the WNZ of FSWed 6N01-7N01 dissimilar aluminum alloys joint showed higher FCG resistance compared to the WNZ of FSWed 6N01 similar aluminum alloy joint but showed lower FCG resistance compared to the WNZ of FSWed 7N01 similar aluminum alloy joint.

Fatigue crack growth curves were almost coincided into a single curve when the curves arranged by $\Delta K_{eff}$ for WNZ of FSWed 5052, 6N01 similar and 6N01-5052 dissimilar aluminum alloys joints. It can be suggested that the difference in FCG behavior was mainly due to the difference in crack closure behavior. The WNZ of FSWed dissimilar aluminum alloy joint in which the materials combination between 5052 and 6N01 aluminum alloys is induced the similar FCG and crack closure behaviors as the WNZ of both FSWed 5052 and 6N01 similar aluminum alloys joints. In case of the WNZ of FSWed 6N01, 7N01 similar and 6N01-7N01 dissimilar aluminum alloys joints, FCG curves obtained can be arranged by $\Delta K_{eff}$ at near-threshold region. Fatigue crack growth behavior in the WNZ of FSWed 6N01-7N01 dissimilar aluminum alloys joint was combined the effect of FCG behaviors of the both of combination materials. The effect of

materials on FCG behavior was reduced in the WNZ of FSWed dissimilar materials joints when the FCG curves were arranged by effective stress intensity factor range even if the BM had a significant effect of microstructure produced by the wrought process on FCG curves. Fatigue crack growth resistance in the WNZ was the similar or higher than that of the BMs for the similar and the dissimilar materials FSWed joints when crack closure effect was taken into account.

## 6.4 General conclusions

Conventional FSW process introduced lower heat input into the joining material compared to a bobbin type tool FSW process. Friction stir welded joints joined by using a bobbin type tool showed different fatigue crack growth behavior compared to that FSWed joints joined by using a conventional FSW tool because of the difference in amounts of heat input during FSW process. FSWed joint joined with lower heat input FSW process showed higher FCG resistance compared to FSWed joint joined by higher heat input FSW process. However, the differences in FCG curves due to different FSW processes and positions in FSWed joints were arranged into a single curve when crack closure effect was taken into account. Intrinsic FCG resistance of the FSWed joints were the similar regardless of FSW process.

Different fatigue crack growth resistances were observed at different positions in all FSWed aluminum alloys joints tested in the present study. Microstructure of joined region in FSWed joints obtained showed contradiction trend with the Hall-Petch relation. The WNZ with smaller grain size of fine-equiaxed dynamic recrystallized grains had lower hardness and yield strength compared to the base materials with larger elongated grains. Moreover, lower hardness and yield strength was obtained in the HAZ which showed similar grain size with the base materials.

The effect of grain size and hardness on threshold stress intensity factor range of FSWed material was discussed in the present work. Grain size and sub-grain size was a factor to control the threshold stress intensity factor range. In contrast, hardness of FSWed material is not dominant on threshold stress intensity factor range.

In case of dissimilar materials FSWed joint combined between the two alloys which showed the similar FCG behavior in the WNZ of FSWed similar materials joints, FCG behavior in WNZ of the FSWed dissimilar materials joint was the similar with that of FCG

behavior in WNZ of the FSWed similar materials joints of both alloys. In case of FSWed dissimilar materials joint combined between the two alloys which showed the difference FCG behavior in the WNZ of FSWed similar materials joints, FCG behavior in the WNZ of the FSWed dissimilar materials joint was combined the effect of FCG behaviors in the WNZ of FSWed similar material joints of both alloys.

The difference FCG resistance obtained in weld region by different FSW process and the difference in FCG resistance at different positions in weld region is mainly due to the difference in crack closure behavior. The effect of materials on FCG behavior was reduced in the WNZ of FSWed dissimilar materials joints when FCG behavior was evaluated by effective stress intensity factor range, even if the BM had significant effect of microstructure produced by the wrought process on the FCG behavior. One of an important conclusion obtained in this work for industry is that FCG resistance of the WNZ in both FSWed similar and dissimilar aluminum alloys joints was the similar or higher compared to that of the BM when crack closure behavior was taken into account.

## 6.5 Recommendations for further work

In according to the effect of welding process in this study, FSWed joint joined by conventional FSW tool showed higher FCG resistance compared to FSWed joint joined by using a bobbin type tool. However, conventional FSW process has some disadvantages compared to a bobbin type FSW process such as generated root flaw which reduced fatigue strength of the joints. The root flaw or other defects generated in welding process can be act as an initial crack in fracture mechanics consideration. In generally, fatigue failure in structural component was occurred by including of crack initiation, crack propagation and final failure stage. In case of conventional FSW process, initial crack was generated in FSWed joint as a root flaw, however, the FSWed joint showed higher FCG resistance. On the other hand, FSWed joint joined by using a bobbin type tool had no root flaw, however, the FSWed joint showed lower FCG resistance. The competition of those two conditions in fatigue failure for reaching critical crack length then resulted in catastrophic failure for structural components that under cyclic loading was still unknown. In order to consider the joining process selection point of view, evaluate the criteria to achieve critical crack length in FSWed joints comparing between both of FSW processes was required to study in future.

In addition, improving of FSW tool design in order to achieve optimum quality and mechanical properties of FSWed joints is required. It is benefits for further work if can be combined the advantages of FSWed joint joined by using conventional FSW tool in case of improved the FCG resistance and FSWed joint joined by using a bobbin type tool in case of eliminated the root flaw to obtain in one FSW tool.

Moreover, the result in Chapter 2 showed that FSWed joint joined by using lower heat input FSW process resulting in obtained higher FCG resistance. From these resulted trend in the present study, varying the FSW process parameters such as rotation speed and traveling speed in order to decrease the heat input during joining by a bobbin type FSW process was interested issue. It is not only benefits for eliminating the root flaw which normally generated in conventional FSW process but also might be increasing FCG resistance of the FSWed joint. Therefore, the effect of FSW process parameters and heat input on FCG behavior in FSWed joint joined by using a bobbin type tool is the vital topic to study for improving FCG resistance of the FSWed joint joined by using a bobbin type tool.

Finally, from the result obtained in Chapter 2 and Chapter 3 showed that grain size and sub-grain size was dominant on threshold stress intensity factor range. It will be benefit if can be predict the threshold stress intensity factor range of the FSWed materials by evaluating from the grain size obtained in welded regions. In order to predict those data, the model for evaluating the grain size of FSWed material from their welding parameters and the model correlate between grain size and threshold stress intensity factor range were required in further study. As a result, if we can combined this knowledge as proposed in above, the model will be able to predict and estimate the threshold stress intensity factor range of the FSWed joint by using the welding parameters without conducting fatigue crack growth test. These predicted data would be useful information for material design consideration in fracture mechanics point of view for FSW applications.